Thermal conductivity enhancement of liquid and solid with single-walled carbon nanotubes

（単層CNTを用いた液体／固体の熱伝導率増大効果）

シブシャンカラン　ハリーシュ

Thermal conductivity enhancement of liquid and solid with single-walled carbon nanotubes

（単層CNTを用いた液体／固体の熱伝導率増大効果）

Approved, Thesis committee:

Shigeo Maruyama, Thesis advisor
Professor, Department of Mechanical Engineering
The University of Tokyo, Japan.

Yuji Suzuki
Professor, Department of Mechanical Engineering
The University of Tokyo, Japan.

Hirofumi Daiguchi
Associate Professor, Department of Human and Engineered Environmental Studies
The University of Tokyo, Japan.

Junichiro Shiomi
Associate Professor, Department of Mechanical Engineering
The University of Tokyo, Japan.

Shohei Chiashi
Lecturer, Department of Mechanical Engineering
The University of Tokyo, Japan.

Declaration

I, hereby declare that the investigation presented in the thesis entitled “Thermal conductivity enhancement of liquid and solid with single-walled carbon nanotubes” submitted to The University of Tokyo, Japan for the award of Doctoral degree is the record of work carried out by me during the period from October 2010 to August 2013 under the supervision of Dr. Shigeo Maruyama. The work is original and has not been submitted earlier as a whole or in part for a degree at this or any other academic institutions.

Abstract

Fluids with higher thermal conductivities are necessary for cooling applications especially in micro-electronic devices. The low thermal conductivity of conventional heat transfer fluids remains a limitation in improving the performance of micro-electronic cooling systems. Metallic and metal oxide particles possess significantly higher thermal conductivity than those of the conventional heat transfer fluids. Hence it is speculated that the addition of such highly conductive particles may enhance the thermal conductivity of heat transfer fluids. Advancement in the development of Nano science and Nanotechnology in the last decade have attracted the heat transfer engineers to utilize nano sized particles for this purpose because of their stability against sedimentation and, as a result, reduction in potential for clogging a flow circulating system. Recent experimental reports of anomalous enhancements in thermal conductivity above the predictions of classical Maxwell theory with low volume fraction of metallic and metallic oxide nano-particles have drawn much focus among the heat transfer researchers. This has led to numerous experimental and numerical investigations on the thermal conductivity of nanofluids suspensions.

Despite numerous efforts, it still remains unclear whether the thermal conductivity enhancement in nanofluids is anomalous or within the predictions of classical theories. Non reproducibility and lack of agreement among the nanofluids community is due to the lack of proper materials synthesis and characterization techniques and inability to form suspensions with long term stability.

To understand the real potential of nanofluids, systematic investigation of the thermal conductivity enhancement is carried out with spherical, one-dimensional and two dimensional carbon allotropes is carried out in this present research. Single-walled carbon nanohorns, single-walled carbon nanotubes and exfoliated graphite nanoplatelets were used as the nano inclusions. Stable nanofluids suspensions were created using sodium deoxycholate as the surfactant in water and ethylene glycol. The nanofluid suspensions were thoroughly characterized using transmission electron microscopy, optical absorbance spectroscopy, dynamic light scattering, photoluminescence spectroscopy and atomic force microscopy.

Thermal conductivity measurements were carried out using a custom built transient hot-wire technique for different temperature and loadings of nano inclusions. Thermal conductivity enhancement results were analyzed based on effective medium theory considering the role of interfacial thermal resistance into account. The experimental results reveal that the aspect ratio of the nano inclusion plays a significant role in the thermal conductivity improvement owing to its high specific surface area and ability to form high heat transport pathways.

Experimental results show that two-dimensional inclusions lead to higher thermal conductivity improvement followed by one-dimensional and spherical inclusions. It was also found that the thermal conductivity enhancement in ethylene glycol is higher than the case of water irrespective of the nature of nano inclusion. Dynamic light scattering studies, optical absorbance and atomic force microscopy clearly reveals the nature of

agglomeration is different in the case of ethylene glycol compared to the case of water. This leads to the conclusion that the particle agglomeration has a profound effect in the thermal conductivity enhancement of nanofluid suspensions. The experimental results are in reasonable agreement with the predictions of effective medium approach which leads to the conclusion that the thermal conductivity enhancement in nanofluids is 'not anomalous' and the classical heat conduction approach holds for well characterized and stable suspensions.

In the last part of this work, fine tuning the thermal conductivity enhancement via temperature regulation is demonstrated for a phase change alkane by successively melting and freezing the alkane with different nano inclusions. Solidification of *n*-Octadecane resulted in higher thermal conductivity enhancement in the solid state compared to the liquid state irrespective of the dimensionality of the nano inclusion. In the solidified state carbon nanotubes outperformed graphite nanoplatelets and carbon nanohorns due to their ability to form percolating networks at low loading. It is hypothesized that this phase-dependent enhancement is due to the formation of a quasi-two-dimensional percolating structure, which is formed by the nanotubes during the phase transition. The present experimental results will stimulate further theoretical research on developing models to explain such behaviour, and will contribute to the development of high conductivity thermal energy storage materials for buildings and in solar power plants.

Acknowledgements

I would like to express my sincere heart of gratitude to my advisor Professor Shigeo Maruyama for his support and encouragement to complete my research successfully. He gave me the freedom to choose a topic and mold my project together and provided invaluable insight and support. His valuable suggestions and guidance filled me with courage and confidence whenever I was let down by various problems during the research.

I am particularly grateful to Dr. Junichiro Shiomi who gave consistent feedback on my research topic throughout my stay. I would also like to thank Dr. Shohei Chiashi for helping on many occasions in the laboratory, and giving feedback on my thesis. I also like to thank Professor Yamaguchi in Chemical Engineering department for providing facilities to perform Dynamic Light Scattering measurements. I would also like to thank Yamamoto san at AIST for his willingness to help performing viscosity measurements. I also appreciate the technical support from Mr. Watanabe in the laboratory.

I also wish to thank all my colleagues in the lab for their kind help and friendship during the period of my graduation thesis. I would like to thank Dr. Kei Ishikawa who helped me in many ways while the design of my experimental setup. I would also like to thank Dr. Shinya Aikawa and Taiki Inoue for their tremendous support in TEM and AFM

measurements. I would also like to thank Dr. Erik Einarsson and Dr. Pei Zhao who spent plenty of time to discuss the spectroscopic analysis results. I also like to thank my friend Theerapol Thurakitseree and junior members Sho Hida, Takuma Hori and Yoshinori Nakamura who helped me in many ways throughout my stay.

I also could not have reached this milestone without the support and tolerance of my family and friends. I owe my mother big thanks for providing me with all of the opportunities and support. I also wish to thank my soon to be wife Sowmyaa for her patience and affection which helped to get to this point.

List of Tables

List of Figures

0.25 wt %. (c) Thermal conductivity enhancement as a function of temperature for different SWCNT loading.

Figure 5.3: Recycling behaviour of thermal conductivity during successive phase transition cycles at SWCNT loading of 0.25 wt %. Arrows indicate the sequence of cycles.

Figure 5.4: (a) Thermal conductivity enhancement in liquid state as a function of SWCNT loading. Modified Yamada-Ota model predict the present experimental results with a TBR of 2.5 x 10^{-8} m^2KW^{-1}. EMT model prediction for the same TBR in the liquid state is marginally lesser compared to modified Yamada-Ota model. (b) Thermal conductivity enhancement in solid state as a function of SWCNT loading. The theoretical models fail to predict the enhancement in solid state as the influence of aggregation during first order phase transition is not included in the models. The experimental results were fitted with a power law equation of form $A\phi_w^b$ where A and b were fitting constants and ϕ_w is the SWCNT weight fraction. The fit parameters were 12.6 and 1.53 for A and b respectively.

Figure 5.5: (a) Differential Scanning Calorimetry plot of melting cycle in *n*-octadecane and *n*-octadecane/SWCNT nano composite. (b) Differential Scanning Calorimetry plot of freezing cycle in *n*-octadecane and *n*-octadecane/SWCNT nano composite. Note that the peaks are shifted by 3.5 ºC for calibration correction of the DSC.

Table of Contents

Chapter 3

Enhanced Thermal Transport in Ethylene Glycol and Water with Single Walled Carbon nanotube Inclusions

Chapter 4

Effect of Carbon Nano Additive Dimensionality in the Thermal Conductivity Enhancement of Nanofluids

Chapter 5

Enhanced Thermal Conduction Characteristics of Phase Change Composites with Single Walled Carbon Nanotube Inclusions

Chapter 6

Chapter 1

Introduction

1.1 Electronics Cooling

Cooling has become one of the major challenges in the generation of micro/nanotechnology. In a broad spectrum of fields such as micro and nano electronics, automobiles and manufacturing, the performance of the systems are greatly hindered by the absence of efficient cooling methods. Micro and nano electronic devices unavoidably produce heat, which need to be minimized to prevent the failure of the device. The necessity to reduce the chip size and increase the speed and performance of such electronic devices has lead to the development of high density multi-chip packaging which has lead to high heat dissipation requirements.

The International Technology Roadmap for Semiconductor (ITRS), 2012 report [1] projects the performance of the processors to increase from 6.82 GHz in 2012 to 16.18 GHz in 2026. The ITRS projection for the performance of single-chip microprocessor is shown in Figure 1.1. Increasing the processor performance often results in the dissipation of higher power density which in turn demands a proper cooling system. However, the lack of a sufficient cooling system remains a concern to meet the projected trajectory of ITRS. It is apparent

from these predictions that meet the roadmap set by ITRS, more efficient cooling solutions are required.

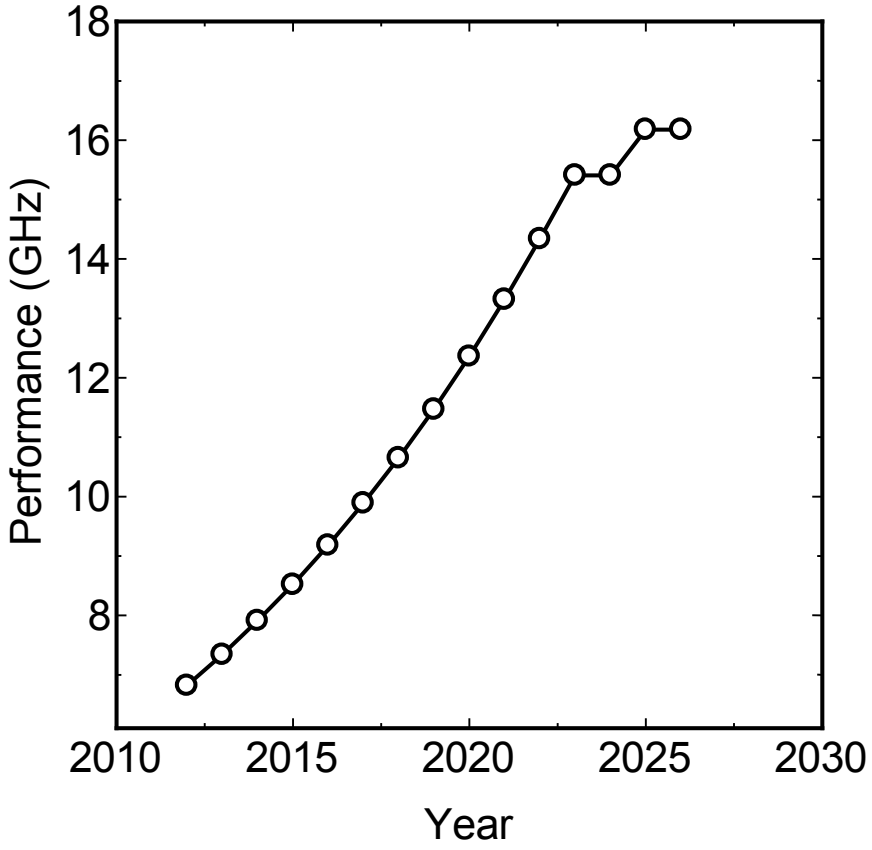

Figure 1.1: ITRS prediction of the performance of single chip microprocessors [1].

The most widely used cooling method adapted to this date for electronics cooling has been forced air convection, but this method has a serious limitation due to its inability to meet with the increasing level of heat flux due to the necessary increase in size of the metal fin-array heat sinks [2]. An alternative to this approach is the utilization of single phase micro-fluidic heat sinks [3]. However, this technology also has significant limitation owing to the thermal

properties of the cooling fluid. Conventional heat transfer fluids exhibit poor heat transfer performance due to their inherent low thermal conductivities.

1.2 Concept of Nanofluids

Fluids with inclusions of higher thermal conductivity particles are being considered as an option to improve the thermal properties of such fluids with a minimal increase in viscosity. Many research activities have been carried out in the past to improve the thermal properties of these fluids by seeding a small quantity of highly thermally conductive macro/micro sized particles in it [4]. However, this has not been very successful because of settling of the solid particles due to their large size [4]. Recent developments in the field of nanoscience have led to the development of a new class of fluids termed "nanofluids" [5]. Over the past decade, nanofluids—colloidal dispersions prepared by uniformly dispersing nanostructures such as nanoparticles, nanotubes and nanosheets in conventional heat transfer fluids—have gained attraction worldwide because of their superior thermal performance [6-8].

1.3 Enhanced Thermal Conductivity of Nanofluids with Spherical Inclusions

Many research groups experimentally reported a substantial increase in the thermal conductivity [7] and the convective heat transfer coefficient [6] of such fluids. The first measurements of the thermal conductivity enhancement with ultrafine particles in fluid were reported by Masuda et al [9]. They reported thermal conductivity enhancements of SiO_2, TiO_2, and Al_2O_3 in water at various particle volume fractions. Later, Argonne National

Research Laboratory reported an 'anomalous' enhancement in the thermal conductivity up to 40 % at 0.3 vol % of dispersed copper and copper oxide nanoparticles in ethylene-glycol and termed such fluids as "nanofluids" [10]. Patel et al. [11] showed that ultra-low inclusion of 0.026 vol % of silver nanoparticles in water and toluene, resulted in a thermal conductivity enhancement of 5-21 % [8]. The reported enhancements in thermal conductivity were considered to be "anomalous" and cannot be predicted by Maxwell's theory [12].

Nanofluids consisting of spherical particles have used various metals and metallic oxides. These predominantly include copper, copper oxide, aluminum, aluminum oxide, zinc oxide, titanium dioxide, gold, silver etc [6-8]. Studies on thermal conductivity enhancement of nanofluids for varying particle volume fraction show conflicting results. Very high improvement in the thermal conductivity was reported with the inclusion of spherical particles by few researchers [10, 11, 13-15] while many research groups failed to observe such anomalous improvement [16-20].

Most importantly the dependence of thermal conductivity enhancement as a function of temperature reported by Das et al. [21] sparked much interest on the mechanism surrounding the thermal conductivity enhancement in nanofluids. Many reports show an increase in thermal conductivity with increase in temperature of the base fluid [22-25] while a least/no significant effect was shown by few groups [26-28]. There also exist few reports which report a reduction in thermal conductivity as a function of temperature [29, 30].The effect of temperature on the thermal conductivity enhancement and the mechanism surrounding the contradictory results still remains unclear and highly controversial.

There are also conflicting reports on the effect of nanoparticle size on thermal conductivity enhancement of nanofluids. Few reports show an enhancement with decrease in particle size because of the increase in specific surface area as the size of the nanoparticle decreases [13, 15, 24] whereas few reports show a contradictory behaviour [22]. Many reports show an increase in thermal conductivity enhancement with decrease in base fluid conductivity while a recent study show the thermal conductivity of base fluid has least effect on the thermal conductivity enhancement [20]. Similarly, the role of thermal conductivity of nano material also remains unclear. Significant reports show that higher the thermal conductivity of the nanomaterial greater is the thermal conductivity enhancement while other reports show that the thermal conductivity of nano particles is not necessarily a primary factor for it. Thermal conductivity enhancement studies in alumina based nanofluids with particle shapes of platelets, blades, cylinders and bricks showed that the enhancement follows the sequence as platelets<bricks<cylinders indicating the role of particle shape in the thermal conductivity enhancement [31]. A recent benchmark study carried out by 33 research groups found no such anomalous improvement happens with spherical nanoparticles but high improvement for the inclusion of cylindrical structures [32]. Their results show that the particle shape/aspect ratio is an important factor to increase the thermal conductivity of fluids. The influence on thermal conductivity increment caused by seeding the above-mentioned spherical particles in different base fluids has been well summarized by several researchers [7, 8, 33-35].

1.4 Thermal Conductivity of Carbon Nanotubes

Among nano suspensions, those seeded with cylindrical structures namely carbon nanotubes have gained interest recently. The discovery of carbon nanotubes (CNTs) by Iijima in 1991 [36] spawned a tremendous amount of research, largely due to its remarkable mechanical, thermal and electrical properties. Experimental and numerical studies have reported very high thermal conductivity for CNTs. Hence, it is natural to expect that the suspensions consisting of CNTs would result in higher thermal conductivity increase compared to other nanoparticles.

The structure of CNT is shown in Figure 1.2. A carbon nanotube consists of an atomic layer of carbon atom which is rolled into the form of a tubular structure. The axis of the CNT can form along many different directions (*i.e.* chiral vectors *(n,m)*) in the carbon layer, yielding CNTs with different chiralities and diameters. Multi-walled carbon nanotubes (MWCNTs) include several concentric tubes that can have varying chiralities and diameters. Single walled carbon nanotubes usually have armchair *(n,n)* or zigzag *(n,0)* and other chiralities *(n,m)*. Armchair *(n,n)* nanotubes are always metallic, while zigzag *(n,0)* and other *(n,m)* chiralities are semiconducting [37]. Heat conduction in CNTs is always dominated by the phonons rather than electrons even in the metallic nanotubes. The phonon conduction in CNTs is influenced by several factors such as the number of phonon active modes, boundary scattering, the diameter and length of the nanotubes, structural defects and also on the presence of impurities [38]**.**

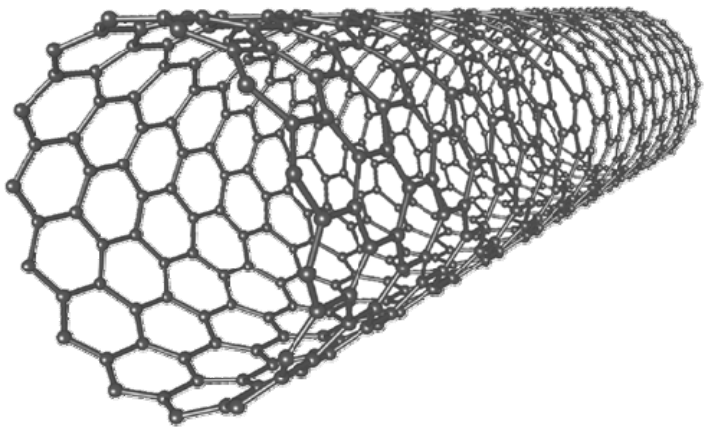

Figure 1.2: Structure of CNT (Image Source: Wikipedia)

1.4.1 Experimental Measurements of Thermal Conductivity of CNTs

Table 1.1 summarizes the reported values of thermal conductivity of SWCNTs and MWCNTs based on experimental methods. Hone et al. [15] estimated a room temperature thermal conductivity of 1750-5800 $Wm^{-1}K^{-1}$ for single-walled CNTs (SWCNT) based on the thermal conductivity measurements of SWCNT mats of tangled nanotube bundles. Kim et al. [40] reported a thermal conductivity value of over 3000 $Wm^{-1}K^{-1}$ for an individual suspended MWCNT of 2.5 μm long and 14 nm diameter. They made use of an external heat source and passively generated a temperature difference by placing a heat source at one end of the nanotube. The heat generated by one resistor was detected using sensors at the other end. Yu et al. [41] measured a thermal conductivity of greater than 8000 $Wm^{-1}K^{-1}$ for SWCNTs of diameter 1 nm using the similar measurement technique. Pettes and Shi [42] recently found that the thermal conductivity of CNTs decreased with the number of walls but this is also correlated to the defect concentration of CNTs with increasing number of walls. The authors

also made use of the measurement method reported by kim et al. [40] but applied a sinusoidal heating pulse in their measurements.

Table 1.1: Summary of experimental thermal conductivity values reported for SWCNTs and MWCNTs

Reference	CNT diameter (nm)	CNT Length (μm)	Thermal Conductivity ($Wm^{-1}K^{-1}$)
Kim et al. [40]	14	2.5	3000
Yu et al. [41]	1-3	2.6	1800-8000
Pettes and Shi [42]	1.5-12	2-4	600 - 40
Fujii et al. [43]	9.8,16.1,28.2	3.7,1.9,3.6	2800,1800,500
Choi et al. [44,45]	20,42,46	1-1.4	300,650,830
Wang et al. [46,47]	1.9	0.5,4.9,6.9	2600,3160,3210
Pop et al. [48]	1.7	2.6	3500
Li et al [49]	1.8	41	2749

Fujii et al. using a T-type sensor experimentally measured a room temperature thermal conductivity of 2069 $Wm^{-1}K^{-1}$ for an individual multi-walled nanotube (MWCNT) of 9.8 nm diameter [43]**.** Choi et al. [44] used the 2 pad 3ω technique and reported a lower thermal conductivity value of 300 $Wm^{-1}K^{-1}$ for an MWCNT of diameter 20 nm and length 1.4 μm at room temperature. Choi et al. [45] previously reported a thermal conductivity in the range of 650 - 830 W m^{-1} K^{-1} for MWCNTs of diameter 46 nm and 42 nm respectively using a 4 pad

3ω technique. Wang et al. [46, 47] reported a thermal conductivity value of 4500 $Wm^{-1}K^{-1}$ for a SWCNT of 1.7 nm diameter and 6.9 µm in length using 3 ω technique. Besides, they also showed that thermal conductivity of the nanotube is length dependent [46].

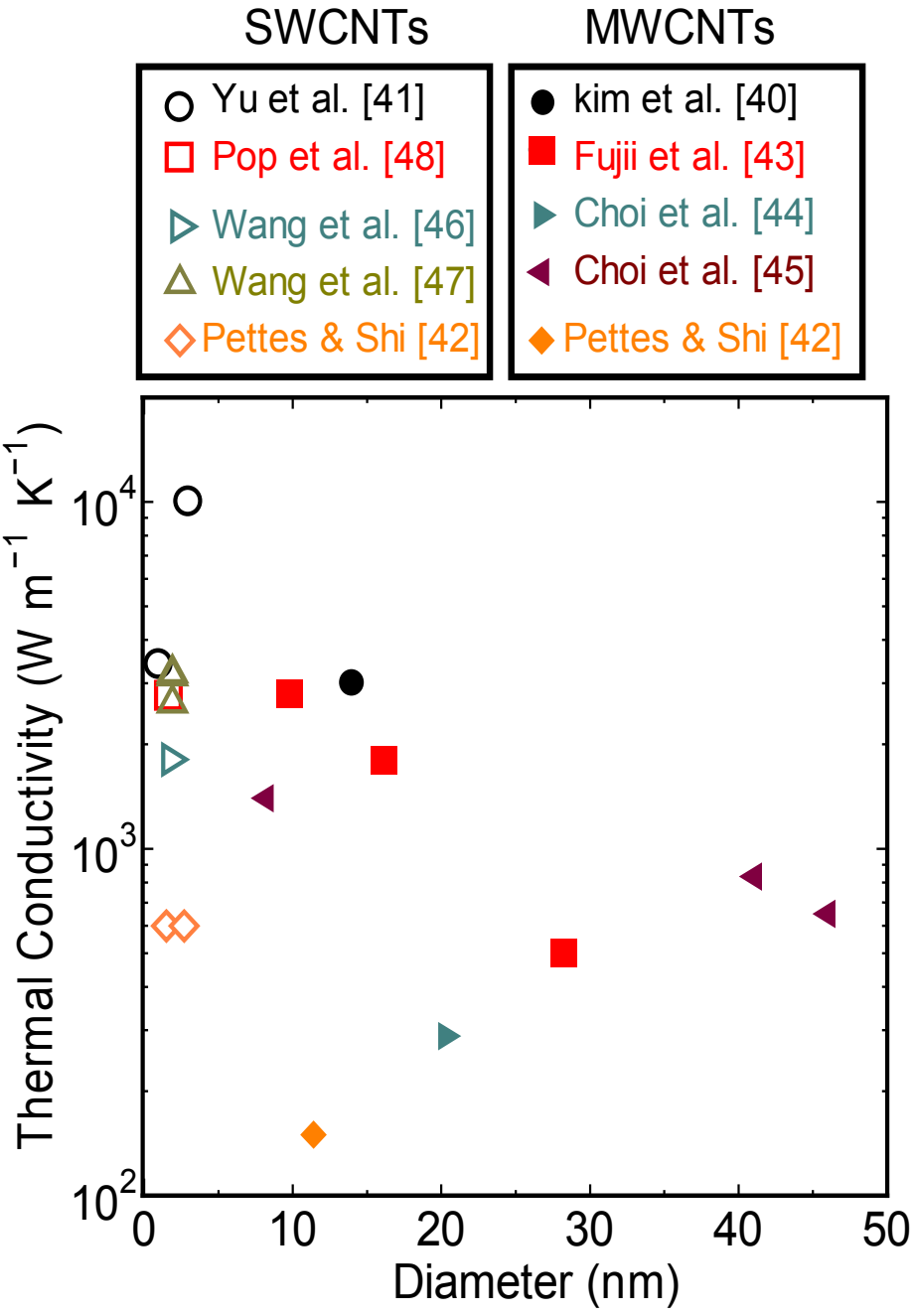

Figure 1.3: Diameter dependent thermal conductivity of CNTs

Pop et al. [48] measured the room temperature thermal conductivity to be around 3500 $Wm^{-1}K^{-1}$ for individual SWCNT of 1.7 nm diameter. They also reported that the thermal conductivity decreases to 1200 $Wm^{-1}K^{-1}$ when the temperature increases to 800 K. Pop et al. [48] made use of self-heating technique to measure the thermal conductivity of suspended nanotube. In this technique, heat is generated by applying a voltage across the CNT which results in an electrical heating of the CNT. In this case the temperature distribution is deduced from the resulting electrical resistance change. Li et al. [49] reported a novel measurement technique using self-heating of CNTs and made the temperature measurements using Raman spectroscopy. They reported a thermal conductivity 1810 $Wm^{-1}K^{-1}$ and 1400 $Wm^{-1}K^{-1}$ for SWCNT of diameter 1.8 nm and MWCNT of diameter 8.2 nm respectively. A summary of the thermal conductivity of CNTs as a function of CNT diameter is shown in Figure 1.3.

1.4.2 Molecular Dynamics Simulations of Thermal Conductivity of CNTs

Another approach to compute the thermal conductivity of CNTs is using molecular dynamics (MD) simulations. MD simulations calculate the thermal transport based on the interaction potentials between the carbon atoms. In general, there are three ways to compute the thermal transport in CNTs using atomistic simulations. They are equilibrium molecular dynamics (EMD), Non-Equilibrium Molecular Dynamics (NEMD) and Homogeneous Non-Equilibrium Molecular Dynamics (HNEMD) respectively. EMD simulations use the Green – Kubo formula derived based on the linear response theory [50]. NEMD simulations use the Fourier's conduction law to obtain the thermal conductivity by applying either a fixed

temperature gradient or heat flux to the system. HNEMD simulations apply an external field to mimic the system without actually imposing a temperature gradient or the heat flux to the system [51]. Table 1.2 summarizes the results of thermal conductivity of CNTs obtained from many of the molecular dynamics simulations in the literature.

Most of the thermal conductivity of CNTs based on MD simulations reported in the literature was performed with the chiral vector (10, 10). Based on HNEMD simulations, Berber et al. [52] obtained a thermal conductivity of 6600 $Wm^{-1}K^{-1}$ for an isolated SWCNT. The results of their simulation showed that the thermal conductivity increases with increasing temperature and reaches a maximum at 100 K. Above this temperature the thermal conductivity decreases to 6600 $Wm^{-1}K^{-1}$ at room temperature. Periodic boundary conditions along the axis of the nanotube are utilized to approximate nanotubes of infinite length in their calculations. Similar behaviour was reported by Osman et al. [53] with the thermal conductivity peak at 400 K. However they reported lower room temperature thermal conductivity of 1700 $Wm^{-1}K^{-1}$. Padgett and Brenner [54] and Moreland et al. [55] found much lower thermal conductivity values compared to previous results, reporting only 160 $Wm^{-1}K^{-1}$ and 215 $Wm^{-1}K^{-1}$ respectively at room temperature at 300 K. Moreland et al. [55] found that the thermal conductivity of the CNT is length dependent. They reported that the thermal conductivity at 300 K increases from 215 $Wm^{-1}K^{-1}$ to 831 $Wm^{-1}K^{-1}$ when the length of the CNT increased from 50 nm to 1000 nm.

Maruyama [56] for a finite length of CNT also reported this length–dependence of thermal conductivity for SWCNTs up to 400 nm. However, length convergence was not found in

either of these studies. Che et al.[57] reported a length-convergent thermal conductivity of 2980 $Wm^{-1}K^{-1}$ for a 40 nm long SWCNT at 300 K. Lukes and Zhong [51] also reported a length dependent thermal conductivity of up to 375 $Wm^{-1}K^{-1}$, also for a 40 nm long SWCNT. Mingo and Broido [58] solved the linearized Boltzmann-Peierls phonon transport equation to predict the thermal conductivity values of SWCNTs. They reported that ballistic transport occurs for short SWCNTs, thus length-convergence was not achieved. However, the thermal transport becomes diffusive as the length increases, and they report a length-convergent thermal conductivity value of 9500 $Wm^{-1}K^{-1}$ for a 100 nm long (10, 0) CNT at 316 K.

Table 1.2: Summary of Molecular dynamics results of thermal conductivity of SWCNTs

Reference	**CNT Chirality**	**CNT Length (nm)**	**Thermal Conductivity ($Wm^{-1}K^{-1}$)**
Berber et al. [52]	(10, 10)	2.5	6600
Osman et al. [53]	(10, 10)	30	1700
Padgett and Brenner [54]	(10, 10)	20-300	160
Moreland [55]	(10, 10)	50-1000	215
Maruyama [56]	(10, 10)	250-400	250-400
Che at al. [57]	(10, 10)	40	2980
Lukes and Zhong [51]	(10, 10)	40	375

The thermal conductivity values obtained by numerical methods span a wide range, and in most cases are lower than the experimentally obtained values. One major reason for this discrepancy is the choice of CNT area which influences the calculated thermal conductivity value. Berber et al. [52] calculated the area based on the assumption that tubes have an inter-wall separation of about 3.4 Å in nanotube bundles. Maruyama [56] used a ring of van der Waals thickness of 3.4 Å, while Che et al. [57] used a ring of 1 Å thickness for the cross-sectional area. The rest of the simulations calculated the area as a circle with circumference defined by the centers of the atoms around the nanotube [51, 53-55]. Variations in the length of CNT, boundary conditions, simulation methods (EMD, NEMD, and HNEMD), and interatomic potentials also contribute to the range of simulated values.

Berber et al. [52] and Lukes and Zhong [51] utilized periodic boundary conditions along the axis of the nanotube to approximate nanotubes of infinite length. Lukes and Zhong [51] reported that with periodic boundary conditions, increasing the simulated length of the SWCNT increased the predicted thermal conductivity. They suggested that longer nanotubes have more vibrational modes which provide new pathways for heat transfer. The phonon mean free path in SWNCTs is of the order of few microns [37]. For CNTs of length shorter than the phonon mean free path, phonon scattering from free boundaries will be important. Hence Lukes and Zhong [51] argued that CNTs modeled with periodic boundary conditions have no free boundary which artificially eliminates boundary scattering. This allows the possibility of phonon–phonon interactions as the only scattering mechanism which is the reason for high thermal conductivity values obtained by this boundary condition.

For a finite-length CNT in which the phonons are scattered at the tube ends, it is more physically meaningful to use free boundary conditions in the simulations to obtain accurate thermal conductivity values. However, in all these MD simulations, the simulated CNT length is shorter than the expected phonon mean free path and the conduction is not completely diffusive. The thermal conductivity may saturate if the simulation is extended to further longer lengths of CNTs. The simulations discussed above were usually performed using isolated (5, 5) or (10, 10) SWCNTs [51-58]. Since the structural details of the SWCNTs used for experiments were not clearly stated, it is quite difficult to directly compare the thermal conductivity values obtained from simulations. It can be concluded that there still exist a significant uncertainty in the thermal conductivity of CNTs, especially for the case of SWCNTs.

1.5. Review of Thermal Conductivity Enhancement in CNT Based Nanofluids

From the experimental and simulation results on the thermal conductivity of CNTs, it is natural to expect that nanofluids seeded with carbon nanotubes would outperform nanofluids seeded with spherical particles due to their high thermal conductivity and large aspect ratio. In the past decade, several groups have made use of CNTs for making nanofluids and have reported thermal conductivity values of such fluids. The first experimental results on CNT-based nanofluids were reported by Choi et al. [59] They reported an enhancement of 160 % for MWCNTs dispersed in poly alpha olefin oil (PAO), and termed the enhancement 'anomalous'. The reported results were much higher than theoretical predictions, and also found a non-linear relationship with respect to the nanotube loading. The magnitude of

enhancement they reported was also very high, and much greater than the earlier reports for fluids seeded with nanoparticles. However, the authors of this work failed to describe in detail the sample preparation procedure for their experiments.

Following the work by Choi et al. [59] Xie et al. [60] measured the thermal conductivity enhancements of water, ethylene glycol and decene seeded with MWCNTs. They functionalized the CNTs by acid treatment to make the suspensions stable. Their experimental results indicate that the thermal conductivity enhancement increased with respect to the CNT volume concentration but decreased with increase in the thermal conductivity of the base fluid.

Assael et al. [61] prepared stable MWCNT dispersions in water consisting of 0.1 wt % SDS as the surfactant. They reported a maximum thermal conductivity enhancement of 38 % with 0.6 vol % MWCNT at room temperature. Assael et al. [62] also performed similar measurements with MWCNTs in water dispersed using CTAB and nanosphere AQ as the surfactants. They found an enhancement of 34 % at 0.6 vol % loading for CTAB dispersed MWCNTs. Hwang et al. [63] reported an 11.3 % increase in thermal conductivity of MWCNTs in water at 1 vol % loading. Choi et al. [64] reported a 19.4 % increase in thermal conductivity of water consisting of 1.14 wt % of SWCNTs. Liu et al. [65] measured the thermal conductivity of MWCNTs in ethylene glycol (EG) and synthetic oil. The increase of thermal conductivity was 12.4 % for ethylene glycol/MWCNT suspensions at 1 vol % while a 30 % increase was seen for synthetic oil/MWCNT suspensions at 2 vol %. Yang et al. [66] reported an enhancement of up to 300 % for PAO consisting of only 0.35 vol % of CNTs.

Nanda et al. [67] reported an enhancement of 36 % at for SWCNT/EG nanofluids at 1 vol %. Cherkasova et al. [68] reported a thermal conductivity enhancement of 7 % at 0.1 vol % for SDBS functionalized MWCNTs.

Wen and Ding [69] reported the temperature-dependent thermal conductivity enhancement of SDBS-dispersed MWCNTs in water. They report an approximately linear dependence of thermal conductivity enhancement for temperatures below 303 K. The dependence levels-off, however, when the temperature becomes higher than 303 K. Ding et al. [70] also reported the temperature-dependent enhancement of MWCNTs dispersed using Gum Arabic. Nasiri et al. [71] systematically studied the temperature-dependent enhancement of SDS-encapsulated and chemically functionalized SWCNTs, DWCNTs and MWCNTs in water. They reported a linear increase in thermal conductivity with increase in temperature for SDS-encapsulated dispersions. On the other hand, level-off behaviour at temperatures above 313 K was found for dispersions consisting of chemically functionalized CNTs. Their experiments showed that suspensions consisting of SWCNTs had the highest enhancement of approximately 40 % at a loading of 0.25 wt %. From their experiments, they also showed chemically functionalized CNTs performed marginally better compared to SDS-encapsulated CNTs. A summary of the existing experimental results for CNT nanofluids are also tabulated in Table 1.3.

Table 1.3: Summary of thermal conductivity enhancement of CNT nanofluids

Type of CNT	Base Fluid	Preparation Technique	Observations	Reference
MWCNT	PAO	No information	Non-linear enhancement. 250 % at 1 vol % loading	Choi et al. [59]
MWCNT	Water, EG, decene	Chemical Functionalization	20 %, 12 % and 8 % at 1 vol % loading for Water, EG, Decene respectively	Xie et al. [60]
MWCNT	Water	SDS	38 % increase at 0.6 vol % loading	Assael et al. [61]
MWCNT	Water	CTAB	34 % increase at 0.6 vol % loading	Assael et al. [62]
MWCNT	Water	SDS	11.4 % at 1 vol % loading	Hwang et al. [63]
SWCNT	Water	No information	19.4 % at 1.14 wt % loading	Choi et al. [64]
MWCNT	EG, Synthetic oil	N-hydroxysuccinimide	12.4 % increase at 1 vol % for EG. 30 % increase at 2 vol % for synthetic oil	Liu et al. [65]
MWCNT	PAO	Polyisobutene succinimide	300 % at 0.35 vol % loading	Yang et al. [66]

SWCNT	EG	Chemical Functionalization	36 % at 1 vol % loading	Nanda et al. [67]
MWCNT	water	SDBS	7 % increase at 0.1 vol %	Cherkasova et al. [68]
MWCNT	Water	SDBS	Upto 50 % increase.	Wen and Ding [69]
MWCNT	Water	Gum Arabic	Non-linear increase at temperature above 300 K.	Ding et al. [70]
SWCNT, DWCNT, MWCNT	Water	SDS	Non-linear increase with respect to temperature.	Nasiri et al. [71]

1.6 Mechanism of heat conduction in nanofluids

The reported thermal conductivity enhancements sparked interests among researchers to understand the mechanism behind the nanofluids. Keblinski et al. [72] and Eastman et al. [73] proposed four possible heat conduction mechanisms. They are: Brownian motion of the nanoparticles, molecular level layering of the liquid at the liquid/solid interface, nature of heat transport (diffusive or ballistic), and the influence of nanoparticle aggregation. Analytical calculations by Keblinski et al. [74] showed that the contribution of Brownian motion to heat transport is insignificant because the contribution due to thermal diffusion is much higher than the Brownian motion. Tsai et al. [75] performed systematic experiments on fluids with different viscosities seeded with Fe_3O_4 particles. From their experiments, they

showed that Brownian motion could play an important factor in the thermal conductivity enhancement. In addition to Brownian motion, liquid layering, nature of heat transport, and clustering of particles, Lee et al. [76] showed that the particle charge state influences the thermal conductivity enhancement.

Recently Gao et al. [77] performed thermal measurements and structural analysis of phase reversible materials. From their investigations they showed that particle aggregation is the major reason for thermal conductivity improvement. Biercuk et al. [78] also suggested the formation of three dimensional percolating networks as the primary reason for the conductivity enhancement from their investigation on CNT composites. Wen and Ding [69] argued that the formation of ordered nano layer was not possible, especially in the case of surfactant-encapsulated CNTs. Due to the large diameter of CNTs they also ruled out the possibility of Brownian motion playing a significant role in heat conduction. However, the authors were not able to explain the conductivity enhancement at higher temperatures.

To summarize, all studies performed so far have reported a thermal conductivity enhancement with respect to the CNT loading. Temperature-dependent enhancement has also been reported in some cases. Attempts to interpret these contradictory thermal conductivity enhancements with CNT inclusions in the light of existing classical theoretical models showed anomalous under-estimate of measured conductivities. Classical models such as Maxwell [12], Hamilton-Crosser [79], Hashin-Shtrikman [80] did not take the aspect ratio of CNTs into account and often restricted to spherical particles. The data from different groups vary to a great extent, making it impossible to obtain a trend line directly from the available

data for CNT nanofluids. In general, most of the reports on CNT based nanofluids shows anomalous enhancement beyond the predictions of effective medium theory. The possible reasons for this discrepancy is that the lack of proper characterization techniques and knowledge on the thermal conductivity of the CNT itself. In addition, sample preparation techniques, aspect ratio of the CNTs after sonication, and purity level of the material used have not been explained in detail by many groups. Moreover there are no general mechanisms available to explain the superior thermal performance of nanofluids. Especially for nanofluids seeded with CNTs, the mechanism is far more difficult to understand due to the surface chemistry involved and the complex structure of the percolating network. The above discussion indicates other factors such as surface functionalization, aspect ratio, purity level, and straightness factor would significantly impact the thermal conductivity of CNT nanofluids.

1.7 Objective of Present Work

The objective of present work is an experimental investigation of the thermal conductivity of aqueous and non-aqueous fluids with different carbon nano additives to better understand the potential of nanofluids. The goals of the proposed work are as follows:

1) To measure the thermal conductivity increase of carbon based nanofluids in water and ethylene glycol using transient hot wire technique with well characterized single walled carbon nanotubes. SWCNT based nanofluids in water and ethylene glycol were prepared using sodium deoxycholate as the surfactant for this purpose. SWCNT

were characterized using transmission electron microscopy, resonance Raman spectroscopy, atomic force microscopy, optical absorption spectroscopy, dynamic light scattering and photoluminescence excitation spectroscopy.

2) To understand the role of temperature in the thermal conductivity enhancement and the associated mechanism behind the nanofluids. For this purpose experiments were carried out with fluids of different viscosities. Further to understand the role of Brownian motion, freezing experiments are carried out using a phase change material.

3) The role of carbon nano filler dimensionality in enhancing the thermal conductivity is investigated systematically. Single walled carbon horns and exfoliated graphite nanoplatelets are used for this purpose.

4) The experimental results of thermal conductivity enhancement with different carbon allotropes were modeled using classical theories. The possible mechanism behind the thermal conductivity enhancement, the role of nano filler shape and thermal boundary resistance is discussed.

5) Experimental prediction of viscosity of nanofluids with different carbon allotropes to probe the feasibility of nanofluids for engineering applications.

1.8 Organization of the Thesis

This thesis aims at investigating the thermal conductivity enhancement in aqueous and non-aqueous suspensions with carbon nanofillers of different dimensionality though the material of most interest is single walled carbon nanotubes. The thesis is organized as organized as follows.

Chapter 1 introduces the concept of nanofluids and gives a review of literature on thermal conductivity of single walled carbon nanotubes and thermal conduction in nanofluids.

Chapter 2 explains the synthesis of carbon nanotubes and material characterization techniques, thermal, electrical and viscosity measurement methods and theoretical models used in this research for analyzing the experimental results.

Chapter 3 reports the thermal conductivity and viscosity measurement results with single walled carbon nanotube suspensions. The experimental results are analyzed with the theoretical models and the possibility of utilizing SWCNT based nanofluids is discussed in this chapter.

Chapter 4 reports the results on thermal conductivity enhancement with single walled carbon nanohorns and exfoliated graphite filler materials.

Chapter 5 presents the unusual thermal conductivity improvement results in the solid and liquid state of phase change alkanes.

Chapter 6 summarizes the thesis and discussions for future research.

Chapter 2

Materials, Experimental Methods and Models

2.1 Synthesis of Single-Walled Carbon Nanotubes from Alcohol

Single walled carbon nanotube (SWCNTs) synthesis was synthesized by the alcohol catalytic chemical vapour deposition (ACCVD) technique. This technique employs cobalt and iron bi-metallic catalysts supported on a zeolite particle (HSZ-390HUA). It utilizes ethanol vapour as the carbon feedstock, and the reaction temperature was maintained at 800°C. Amorphous carbon impurities and metal particle impurities were dramatically suppressed at the reaction temperature of 800°C. The etching effect caused by the decomposed hydroxyl (-OH) radical, which removes carbon atoms with dangling bonds during the CVD process was reported as the reason for the high purity of the SWCNTs [81]. After CVD synthesis zeolite particles were removed by dissolving in sodium hydride solution.

2.2 Transmission Electron Microscopy (TEM) Raman Spectroscopy and Thermogravimetric Analysis (TGA) Characterization

The SWCNTs were analyzed using transmission electron microscopy (JEOL, JEM-2000EX) and resonance Raman spectroscopy. For TEM imaging, the samples were prepared by sonicating in ethanol for 30 minutes, after which 10 μl of the solution was dropped on a TEM microgrid and allowed to evaporate. A typical TEM image of the SWCNTs synthesized from

ethanol feedstock is shown in Figure 2.1. The TEM image clearly shows that the SWCNTs were devoid of both amorphous carbon and metal nanoparticle impurities.

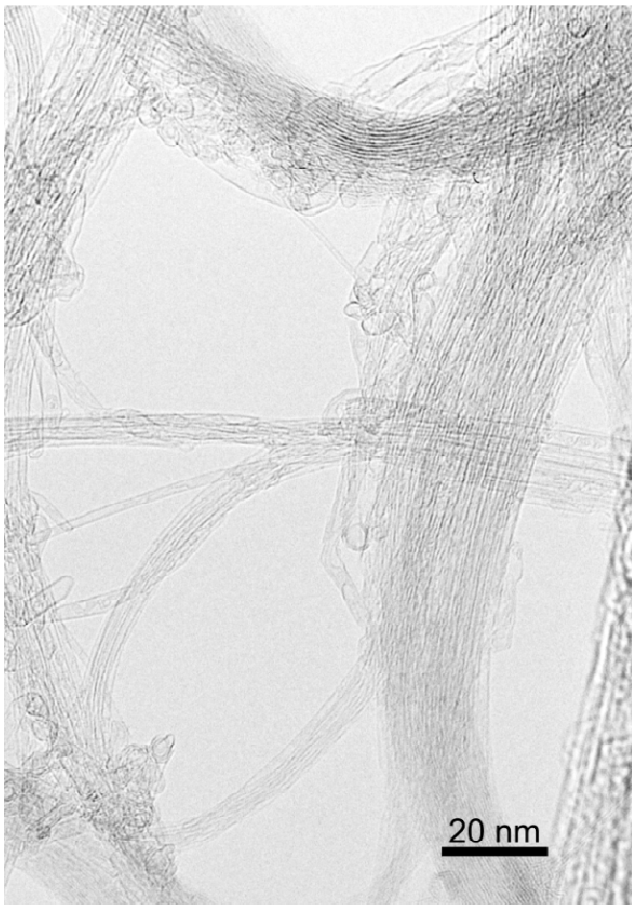

Figure 2.1: TEM image of SWCNTs synthesized from ethanol feedstock. Image captured at an acceleration voltage of 120 kV.

Raman spectra of the SWCNTs were acquired using a micro-Raman apparatus with a 50 cm single monochromator and a CCD detector (Chromex 501is with Andor DV401-F1). An argon ion laser with a wavelength of 488 nm (2.54 eV) and a Helium–Neon laser with a wavelength of 633 nm (1.96 eV) were used to obtain the spectra. Raman scattering is an inelastic scattering of light which is used to investigate the vibrational and rotational

frequencies of atoms. In Raman scattering, an electron is excited from the valence band to the conduction band by absorbing a photon. Then the excited electron is scattered by emitting (or absorbing) phonons, and gradually reaches the valence band by emitting a photon. During this process, the interaction between phonon and electron results in the energy of the laser photons being shifted. This shift in photon energy corresponds to the vibrational frequencies of the material. A typical spectrum obtained from the SWCNT sample is shown in Figure 2.2. Two dominant features noticed in RRS are the radial breathing mode (RBM) at low frequencies and the tangential multi-feature (G-band) at higher frequencies.

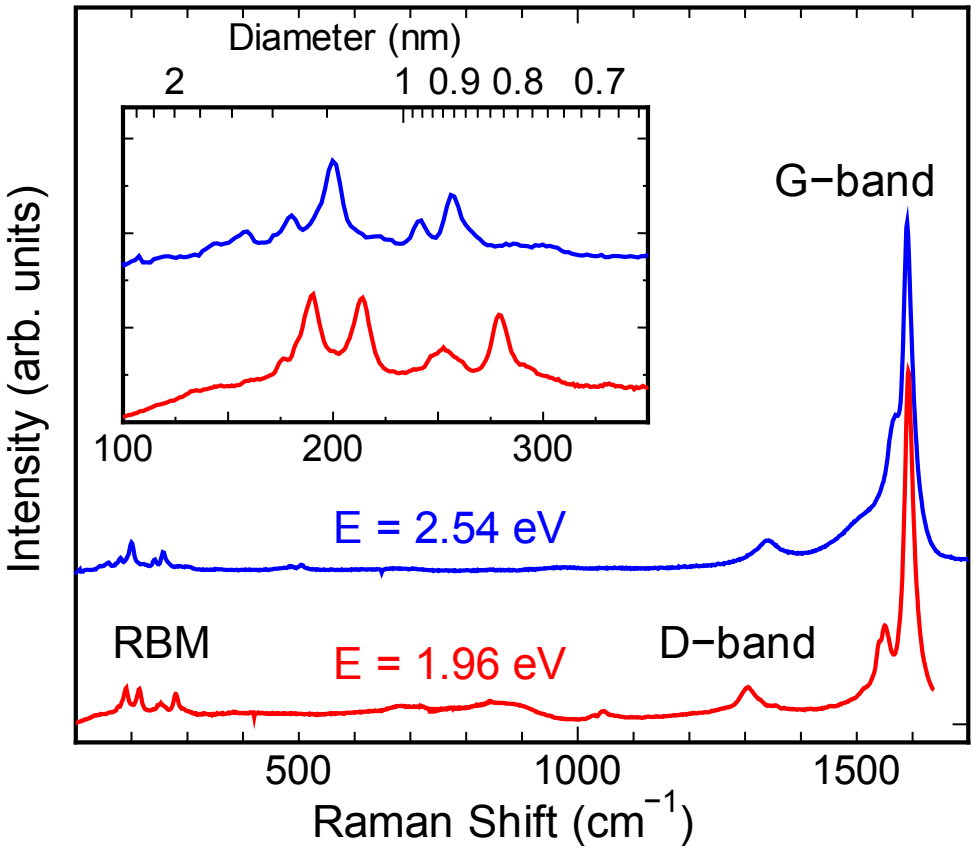

Figure 2.2: Resonance Raman spectra of ACCVD SWCNTs. The G-band, D-band and the radial breathing mode (RBM) peaks are shown. An expanded view of the RBM signals with an added diameter scale is shown in the inset.

RBM peaks seen in the low-frequency region (100–400 cm^{-1}) are unique to SWCNTs and are not observed in other carbon allotropes [82]. An interesting feature of the RBM is that the RBM frequency (ω_{RBM}) is proportional to the inverse of the nanotube diameter, following the equation $\omega_{RBM} = A/d_t + B$, where d_t (nm) is the diameter of the nanotube, and A (cm^{-1} nm) and B (cm^{-1}) are empirical constants. For the present case, values of 217.8 and 15.7 are used for A and B respectively [83]. The expanded RBM signal along with the diameter scale is shown in the inset of Figure 2.2. From the inset it can be seen that the sample contains SWCNTs with diameters ranging from 0.8-1.6 nm [81].

The G-band observed at 1592 cm^{-1} is a characteristic feature of sp^2-bonded graphitic carbon and corresponds to in-plane vibrations of the carbon atoms. In addition to the G-band and RBM, a third feature found near 1350 cm^{-1} (the D-band) arises from defects in the tube walls or from amorphous carbon impurities. The relative intensity of the G-band with respect to the D-band (I_G/I_D) is representative of the crystallinity of the SWCNTs. In the as grown sample, a large I_G/I_D indicates good crystallinity of the SWCNTs.

Thermo Gravimetric Analysis (TGA) is a commonly used technique to determine a material's thermal stability and the fraction of volatile components by continuously monitoring the weight change of the material when it is heated. The SWCNTs are placed in a platinum cup that is supported on a mass balance located outside the furnace chamber. The balance is zeroed, and the SWCNTs are gradually heated at a heating rate of 0.5 °C. The TGA curve plots the TGA signal, converted to percent weight change on the Y-axis against the reference material temperature on the X-axis. Thermo gravimetric analysis of the

SWCNTs shown in Figure 2.3 reveals that the SWCNTs uniformly burnt at a temperature of 600 °C. Since amorphous carbon decomposes at around 300 °C - 500 °C, which is lower than the decomposition temperature of SWCNTs, the TGA result proved absence of amorphous carbon impurities. The TEM investigation, the Raman spectra, and the TGA analysis showed the absence of structural defects or impurities such as metals or amorphous carbons in the ACCVD grown SWCNTs.

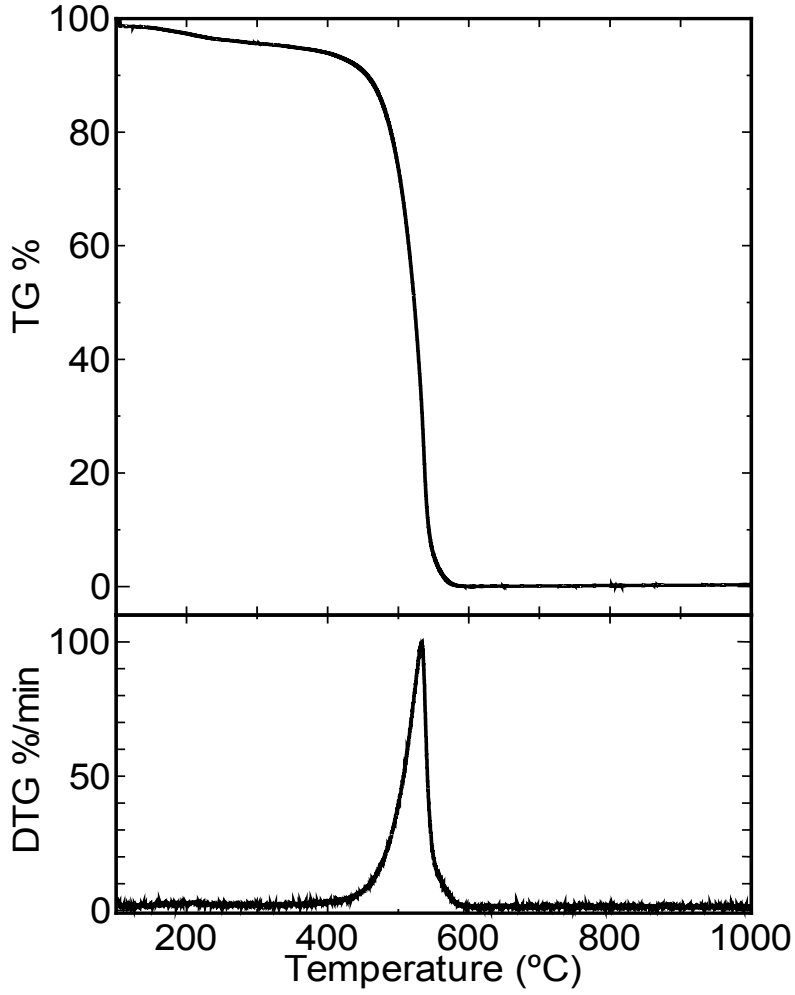

Figure 2.3: Thermogravimetric analysis of SWCNTs. Measurement was performed at a heating rate of 0.5 °C/min.

2.3 Nanofluid Preparation and Characterization

2.3.1 Preparation of SWCNT-Based Nanofluids

An important prerequisite for a nanofluid is the preparation of a stable and homogenous suspension. Single-step and two-step synthesis techniques have been commonly adopted to prepare nanofluid dispersions. The single-step technique was often used to prepare nanofluids seeded with metallic/metal oxide spherical nanoparticles. However, for the case of CNTs, single-step synthesis techniques have not yet been achieved. CNT nanofluids are usually prepared by two-step methods. In the first step, CNTs (SWCNTs/MWCNTs) are synthesized by arc discharge, laser ablation, and chemical vapour deposition. In the second step, stable and homogenous suspensions are prepared by dispersing the 'as grown' CNTs in the required base fluid.

The van der Waals force of attraction between carbon nanotubes makes 'as grown' CNTs extremely difficult to disperse in polar/non-polar fluids. Furthermore, the forces between CNTs are heavily influenced by both chirality and curvature of the surface. According to theory, the sidewall in a CNT consists of strained double-bonds, resulting in sp^2/sp^3 orbital hybridization. The strained double bonds would have partial single bond character resulting in a partially unsaturated bond. This phenomenon would explain the high force of attraction between the outer walls of CNTs. Thus the force of attraction can be more pronounced in SWCNTs than for MWCNTs. Henceforth, to create stable CNT dispersions two popular techniques prevail in the open literature. The first technique is to attach a hydrophilic

functional group onto the sidewalls by chemical functionalization. The other method is to encapsulate the CNTs using anionic/cationic surfactants.

Xie et al. [60] first employed a nitric acid/sulfuric acid mixture in the ratio of 1:3 to chemically functionalize CNTs. A known quantity of pristine CNTs were treated with the acid mixture, boiled, and refluxed for a short time period. After the reaction, the samples were collected and diluted using distilled water until a pH of 7 was obtained. The CNTs were further dried to eliminate the water content. Following the work of Xie et al. [60] , more recently Chen et al. [84] have employed mechanochemical reactions to chemically functionalize CNTs. However instead of an acid mixture they made use of an alkaline medium for the nanofluid preparation. They mixed CNTs with potassium hydroxide and ball-milled the mixture.

Chemical functionalization of CNTs heavily damages the structure of the CNTs and reduces the thermal properties of the CNTs. Therefore acid treatment may not be a suitable method to prepare CNT dispersions. Thinner nanotubes are susceptible to more structural damage than large-diameter nanotubes due to the greater strain induced on the bonds in thinner tubes. The mechanochemical reaction method has been found to limit the aspect ratio distribution. On the other hand, when the ball milling time is long, it was reported that the tubes were heavily damaged, which lead to the formation of a large amount of amorphous carbon [85]. The presence of amorphous carbon may modify the thermal properties of the dispersion. Hence, chemical functionalization and mechanochemical reactions may not be a proper method to make efficient, high-quality CNT dispersions.

Apart from chemical functionalization, the other commonly adopted method by many researchers is to encapsulate the CNTs using anionic/cationic surfactants. Jiang et al. [86] prepared stable CNT suspensions using an anionic surfactant, namely sodium dodecyl sulfate (SDS). They reported that SDS, which consists of a single, straight hydrophobic segment and a terminal hydrophilic segment, tends to modify the interface of the CNTs with the surrounding base fluid thereby creating stable suspensions. Assael et al. [61], Zhang et al.[87], Garg et al. [88] and Nasiri et al. [71] also used SDS to prepare nanofluid dispersions. Ding et al. [70] used Gum Arabic (GA) to disperse CNTs in water. Wen and Ding [69] used Sodium dodecylbenzene sulphonate (SDBS) to prepare nanofluid dispersions, and reported that the quality of the dispersions was very good compared to SDS and GA. However, they also demonstrated that the surfactant failed when heated to higher temperature, and the suspensions became no longer stable. Cherkasova et al. [68] also used SDBS to prepare CNT nanofluids, but did not report any measurements at different temperatures. Assael et al. [62] dispersed double walled nanotubes (DWCNTs) and MWCNTs using Nanosphere AQ and hexadecyltrimethylammonium bromide (CTAB), a cationic surfactant. They studied different parameters like surfactant type, surfactant loading, and sonication time. Based on their studies they concluded CTAB is a suitable surfactant to disperse DWCNTs and MWCNTs. They suggested that the cationic surfactant interacts well with the outer walls of the DWCNTs and MWCNTs, thereby creating a stable dispersion [62].

The highly hydrophobic nature of SWCNTs makes it very difficult to disperse them. An important prerequisite for a nanofluid is the preparation of a stable and homogenous dispersion. In this research work, a surfactant was used to prepare the nanofluid dispersion.

Sodium deoxycholate (DOC), a bile salt, commonly used for Density Gradient Ultracentrifugation experiments was used as the surfactant in the present study [89-91]. The chemical structure of DOC is shown in Figure 2.4. DOC possesses a rigid structure consisting of a cholesterol group with dissimilar sides [92]. It consists of a steroid skeleton with a carboxylic acid side chain at one end and two hydroxyl groups on its steroid backbone. The two polar hydroxyl groups on the α-face and the methyl group on the β-face facilitate strong adsorption of DOC onto the surface of SWCNTs [90].

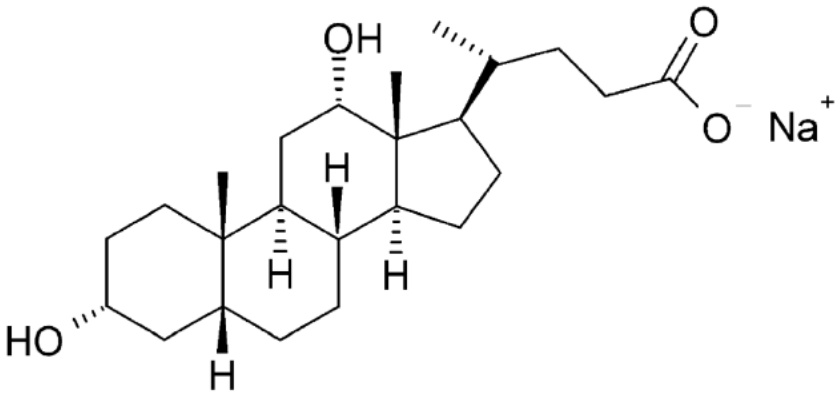

Figure 2.4: Chemical structure of sodium deoxycholate ($C_{24}H_{39}NaO_4$)

Stable nanofluid dispersions were prepared by adding necessary loading of SWCNTs using DOC as the surfactant. For this purpose the SWCNT density was considered to be 1.6 g/cm^3 (assuming a SWCNT diameter of 1 nm and Van der Waals spacing of 0.342 nm). DOC loading of 0.75 wt % was employed. The dispersions were subjected to bath sonication for 6 hours followed by tip sonication using an ultrasonic processor (Hielscher GmbH, UP-400S with H3/Micro Tip 3) for 2 hours at a power flux level of 320 W (80 % amplification). Same sonication conditions are adopted for samples of different concentrations tested. Furthermore,

it was also assumed that 5 % of the mass is lost during the tip sonication and the losses are taken into account during the sample preparation. The pH of the SWCNT/water nanofluids was measured to be 7.

2.3.2 Nanofluid Characterization

DOC-encapsulated SWCNTs were further characterized using TEM (Hitachi H-9500) to see how the nanotubes are dispersed by the surfactant. TEM samples were prepared by performing dialysis for 24 hours to remove excess surfactant. Figure 2.5 shows the TEM image of DOC dispersed SWCNT.

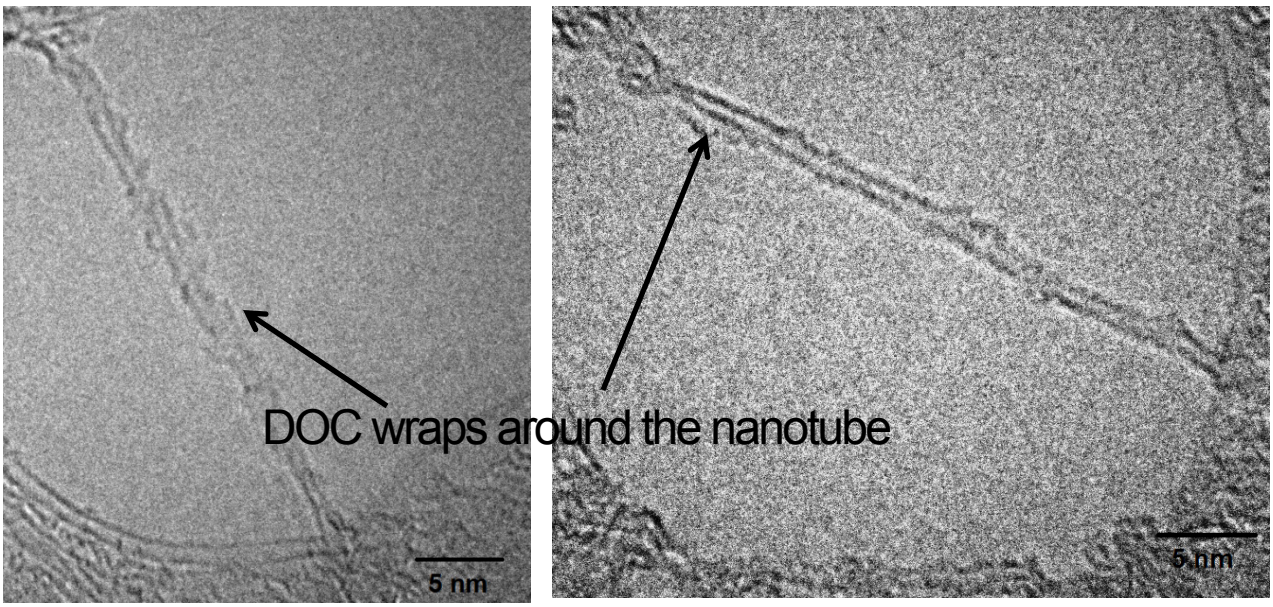

Figure 2.5: TEM visualization of surfactant-encapsulated SWCNTs. Image captured at an acceleration voltage of 200 kV.

Anionic surfactants like SDS form ellipsoidal or spherical micelles on the CNT surface. Unlike SDS, DOC having one hydrophilic side and one hydrophobic side wraps around the

SWCNT instead of forming spherical or ellipsoidal micelles [90]. The hydrophobic α-face contacts intimately with the side walls of the nanotube, while the hydrophilic β-face interfaces with water. The strong interaction between the hydrophobic side of DOC and the SWCNT sidewalls causes the surfactant to wrap around the SWCNT with a preferred orientation [89, 90]. TEM image shown in Figure 2.5 support the mechanism of DOC wrapping reported in the literature [89-91] based on Density Gradient Ultracentrifugation experiments.

2.3.3 Dynamic Light Scattering

Dynamic Light Scattering (DLS) is a popular technique to measure the size distribution of the nano inclusions in a solution. When a laser beam is illuminated through a liquid medium with suspended nano inclusions, the beam scatters off those inclusions in all directions (Rayleigh scattering), resulting in a scattering-angle-dependent intensity pattern. Especially when the nano inclusions are experiencing Brownian motion, the intensity pattern fluctuates randomly. Constructive and destructive interference occurs as the illuminated light is scattered by the presence of nano materials. As a result, the photon detector measures an average intensity pattern which fluctuates as a function of time. The time required for these fluctuations to decay back to the average intensity depends on the Brownian motion of the particles and the size of the particles. Smaller sized particles experience more rapid Brownian movement which results in faster decaying fluctuations than larger sized particles. Analysis of the intensity fluctuations allows for the determination of diffusion coefficient of the

particles in the liquid from which the particle size distribution can be calculated using the Stokes-Einstein equation.

In a DLS experiment, to quantify the intensity decay time, an auto-correlation function is used to measure the intensity at a time *t,* and with the intensity at a later time $t + \tau$, yielding the correlation as a function of τ. For the case of mono-disperse, non-interacting spherical particles, the correlation is given by,

$$G(\tau) = A\exp(-2\Gamma\tau) + B \tag{2.1}$$

Where A and B are instrument constants, $\Gamma = Dq^2$ is the intensity decay rate where D is the diffusion coefficient which can be determined from Stokes – Einstein equation and q is the scattering vector. The diffusion coefficient is written as follows [92]:

$$D = \frac{k_b T}{3\pi\eta d} \tag{2.2}$$

Where k_b is the Boltzmann constant, T is the temperature of the fluid, η is the fluid viscosity and d is the diameter of the particle. The scattering vector q is given by

$$q = \frac{4\pi n}{\lambda} Sin\left(\frac{\theta}{2}\right) \tag{2.3}$$

Where n is the refractive index of the fluid, λ is the wavelength of the light and θ is the angle at which the scattered light is measured. The size distribution of nano inclusions in this work is determined by using a Zetasizer-Nano (Malvern Instruments). It uses a He-Ne laser (4 mW, λ= 633 nm) and avalanche photodiode detector. Figure 2.6 and 2.7 shows the size distribution of SWCNTs in water and ethylene glycol respectively.

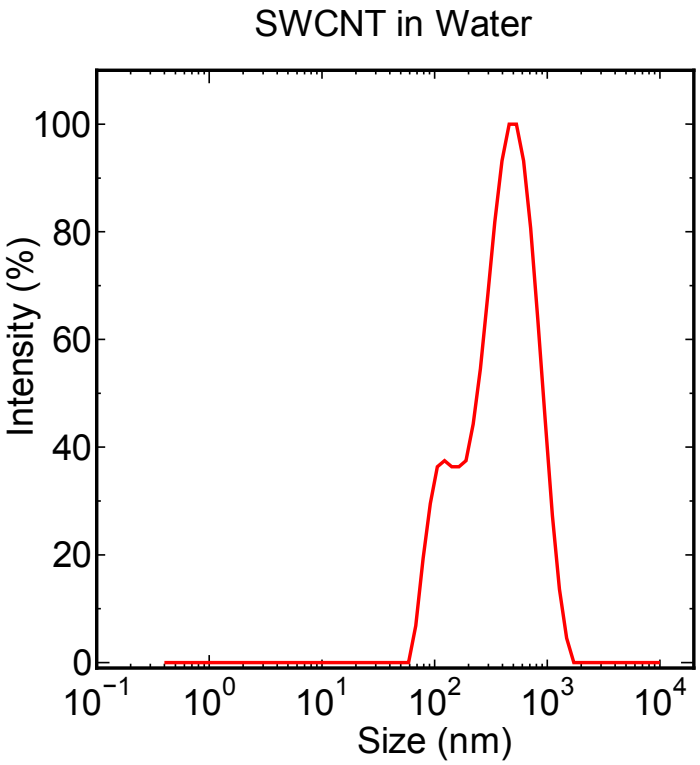

Figure 2.6: Size distribution of SWCNTs in water

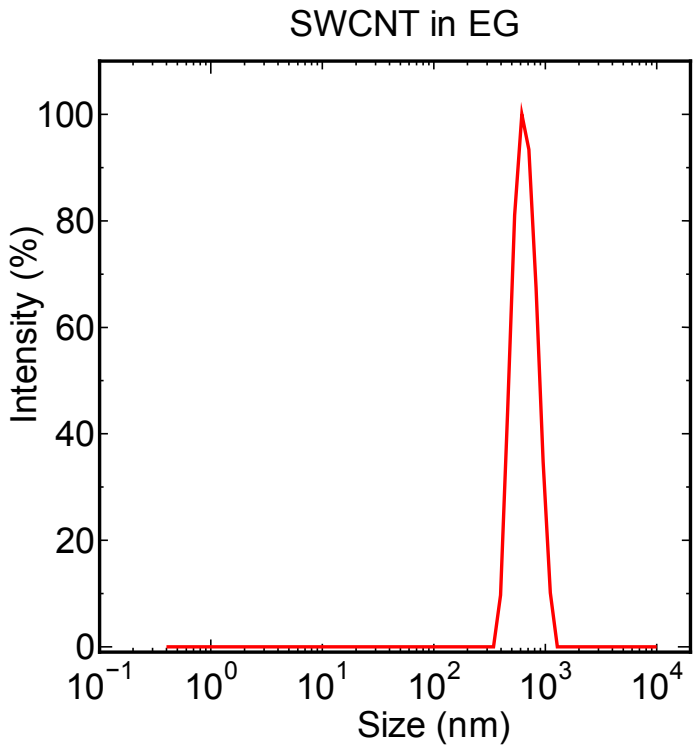

Figure 2.7: Size distribution of SWCNTs in Ethylene Glycol

Figure 2.6 shows the cluster size distribution of SWCNTs in water. Incidentally it shows a double peak and a broad peak width. It indicates a wider size distribution of the SWCNTs. Figure 2.7 shows a different behaviour were only single peaks is present and the peak width is narrow. It can be concluded based on the spectra the dispersion of SWCNTs are well dispersed in aqueous medium compared to the case of ethylene glycol.

2.3.4 Optical Absorption and Photoluminescence Characterization

DOC-dispersed SWCNTs were further characterized using optical absorption spectroscopy (OAS) and photoluminescence spectroscopy (PLE). The nanofluid dispersions were diluted to perform the measurements. In optical absorption spectroscopy, the wavelength of the incident light is scanned through spectral range from the ultraviolet regions to visible and near infrared (UV-vis-NIR) spectral regions. Figure 2.8 shows a typical absorption spectrum obtained from SWCNTs dispersed in water and ethylene glycol using DOC. The absorbance spectrum of water/SWCNT nanofluids shown in Figure 2.8 consists of sharp peaks, which are characteristic of isolated nanotubes. The absorption peaks correspond to the first and second optical transitions (E_{11} and E_{22}) in semiconducting nanotubes and the first optical level of metallic nanotubes [93]. In the case of EG/SWCNT suspensions show a broad absorption peak in the near infra-red region and visible region. Moreover, the peaks are shifted in the near-infra red region which indicates that the SWCNTs are aggregated in EG based nanofluids. This observation is in consistent with DLS results were a larger cluster size distribution is noticed.

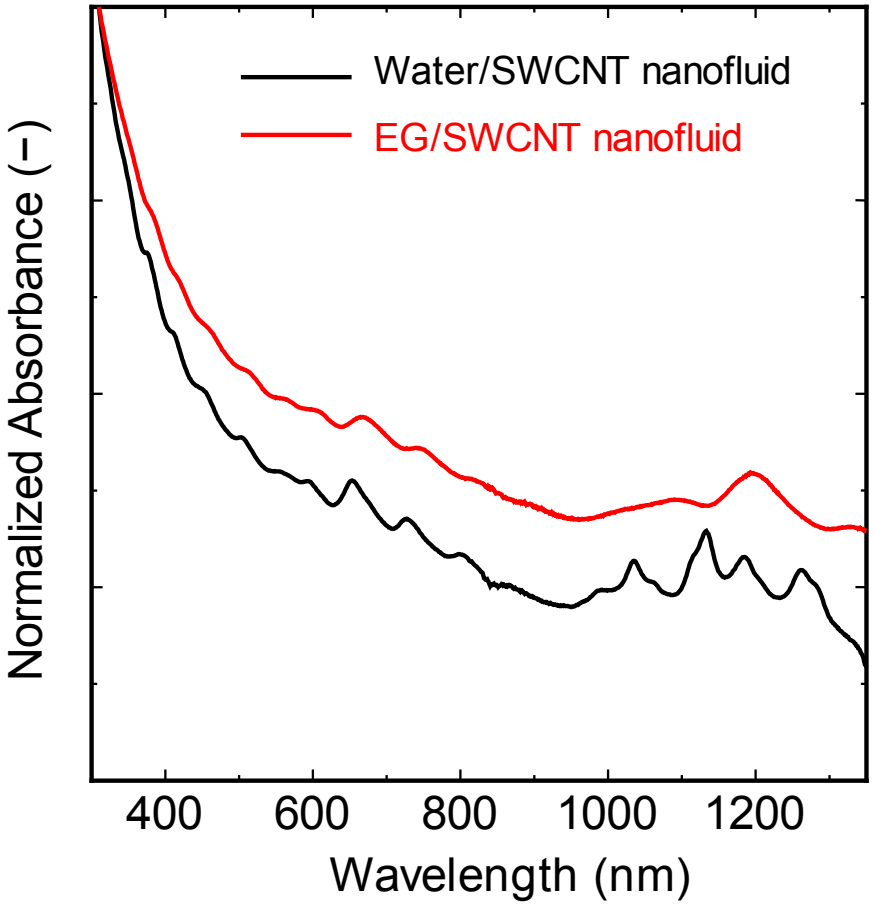

Figure 2.8: UV-Vis-NIR absorbance spectrum of SWCNTs dispersed in water and EG using DOC as the surfactant.

When a semiconductor is electronically excited to a higher energy state by chemical, optical, or electrical energy, it gradually reaches the ground state by photon emission. This process is called as luminescence. If the semiconductor is excited by absorbing photons or other electromagnetic radiation, this form of luminescence is called fluorescence or photoluminescence (PL). PLE mapping is a very powerful approach for the determination of the chirality distribution in a bulk SWNT sample and also to evaluate the quality the

dispersion of SWCNTs. Figure 2.9 shows a PLE map of the dispersed SWCNTs with and without centrifugation. Figure 2.9(a) shows a PLE map of the suspension taken at a concentration of 0.005 vol %. The clear signals from various semiconducting SWCNTs demonstrate that a dispersion of well-isolated SWCNTs can be obtained even without centrifugation [94]. A PLE map of the same sample after ultracentrifugation is shown in Figure 2.9(b). The signal is much more intense due to the removal of bundles, but no changes in spectral positions are evident after ultracentrifugation. This indicates that DOC is an effective surfactant for dispersing relatively high concentrations of SWCNTs, which can then be characterized using common spectroscopic techniques.

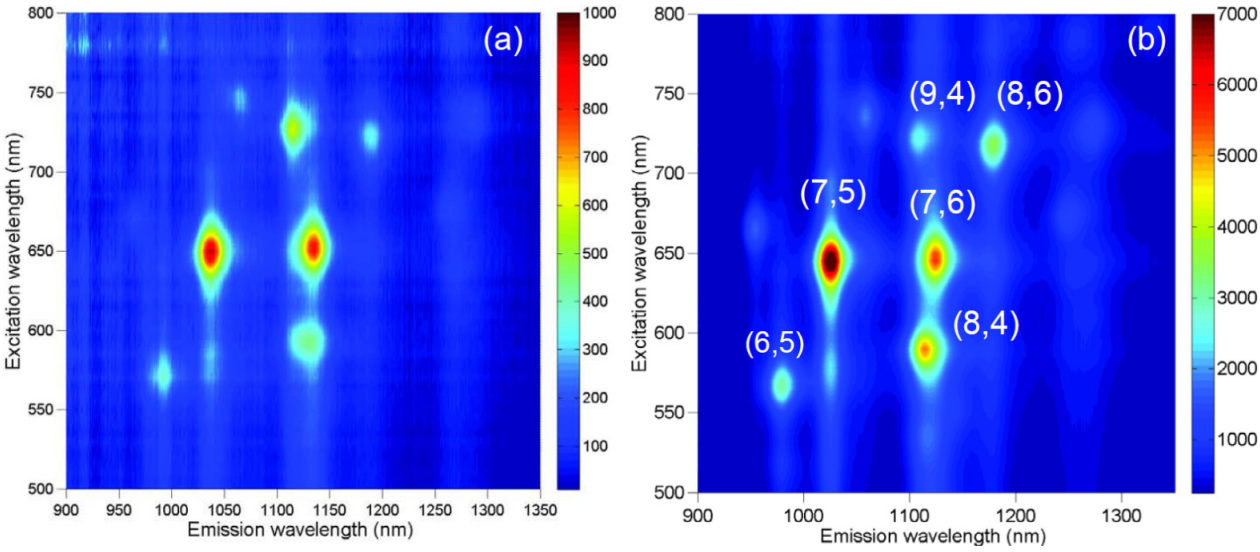

Figure 2.9: Photoluminescence excitation map of SWCNT/water nanofluid. Figure 2.9 (a) corresponds to the PLE map taken at 0.005 vol %. Figure 2.9(b) corresponds to the PLE map taken post centrifugation. Improved signal intensity due to the elimination of bundles is clearly evident in Figure 2.9(b).

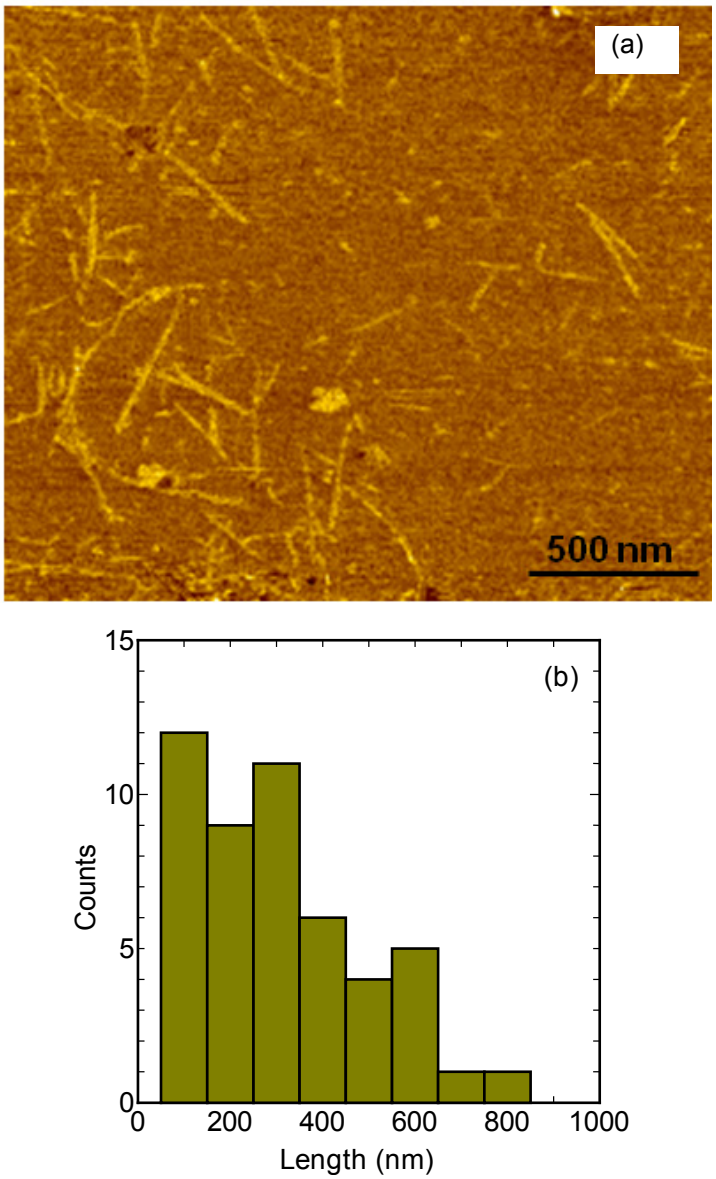

Figure 2.10: (a) AFM image of surfactant-encapsulated SWCNTs post sonication (SWCNT loading – 0.005 vol %). (b): Size wise length distribution of the SWCNTs.

Atomic force microscopy (AFM) measurements (SII, SPI3800N) were performed in order to determine the mean length of the SWCNTs after sonication. The samples were prepared by dropping 10 µL of the SWCNT dispersion on a silicon substrate and the substrate was heated

at 333K for 30 minutes to evaporate the water. Figure 2.10(a) shows a typical AFM image of the DOC-wrapped SWCNTs. Figure 2.10(b) shows the SWCNTs length distribution predominantly ranging from 100 nm to 600 nm post sonication.

2.4 Measurement Methods

2.4.1 Thermal Conductivity Measurement

The prevailing techniques for measuring the thermal conductivity of nanofluids are the transient hot wire method [15,20,22-25], steady-state parallel plate method [42], temperature oscillation method [21] and the 3-ω method [64]. Some research groups make use of non-intrusive optical measurement techniques such as forced Rayleigh scattering [95] and infra-red microscopy [96] for thermal measurements. Non-intrusive techniques eliminate the uncertainty issues associated with steady state and transient hot wire methods due to the diffusion and aggregation of the nanomaterials and the occurrence of natural convection during long measurement times. However, optical measurements are very expensive and least popular among the nanofluid research community. Besides, a recent round robin study carried out by 33 research groups concluded that the effect of measurement technique does not have a significant impact in the anomalous thermal conductivity results prevailing in the literature [32]. Hence in this research the most favored measurement method namely the transient hot wire method (THW) is adopted for experiments. In this chapter, the mathematical principles of measurement method will be explained in detail followed by the apparatus design and calibration results.

2.4.2 Description of the Transient Hot-Wire Method

In the THW technique a hot wire is placed inside the fluid test cell, which acts as both the heater and an electrical resistance thermometer. This technique is based on the measurement of the temporal response of the temperature of a hot wire when it is subjected to an electrical step input. A platinum (Pt) hot wire (diameter 25.4 μm) with an electrically insulating isonel coating (coating thickness 2.0 μm) was employed in this research. The hot wire acts as both the heater and an electrical resistance thermometer. During the experiments, the hot wire is immersed in the test fluid and a step input is passed through it. The temperature rise of the hot wire is determined from the change in resistance of the hot wire, which is measured as a function of time using a Wheatstone-bridge circuit.

The relation between thermal conductivity k and measured temperature T can be summarized as follows [97]. Assuming a thin, infinite line heat source with constant heat output in an infinite medium, the energy equation can be written as

$$\frac{1}{\alpha}\frac{\partial T}{\partial t} = \frac{1}{r}\frac{\partial}{\partial r}\left(r\frac{\partial T}{\partial r}\right) \tag{2.4}$$

With initial condition

$$T(t=0) = T_0 \qquad \left.\frac{\partial T}{\partial r}\right|_{r=\infty} = 0 \tag{2.5}$$

and boundary conditions

$$\lim_{r\to 0}\left(r\frac{\partial T}{\partial r}\right) = \frac{q}{2\pi k} \tag{2.6}$$

The analytical solution is of the form

$$T(r,t) = T_0 + \frac{q}{4\pi k}\left\{-\gamma + \ln(\frac{4\alpha t}{r^2}) + ...\right\} \quad (2.7)$$

Here, α is the thermal diffusivity and γ=0.5772 is Euler's constant. If the temperature of the hot wire at times t_1 and t_2 are T_1 and T_2 respectively, then by eliminating the higher order terms in Eq. (2.4), the thermal conductivity of the fluid can be approximated by:

$$k = \frac{q}{4\pi}\frac{\ln(t_1/t_2)}{T_1 - T_2} \quad (2.8)$$

Nagasaka and Nagashima [98] further improved the analytical solution for an electrically insulated wire to measure the thermal conductivity of surrounding fluid. The solution takes the form as follows:

$$\Delta T = \frac{q}{4\pi k}\left(\ln t + A + \frac{1}{t}\left(B\ln t + C\right)\right) \quad (2.9)$$

In equation (6) A, B and C are constants determined by the geometry of the wire, thermal diffusivity of the fluid, insulation coating, material of the hot wire and the thermal conductivity of the insulation layer. When the $1/t$ term in the equation (2.6) is small, the constant term A shifts the ΔT term without changing the slope of the equation (2.6). Thus, the thermal conductivity of the fluid can be calculated using the simplified expression as shown in equation (2.7). It need to be noted that the equation (2.7) is identical to that (2.5) in the absence of electrical insulation coating.

$$k = \frac{q}{4\pi}\left(\frac{d\ln t}{dT}\right) \quad (2.10)$$

During measurement, the hot wire is heated by a constant DC power supply. The temperature rise of the hot wire is determined from the change in resistance of the hot wire, which can be measured in time using a Wheatstone-bridge circuit. For a known electric power supply and slope of the curve ln(t) versus T, the thermal conductivity k is calculated using equation (2.10).

Low cost and easy implementation are considered to be the advantages of this method. However, assumptions like infinite length of the wire and the ambient acting like a reservoir may introduce some errors. A modified version of this method, namely the short transient hot wire (SHW), has been developed by Zhang et al. [87]. This measurement procedure is similar to that of THW. However, a significant difference is that this method is based on the numerical solution of a two dimensional transient heat conduction equation with the boundary conditions as those used in the actual measurement. This method can be used for test cells of smaller volume and alleviates the uncertainties caused by the boundary effects.

Error associated with the finite length of the wire is calculated using the expression prescribed by Healy et al [99]. The expression is written in the form as follows:

$$\frac{dT}{d\ln t} = \frac{q}{4\pi k}(1-\delta) \tag{2.11}$$

Where δ is the error associated with the finite length of the wire. The error δ is calculated using the expression as follows:

$$\delta = -\frac{e^{-L^2/16\alpha t}}{\pi}\left\{\frac{\sqrt{16\alpha t}}{L} + \frac{L}{r}\left[\frac{k_w}{k} - \frac{(\rho C_p)_w}{\rho C_p}\right]\frac{\ln(4\alpha t/r^2 k)}{(4\alpha t/r^2 k)^{3/2}}\right\} \tag{2.12}$$

In equation (2.9), the subscript *w* denotes the properties of the hot wire. For the present system of the hot wire diameter (*2r*) 25.4 μm and length (*L*) 40 mm, the error is calculated to be of the magnitude 10^{-5}.

Similarly for sufficiently long wire the effect of axial conduction can be ignored. The applied power ($q = v^2/RL$) where the length of the wire and applied voltage is constant but the resistance *R* of the wire depends on the temperature which in turn is a function of time. However, for a limited increase in temperature this can be assumed constant. Other errors associated with the assumptions on finite thermal conductivity and heat capacity of the wire can be safely ignored due to the high thermal conductivity of the hot wire used.

2.4.3 Experimental Setup

The schematic of the transient hot wire system is shown in Figure 2.11. The experimental setup consists of a platinum (Pt) hot wire (diameter 25.4 μm) of length 40 mm with an electrically insulating isonel coating (coating thickness 2.0 μm). The hot wire is soldered to electrically insulated lead wires to keep the wire straight and also to connect it to the electrical system. The test cell is made of copper of length 65 mm and inner diameter 15 mm. The test cell is immersed in a thermostatic bath to precisely control the temperature of the fluids in which the experiments were performed.

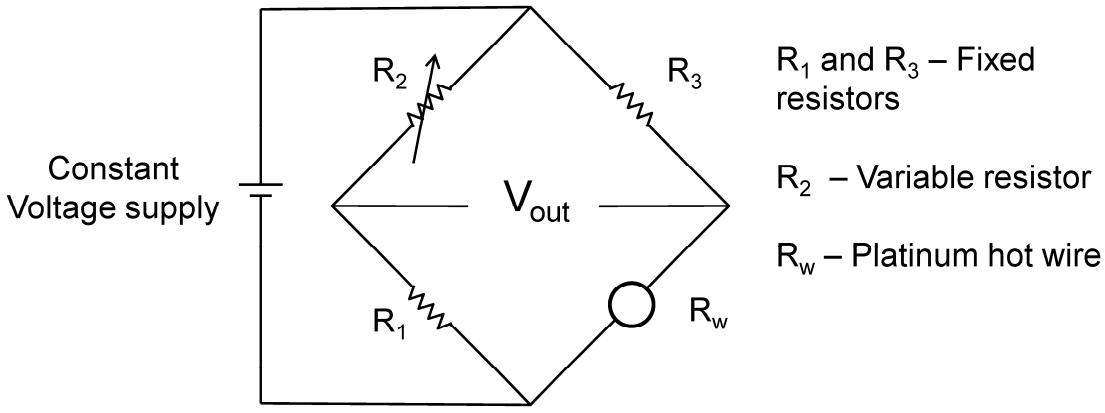

Figure 2.11: Schematic representation of the Transient Hot Wire (THW) setup

The soldered hot wire is connected to the Wheatstone bridge which has two high precision fixed resistors and one variable resistor. Two arms of the bridge were considered as the fixed resistors and the rest two arms were assigned for the variable resistor and transient hot wire. A constant voltage supply is supplied to the system for a period of 5 seconds. This electrical impulse will disrupt the bridge balance and cause a change in resistance of the hot wire due to the change in temperature. The change in resistance of the wire during this period is acquired using a GL 220 Graphtec data logger at a sampling interval of 20 ms. Figure 2.12 shows the raw data profile of the wire resistance change when a constant voltage supply is provided to disrupt the bridge balance.

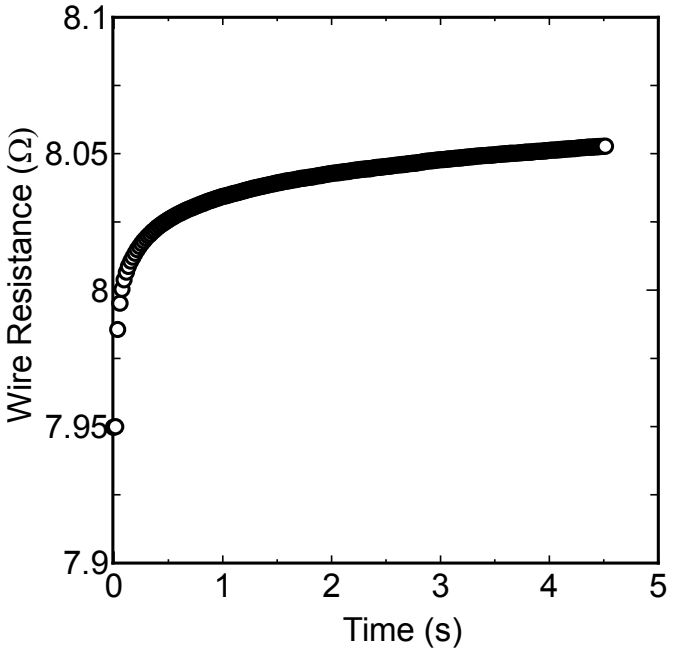

Figure 2.12: Resistance change of the THW when a constant voltage supply is provided.

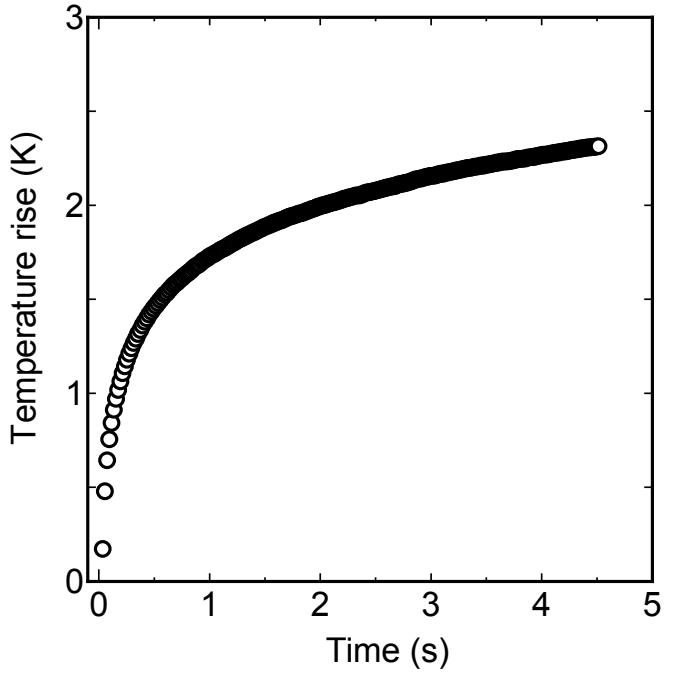

Figure 2.13: Temperature raise as a function of time

Since the temperature coefficient of the platinum wire is known, the temperature profile of the hot wire is acquired from the resistance change which can be seen in Figure 2.13. From the known heat supply per unit length of wire and the temperature change of the wire, the thermal conductivity of the fluid can be calculated using equation (2.10) as mentioned previously.

2.4.4 Calibration of the THW Setup and Uncertainty Analysis

To validate the THW setup, the thermal conductivity of pure deionized water and ethylene glycol were measured at different temperatures. When using equation (2.10) to calculate the thermal conductivity, it is necessary to know the starting time and the ending time to compute the slope. Healy et al. [99] also suggested the initial time to be between 10 ms < t < 100 ms. However, the ending time depends on the system design and varies between every setup. For the present setup, we found that beyond 2s natural convection effect sets in. For the thermal conductivity calculations, the data recorded between 0.2 and 2 s after the step input was used for fitting. Choosing the data in this range eliminates effects associated with the thermal capacitance of the hot wire and the influence of natural convection. Figure 2.13 shows a sample raw data profile obtained from the experiment. Figure 2.14 shows the ln t versus the temperature rise plot. The linear region in Figure 2.14 is fitted using a least squares fit to compute the slope.

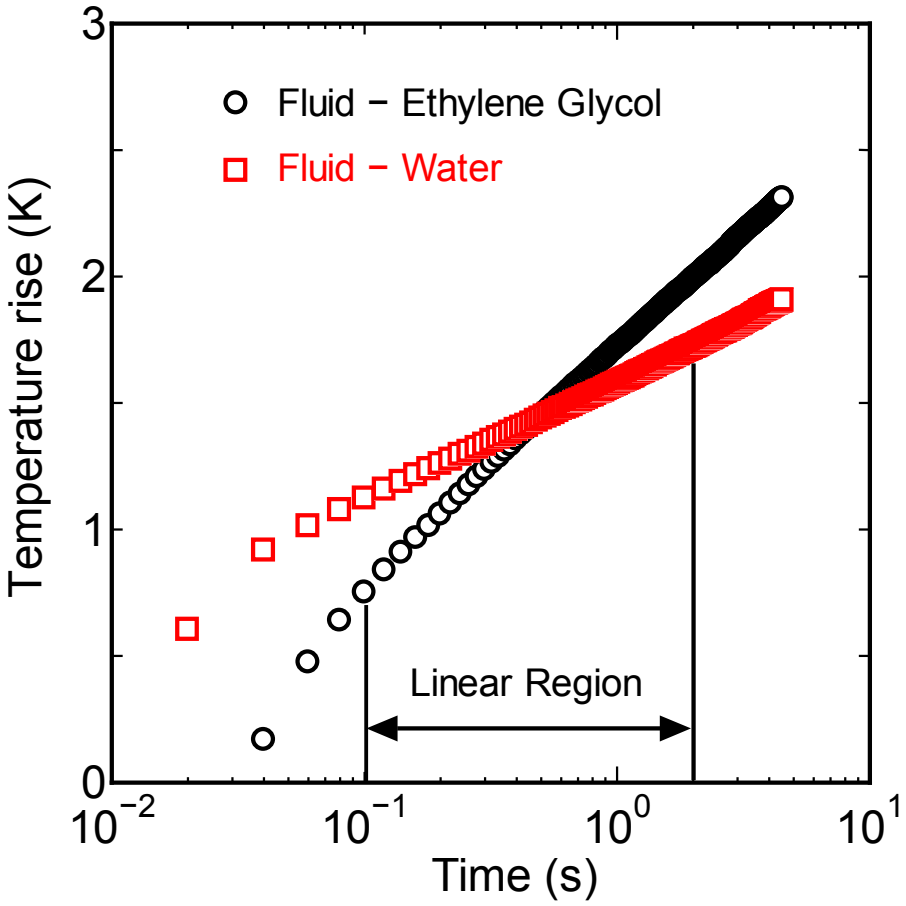

Figure 2.14: Logarithm of time Vs Temperature Rise

A comparison of the measured and reference thermal conductivity data is shown in Figure 2.15. The upper line corresponds to the thermal conductivity of water according to the ASTM-D2717 standard [100]**.** The lower line corresponds to the thermal conductivity of EG reported by Di Guilio & Teja [101]. A detailed uncertainty analysis of the THW setup was carried out and the experimental uncertainty was found to be ± 3 %.

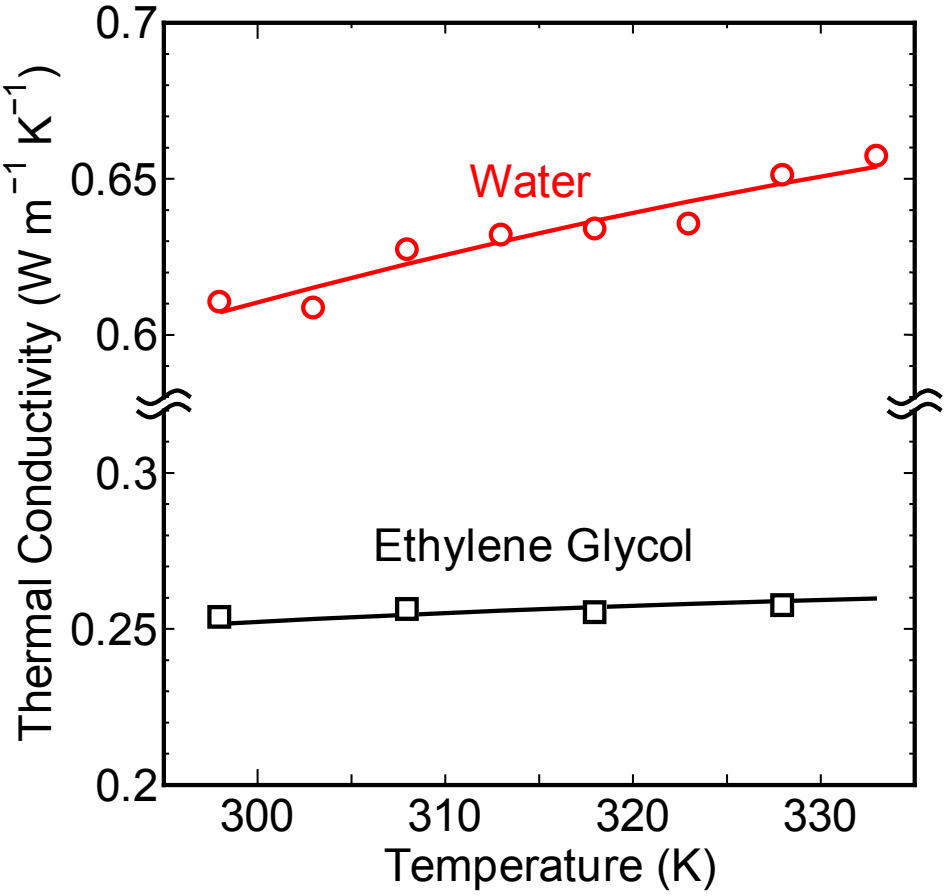

Figure 2.15: Comparison of thermal conductivity values measured in this work with the reference literature. Open and filled circles correspond to the measured thermal conductivity of water (top) and EG (bottom), respectively. Solid lines correspond to the literature data.

2.4.5 Electrical Conductivity Measurement

The electrical conductivity of the SWCNT nanofluids was measured by pouring the dispersions into a specially prepared rectangular test cell made of plexi-glass. The test cell consists of two parallel copper electrodes with an area A of 3 cm^2 separated by a distance L of 6.5 cm. The electrical conductance ρ is calculated using the following equation, where R is

the measured electrical resistance. The reciprocal of electrical conductance gives the electrical conductivity of the nanofluids.

$$\rho = \frac{RA}{L} \tag{2.13}$$

2.4.6 Viscosity Measurements

Various methods exist for the determination of viscosity of fluids. In this work two methods are adopted to measure the viscosity of nanofluids. For water based nanofluids capillary viscometer is used. For ethylene glycol based nanofluids experiments are carried out with capillary viscometer as well as cone-plate viscometer. A capillary viscometer has several designs, but most common is the U-shaped or Ostwald viscometer. In this work, a Cannon-Fenske routine Ostwald viscometer is used. Cannon-Fenske capillary viscometer is a U-shaped piece of glass tubing having two glass bulbs on one arm, separated by a calibrated length of capillary tubing. Another bulb is low on the other arm, to which the fluid to be measured is loaded. The fluid and the capillary viscometer are then suspended in a vertical stand and a constant temperature water bath and allowed to come to thermal equilibrium. Once thermal equilibrium is reached, the fluid is drawn up into the upper bulb and is allowed to flow from the upper bulb to the lower through the capillary tube. The efflux time, or time it takes to traverse the length of the capillary, is measured using a stop watch. Each capillary viscometer has a coefficient of calibration provided by the supplier. Multiplying the efflux time and the coefficient of calibration gives the calculation of the kinematic viscosity of the fluid. The measurement method follows the standards ASTM D 446 and ISO 3105 [102].

To check the rheological behaviour of ethylene glycol based fluids, a cone-plate viscometer is also used in this work. A cone and plate viscometer consists of a stationary flat plate and an inverted cone whose apex just in contact with the plate. The fluid is placed in the narrow gap between the flat plate and the cone. The measurements are performed with a cone and plate geometry (Toki Sangyo TPE 100) with a cone diameter of 50 mm and a cone angle of 1°. The cone is rotated at a specified speed (i.e. angular velocity) and the torque required to turn the cone is measured. The measured torque is converted to a shear stress. Viscosity is calculated from the shear stress shear rate relation. The measurement method follows the standards ASTM D 7395.

2.5 Thermal conductivity models and the Role of Thermal Boundary Resistance

From the experimental results it is evident that the conductivity enhancement depends on multiple parameters including the thermal conductivities of the base fluid and the dimensionality of the material used the volume fraction, surface charge state, preparation method and the temperature. Presently, there is no reliable analytical model to accurately predict the thermal conductivity of nanofluids, and there are no models that incorporate all these factors. The experimental results in the following chapters will be analyzed based on some reasonable theoretical models prevailing in the literature. The models will be discussed in this section.

For heterogeneous mixtures, numerous theoretical models have been performed in the past, dating back to the seminal work by Maxwell [9]. The Maxwell model has been used to

predict the effective thermal or electrical conductivity of solid-liquid mixtures consisting of mono disperse, ignoring the mutual interaction effects, low-volume-fraction mixtures of relatively large-sized spherical particles, and has been the basis for many analytical models developed for nanofluids in the past decade. In this model, the effective thermal conductivity is given by

$$\frac{k_{eff}}{k_b} = \frac{k_p + 2k_b + 2(k_p - k_b)\phi}{k_p + 2k_b - 2(k_p - k_b)\phi} \tag{2.14}$$

Where k_{eff} is the effective thermal conductivity of the nanofluid, k_p is the thermal conductivity of the inclusion, k_b is the thermal conductivity of the base fluid, and ϕ is the volume fraction.

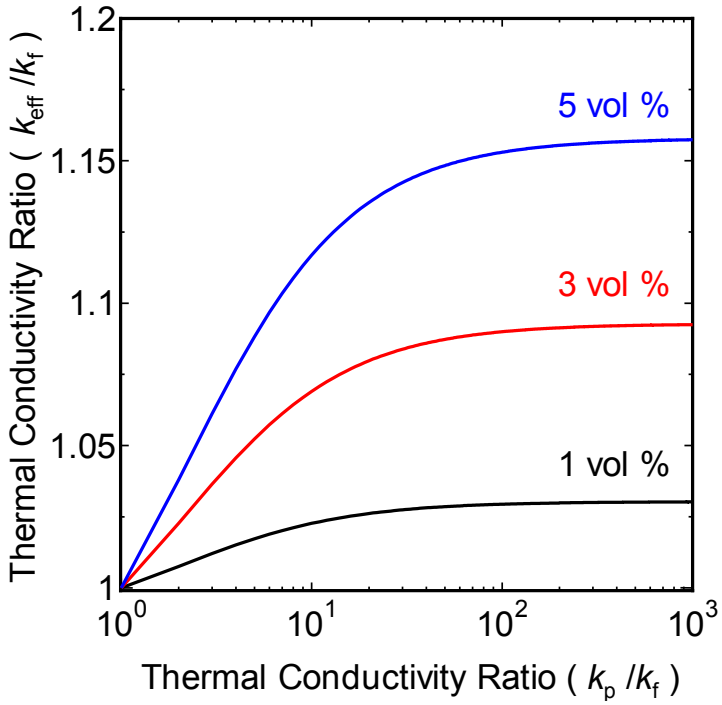

Figure 2.16: Thermal conductivity enhancement as a function of ratio of nanoparticle thermal conductivity to base fluid conductivity from Maxwell's model.

Figure 2.16 shows the predictions of Maxwell's model for varying volume fraction. It can be seen from the figure that the thermal conductivity enhancement saturates when the ratio of nanoparticle thermal conductivity to the base fluid thermal conductivity reaches above 70. This means that just utilizing a higher conductivity spherical particle does not necessarily increase the base fluid conductivity. The predictions of this model contradict the existing experimental reports on nanofluids thermal conductivity which is discussed in the previous chapter of the thesis.

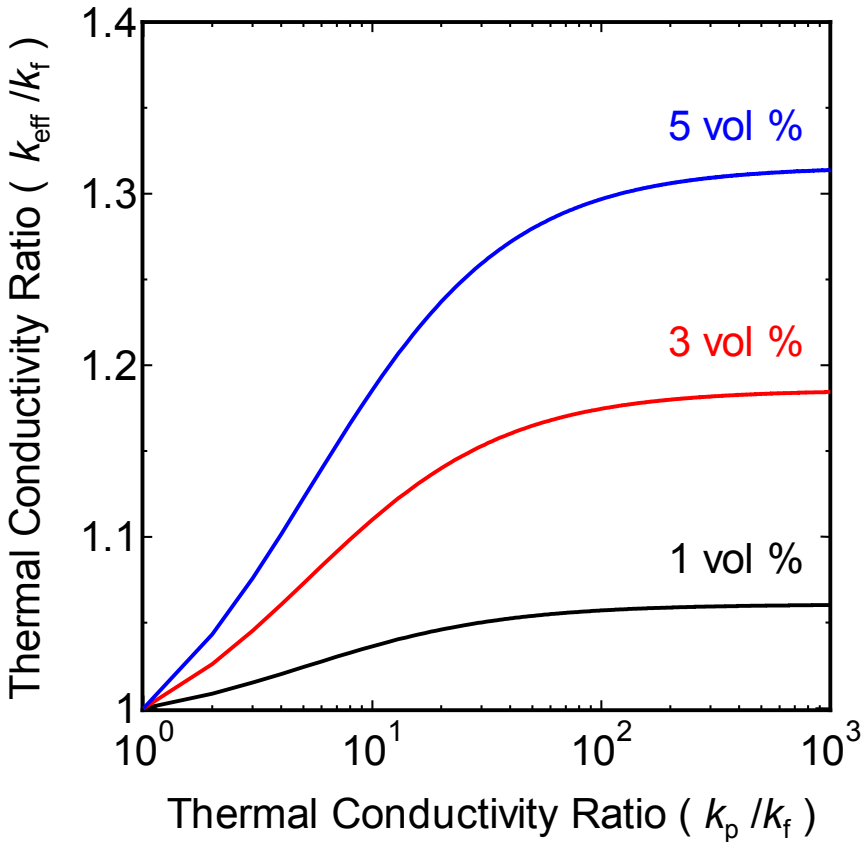

Figure 2.17: Thermal conductivity enhancement as a function of ratio of nanoparticle thermal conductivity to base fluid conductivity from Hamilton – Crosser model for cylindrical inclusions.

Hamilton and Crosser [79] extended the Maxwell's model to non-spherical particles. They introduced a shape factor to account for the particle shape and obtained the following model.

$$\frac{k_{eff}}{k_b} = \frac{k_p + (n-1)k_b + (n-1)(k_p - k_b)\phi}{k_p + (n-1)k_b - (n-1)(k_p - k_b)\phi} \tag{2.15}$$

Where n is the shape factor. They proposed a value of $n=3$ for spherical particles and for $n=6$ cylindrical particles.

Figure 2.17 shows the predictions of Hamilton-Crosser model for varying volume fraction specifically for cylindrical inclusions. This model shows that the presence of cylindrical inclusions enhances the thermal conductivity by a factor of 2 compared to the case of spherical inclusions. However, even in this model the thermal conductivity enhancement saturates when the ratio of nanoparticle thermal conductivity to the base fluid thermal conductivity reaches above 70. This shows that mere presence of higher conductivity cylindrical particle does not increase the base fluid conductivity significantly without increasing the volume fraction of the material.

Nan et al. [103] proposed a simple model to calculate the effective thermal conductivity of CNT-based composites by generalizing Maxwell's formula. Their model is written as follows:

$$\frac{k_{eff}}{k_b} = \frac{3 + (\beta_x + \beta_z)\phi}{3 - \phi\beta_x} \tag{2.16}$$

where

$$\beta_x = \frac{2(k_{11}^p - k_b)}{k_{11}^p + k_b} \quad \beta_z = \frac{k_{33}^p}{k_b} - 1 \tag{2.17}$$

In equation (2.18), k_p^{11} and k_p^{33} are the thermal conductivities along the transverse and longitudinal axes of the CNT. Taking into account the thermal boundary resistance between the CNT and the surrounding host matrix, this model was further modified as follows:

$$\frac{k_{eff}}{k_b} = 1 + \frac{\phi L}{d} \frac{\left(k_p / k_b\right)}{\frac{L}{d} + \frac{2a_k}{L} \frac{k_p}{k_b}} \tag{2.18}$$

Here L and d are the nanotube length and diameter respectively, a_k is the Kapitza, radius which is defined as the product of thermal boundary resistance (TBR) and the thermal conductivity of the base fluid ($a_k = TBR \times K_b$).

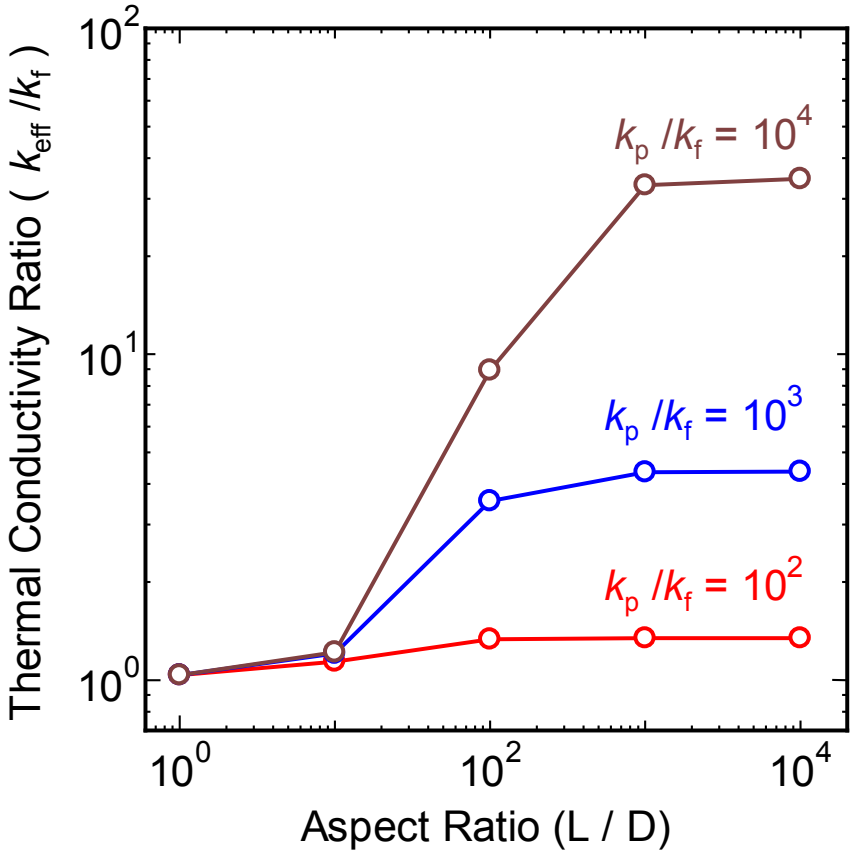

Figure 2.18: Thermal conductivity enhancement as a function of aspect ratio without taking thermal boundary resistance by EMT model.

Figure 2.18 shows the predictions of effective medium model as a function of aspect ratio of the material and for varying contrast ratio of the nanotube to the base fluid conductivity. It can be seen from this figure that when the ratio of CNT thermal conductivity to base fluid conductivity is 100 or less, increasing the aspect ratio of the CNT does not increase the thermal conductivity of the base fluid. However, when the ratio of CNT thermal conductivity to base fluid conductivity is more than 100, effective thermal conductivity enhancement increases as the aspect ratio increases.

In figure 2.18, the role of thermal boundary resistance between the nanomaterial and the surrounding base fluid is not considered for calculations. However, Thermal boundary resistance (TBR) also known as Kapitza resistance exists at solid-solid and solid-liquid interfaces [104]. This effect is considered to play a significant role at the interface between the nanomaterial and the surrounding liquid matrix. The thermal boundary resistance represents a barrier to the heat flow associated with the acoustic mismatch in the phonon spectra of the heat carriers and possible weak contact at the interface. Limited experimental and numerical results exist for the boundary resistance between SWCNT and the surrounding interface for CNT based suspensions [105—108]. Huxtable et al. [105] measured interfacial thermal resistance of SDS encapsulated carbon nanotubes in water to be around 8.3×10^{-8} m^2KW^{-1}.Similar results were reported by Kang et al. [106] for semi-conducting and metallic SWCNTs in water encapsulated using SDS, SDBS and Sodium Cholate (SC) surfactants. Molecular dynamics simulation results of SWCNTs surrounded by octane medium (3.4×10^{-8} m^2 K W^{-1}) report similar order of magnitude and show the interface resistance depends on the length of the CNTs [107]. For sufficiently longer CNTs Carlborg et al. [108] showed the

interface conductance to be in the similar order of magnitude for SWCNTs (1.6-2.4 MW m^{-2} K^{-1}) surrounded by argon matrix and independent of length. Schmidt et al. [109] measured the interfacial thermal conductance of CTAB encapsulated gold nanoparticles in water and reported a higher interface conductance in the range of 150 – 450 MW m^{-2} K^{-1}. Recently Park et al. [110] measured the thermal conductance of the gold nanorod/fluid interfaces of methanol, ethanol, toluene, and hexane. Their experimental results falls within a narrow range: 36 ± 4 MW m^{-2} K^{-1} for methanol, 32 ± 6 MW m^{-2} $K^{-1}$for ethanol, 30 ± 5 MW m^{-2} $K^{-1}$for toluene, and 25 ± 4 MW m^{-2} K^{-1} for hexane.

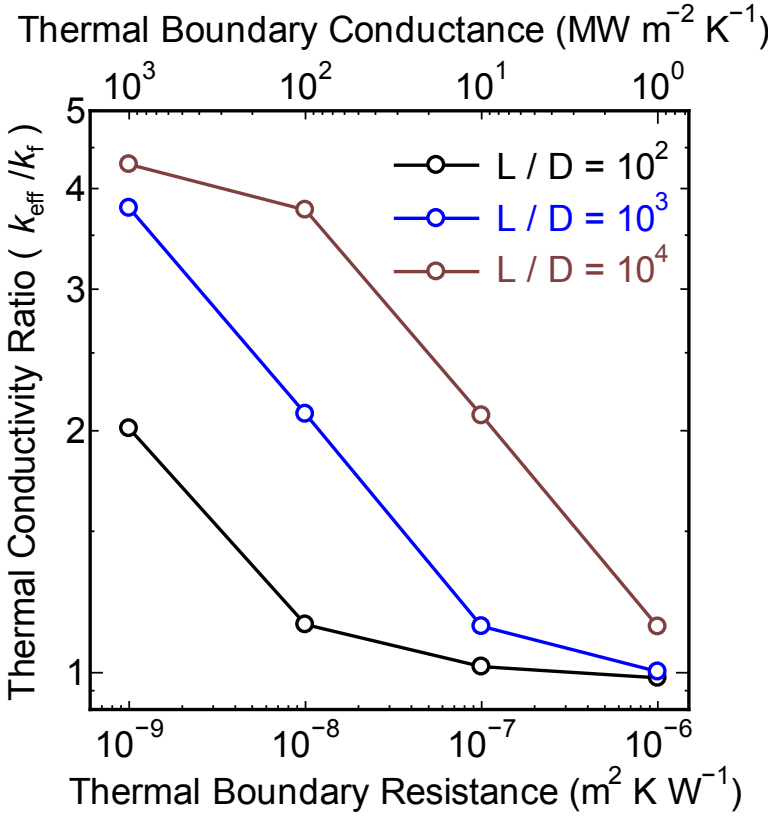

Figure 2.19: Thermal conductivity enhancement as a function of thermal boundary resistance for varying aspect ratio of 1 vol % CNTs.

Figure 2.19 shows the effect of thermal boundary resistance in the effective thermal conductivity enhancement of the 1 vol % CNT based nanofluids. It can be clearly seen that despite the higher thermal conductivity of CNTs, the enhancement is largely limited by the thermal interface resistance. Figure 2.20 shows the thermal conductivity enhancement for varying volume fraction for varying contrast ratio of the nanotube to the base fluid conductivity. This figure shows that when the role of TBR is taken into account, it is sufficient to have a thermal conductivity contrast ratio of 1000 above which mere increase in the thermal conductivity of CNT does not improve the thermal conductivity of the fluid. Figure 2.19 and figure 2.20 clearly show that to achieve high thermal conductivity enhancement it is necessary to have high aspect ratio and low thermal boundary resistance.

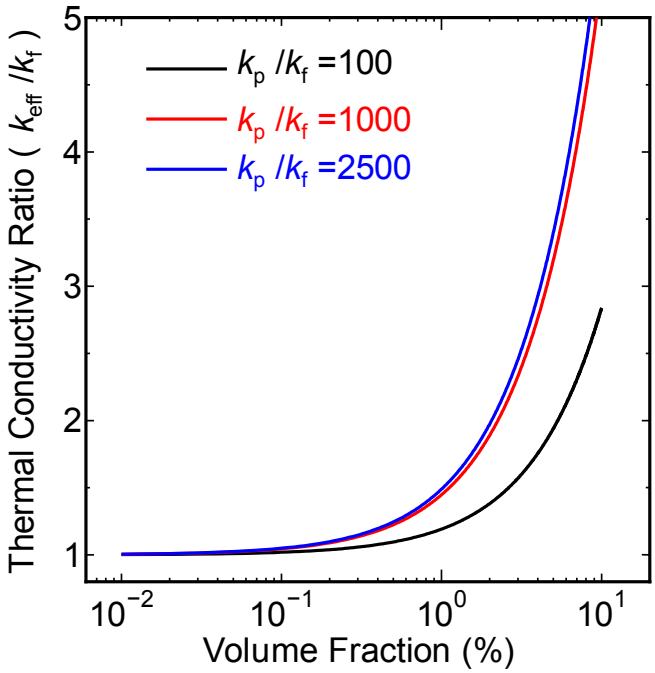

Figure 2.20: Thermal conductivity enhancement as a function of ratio of CNT thermal conductivity to base fluid conductivity from EMT model considering the effect of thermal boundary resistance.

Yamada – Ota model [111] reported an empirical model by assuming a random orientation of the particles having a shape of parallelepiped neglecting the inter-particle interactions and aggregation effects.

$$\frac{k_{eff}}{k_b} = \frac{(k_p/k_b) + \alpha - \alpha\phi[1-(k_p/k_b)]}{(k_p/k_b) + \alpha + \phi[1-(k_p/k_b)]} \tag{2.19}$$

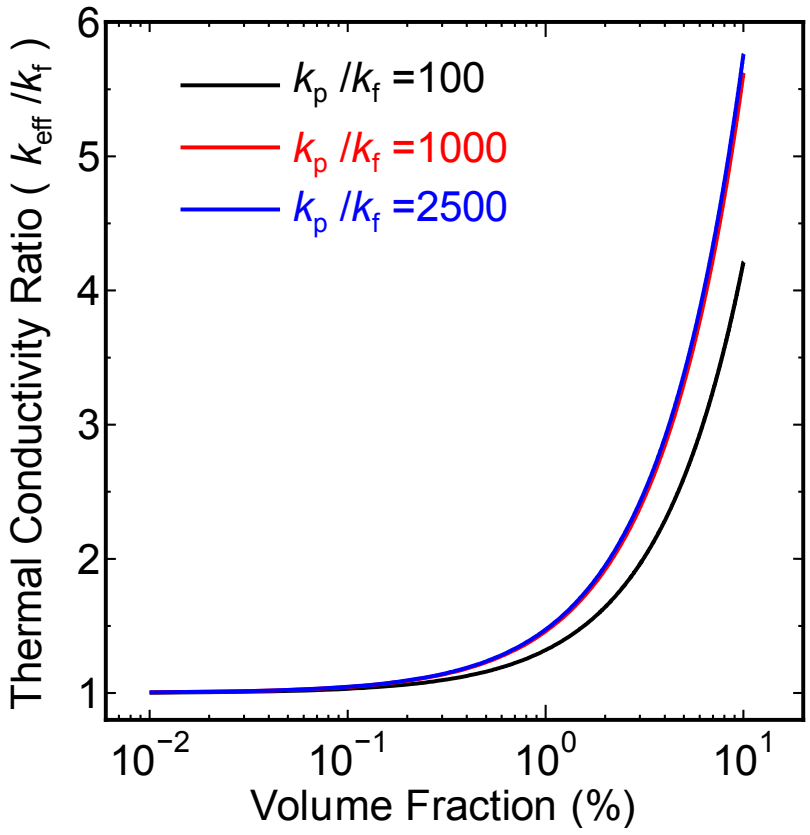

Figure 2.21: Thermal conductivity enhancement as a function of ratio of CNT thermal conductivity to base fluid conductivity from Yamada-Ota model considering the effect of thermal boundary resistance.

Zheng and Hong [112] further improvised this model by incorporating the TBR in the original model, and can be written as follows:

$$\frac{k_{eff}}{k_b} = \frac{(k_x / k_b) + \alpha - \alpha\phi[1-(k_x / k_b)]}{(k_x / k_b) + \alpha + \phi[1-(k_x / k_b)]} \tag{2.20}$$

where $k_x = \dfrac{k_p}{1+\left(\dfrac{2k_p TBR}{L}\right)}$ and $\alpha = 2\phi^{0.2}\dfrac{L}{d}$. The notations in equation (2.20) are same as in equation (2.18). Note that the TBR incorporated in the original Yamada–Ota model follows the same manner as reported by Nan et al [103]. The predictions of Yamada-Ota model including the effect of TBR is shown in figure 2.21. It can be seen that the behaviour of EMT model and the Yamada – Ota model are almost similar. However, the effective thermal conductivity enhancement predicted by the Yamada – Ota model is marginally higher than the EMT model predictions.

2.6 Viscosity Models

The inclusion of a nanomaterial not only increases the thermal conductivity of the material but also increases the viscosity of the base fluid. For the development of nanofluids for practical applications accurate knowledge of the viscosity is also required. The first contribution to the theory of viscosity of suspensions of spheres was developed by Einstein [113].He considered a dilute suspension of rigid spherical particles where the movement of one spherical particle does not influence the other. For such a system he proposed a simple equation which can be written as follows:

$$\frac{\eta_{eff}}{\eta_f} = 1 + \frac{5}{2}\phi \tag{2.21}$$

Here, η_{eff} is the effective viscosity of the fluid and η_f is the viscosity of the base fluid.

For concentrated suspensions of spheres when particle interaction becomes important, Mooney [114] proposed a simple model as follows

$$\frac{\eta_{eff}}{\eta_f} = \exp\left(\frac{\frac{5}{2}\phi}{1-(\phi/\phi_0)}\right) \tag{2.22}$$

In this equation ϕ_0 is an empirical constant which ranges between 0.74 and 0.52. These values correspond to the values of ϕ for closest packing and cubic packing respectively.

For concentrated suspensions of non-spherical particles, the often used equation is the Krieger-Dougherty equation [115]. This equation takes the form

$$\frac{\eta_{eff}}{\eta_f} = \left(1-\frac{\phi}{\phi_{\max}}\right)^{-A\phi_{\max}} \tag{2.23}$$

In this equation A and $\phi_{\max}$ are the fitting parameters which depends on the shape and concentration of the inclusions.

It needs to be noted that the models proposed here are based on the assumption that the fluid is Newtonian and valid only at higher shear rates. However, a non-Newtonian behaviour is reported in the literature for nanofluids especially for CNT based nanofluids [70, 116-118]. This means that the viscosity depends on the velocity gradient and may be different in a shear

rate than it is in gravity driven flow. Therefore, the above proposed models need to be used with some caution.

2.7 Conclusions

In this chapter, synthesis of single walled carbon nanotubes, preparation of nanofluids and several characterization techniques are described. Transmission electron microscopy, Raman spectroscopy and thermogravimetric analysis demonstrate the high quality of SWCNTs synthesized. Dynamic light scattering measurements reveal that the cluster size distribution is wider in water based nanofluids while in the case of EG based nanofluids the cluster size distribution is narrow and the size of the clusters are larger than that of water. This is further confirmed by the broad and red shifted absorption peaks of ethylene glycol based nanofluids. The superior quality of water based suspensions was confirmed by the presence sharper peaks in the optical absorption spectroscopy and photoluminescence signals. The mathematical principles of THW setup and experimental setup are explained in detail. From the calibration measurements of pure fluids it is concluded that the transient hot wire technique is a reliable method for the measurement of thermal conductivity of liquids. In this chapter the electrical conductivity setup and viscosity measurement methods is described in detail. Theoretical models to analyze the experimental data are explained along with its merits and demerits.

Chapter 3

Enhanced Thermal Transport in Ethylene Glycol and Water with Single Walled Carbon nanotube Inclusions

3.1 Introduction

In this chapter, the effective thermal conductivity of SWCNT suspensions dispersed using sodium deoxycholate surfactant in ethylene glycol (EG) and water is presented. Thermal conductivity measurements were performed using the transient hot wire technique which is explained in detail in the previous chapter. Besides, the effective electrical conductivity is measured for water based nanofluids to understand the role of percolation thresholds. The influence of SWCNT loading and temperature on the thermal conductivity enhancement is also investigated in this chapter. The effective viscosity of SWCNT suspensions is also measured using glass capillary viscometer and cone-plate viscometer. The favorability of CNT based nanofluids is discussed based on the thermal conductivity and viscosity measurements.

3.2 Experiments Results of Thermal and Electrical Conductivity Measurements

Thermal conductivities of the SWCNT-dispersed EG samples were measured for different SWCNT loadings ranging from 0.1 to 0.3 wt % using the THW setup. Figure 3.1 shows the thermal conductivities versus different SWCNT loadings measured at room temperature. The thermal conductivity increased with increasing SWCNT loading in a slightly nonlinear

fashion. At a loading of 0.1 wt % no significant improvement in effective conductivity was obtained (only 2.7 %). This minor increase lies very well within the experimental uncertainty limits and cannot be considered as conductivity enhancement. However, on further increasing the nanotube loading, a significant improvement in the effective conductivity was measured. A maximum enhancement of 14.8 % at a loading of 0.3 wt % was found in this study.

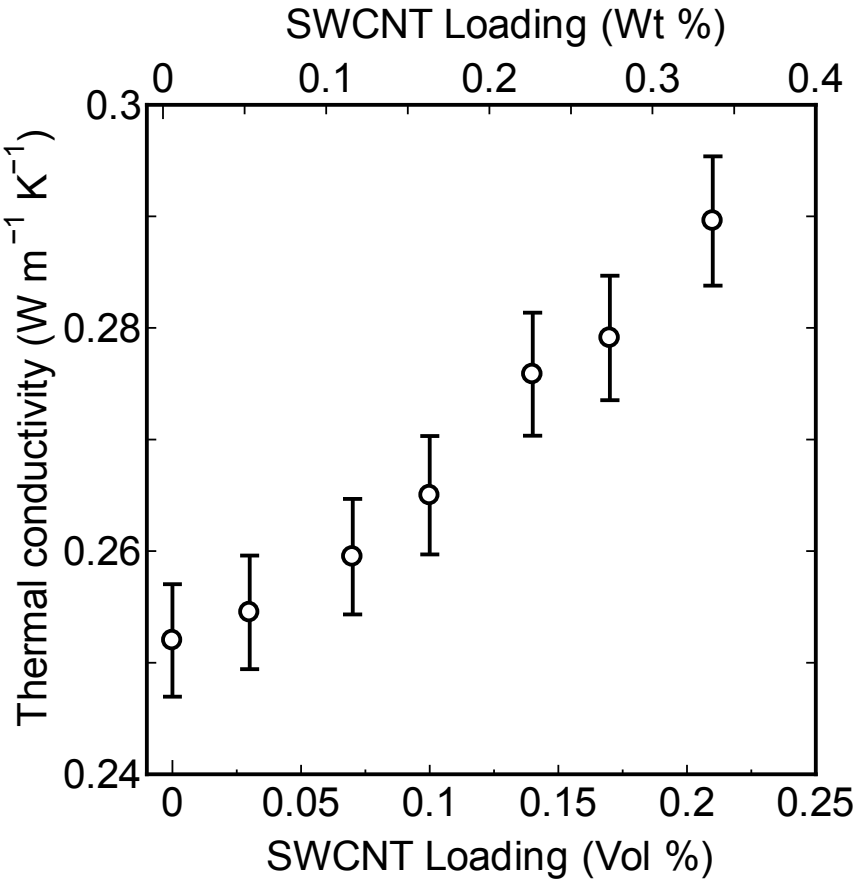

Figure 3.1: Thermal conductivity enhancement of ethylene glycol as a function of SWCNT Loading.

The results of this study show thermal conductivity enhancements are less than those reported by Choi et al [59] for poly-(α olefin) oil seeded with MWCNTs**.** Xie et al. [60] and

Liu et al. [65] reported enhancements of 12.7 % and 12.4 % respectively at 1 vol % loading. Ruan and Jacobi [119] recently reported an enhancement of 9.3 % at a volume fraction of 0.24 % for EG/MWCNT nanofluids. Nanda et al. reported an enhancement of 36 % at for SWCNT/EG nanofluids at 1 vol % [67]. Eastman et al. [10] reported an enhancement of 40 % at 0.3 vol % for Copper/EG based nanofluids. In this work, such a high enhancement was not observed. This difference could be attributed to the aspect ratio of the material used, purity level, and treatment method adopted to prepare the nanofluid dispersion.

Thermal conductivity of the SWCNT/water nanofluid samples was measured using the THW setup for different SWCNT loadings ranging from 0.1 to 0.3 vol %. Figure 3.2 shows the effective thermal conductivity versus different SWCNT loadings measured at room temperature. Thermal conductivity increased with increasing SWCNT loading in a linear fashion.

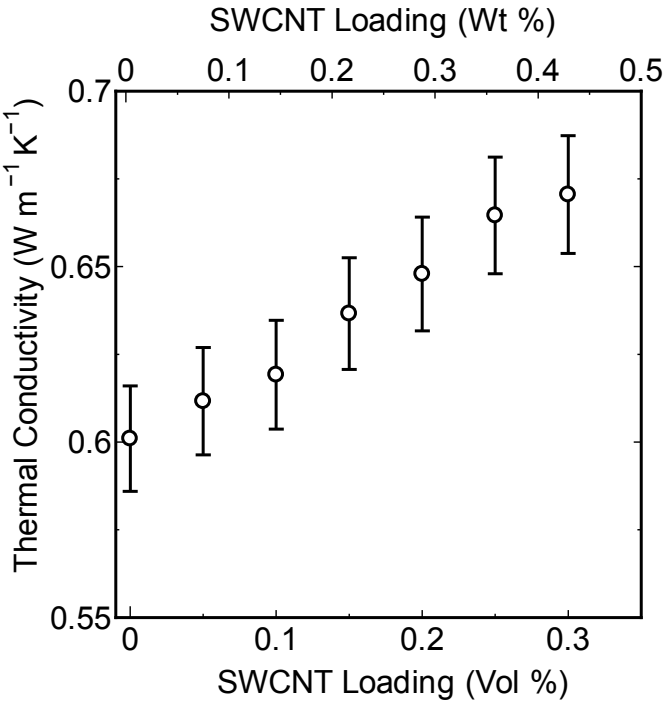

Figure 3.2: Thermal conductivity enhancement of water as a function of SWCNT Loading.

Electrical conductivity of the SWCNT/water nanofluid samples are plotted in Figure 3.3. The Electrical conductivity increased sharply at very low SWCNT loading and then gradually saturated as the SWCNT loading increased, thus exhibiting clear percolation behaviour. Experimental data were fitted using a two-parameter equation $\rho = \rho_o(\varphi - \phi_c)^t$ as per classical percolation theory [120]. Fitting the data using a power law equation shows a very low percolation threshold of $\varphi_c = 0.0152$ vol % (0.025 wt %). The present results are comparable to the electrical percolation threshold of 0.024 wt % and 0.03 wt % reported for SWCNT/Poly (ethylene terephthalate) [121] and SWCNT/Poly (ethylene oxide) composites [122].

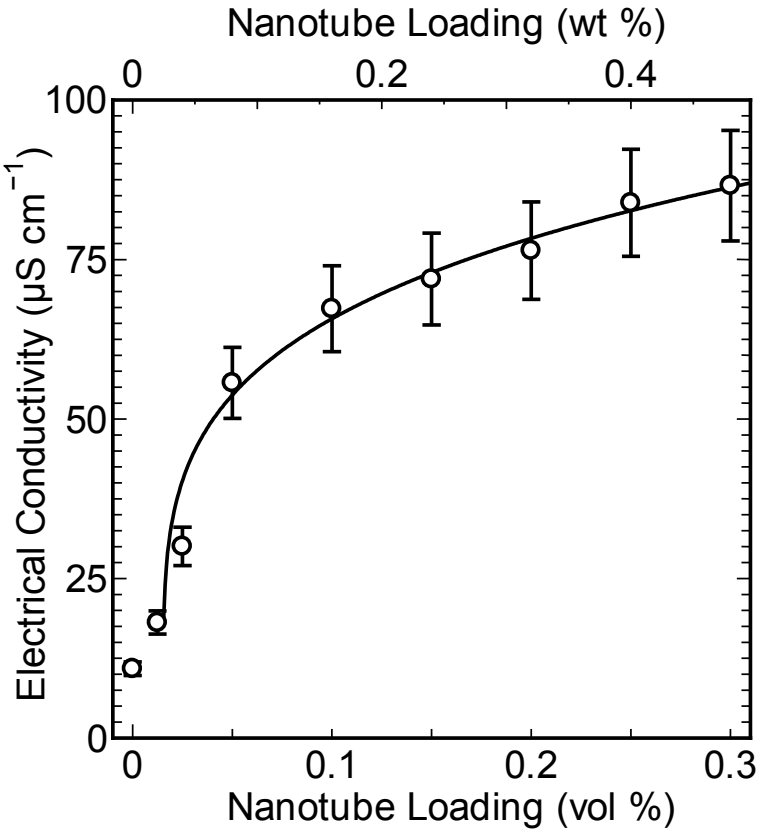

Figure 3.3: Electrical conductivity of SWCNT/water nanofluids. A two-parameter fit as per classical percolation theory [120] yields a low percolation threshold of 0.0152 vol %.

Figure 3.2 shows the effective thermal conductivity of water increases linearly with SWCNT loading which is clearly contradictory to the electrical conductivity results. Electrical conductivity of the fluids showed a percolating behaviour while no obvious sign of percolation was noticed for thermal conductivity. Persistent heat conduction by water and low thermal conductivity contrast ratio (compared to electrical conductivity contrast ratio) between water/SWCNT does not result in a sharp increase in thermal conductivity at the percolation threshold [123].

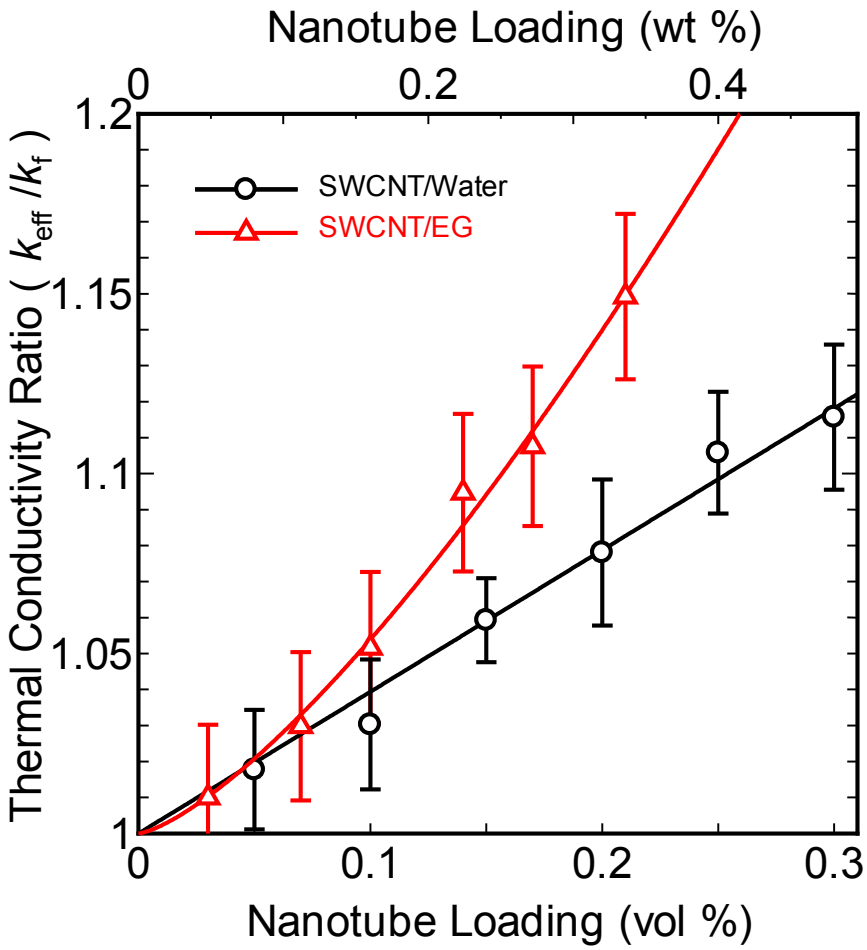

Figure 3.4: Thermal conductivity increase as a function of SWCNT loading in Water and Ethylene Glycol.

In Figure 3.4, effective thermal conductivity enhancement for SWCNT/ethylene glycol (EG) and SWCNT/Water based nanofluids were compared. SWCNT/EG nanofluids showed a higher thermal conductivity enhancement compared to that of the SWCNT/water nanofluids. Moreover, the SWCNT/EG effective thermal conductivity shows a non-linear increase with respect to SWCNT loading, whereas a linear increase is found in the case of the water based nanofluids.

The number of contact points between the SWCNTs increase as a function of the square of the SWCNT loading, therefore one might associate the non-linear increase observed in SWCNT/EG nanofluids to the non-linear increase in the heat transport path [123]. DLS measurements for water and EG based nanofluids show that the aggregate size distribution is narrow in the case of EG compared to the case of water. Besides, broader and red-shifted peaks are clearly noticed in the case of EG based nanofluids whereas in the case of water sharp and distinct features of the peaks are clearly noticed. Furthermore, photoluminescence signals from the water suspensions clearly demonstrate the degree of isolation is more pronounced in the case of water whereas in the case of EG SWCNTs always exist in the form of aggregates. This is more likely due to the compatibility of DOC to stabilize the SWCNTs efficiently in water while in the other case it is less/incompatible. The stability of SWCNT/EG nanofluids was extremely poor compared to the case of SWCNT/water based nanofluids, as the SWCNTs soon settled and formed larger aggregates. The non-linear tendency observed in this work was possibly due to the existence of larger aggregates and larger heat transport paths created by this aggregates.

Efficient isolation of SWCNTs in water (compared to EG) may minimize the number of contact points thereby diminishing the heat transport path because resulting in a linear increase in effective thermal conductivity. Since the electrical conductivity measurements reveal a very low percolation threshold, it can be concluded that the SWCNTs forms a percolating network, which leads to better energy transport thereby increasing the effective conductivity of the fluid. The thermal conductivity increase observed in the present experiments supports the mechanism of particle clustering in increasing the thermal conductivity of the fluid.

3.3 Temperature Dependence

The effective thermal conductivity increase of the SWCNT/water nanofluid was also found to be temperature dependent. Figure 3.5 shows the effective thermal conductivity values for three volume concentrations at different temperatures. Figure 3.5 shows an additional 3-5 % increase in effective thermal conductivity with increasing temperature. A maximum conductivity increase of 16 % is obtained at a temperature of 333 K and a SWCNT loading of 0.3 vol %.

Gharagozloo et al. [96] reported that nano particles tend to aggregate as time progresses, and correlated the temperature dependent increase observed to the increase in the size of the aggregates as a significant amount of time is often spent to heat the fluid during measurements. In order to examine this mechanism we performed a hysteresis measurement, which is shown in Figure 3.6.

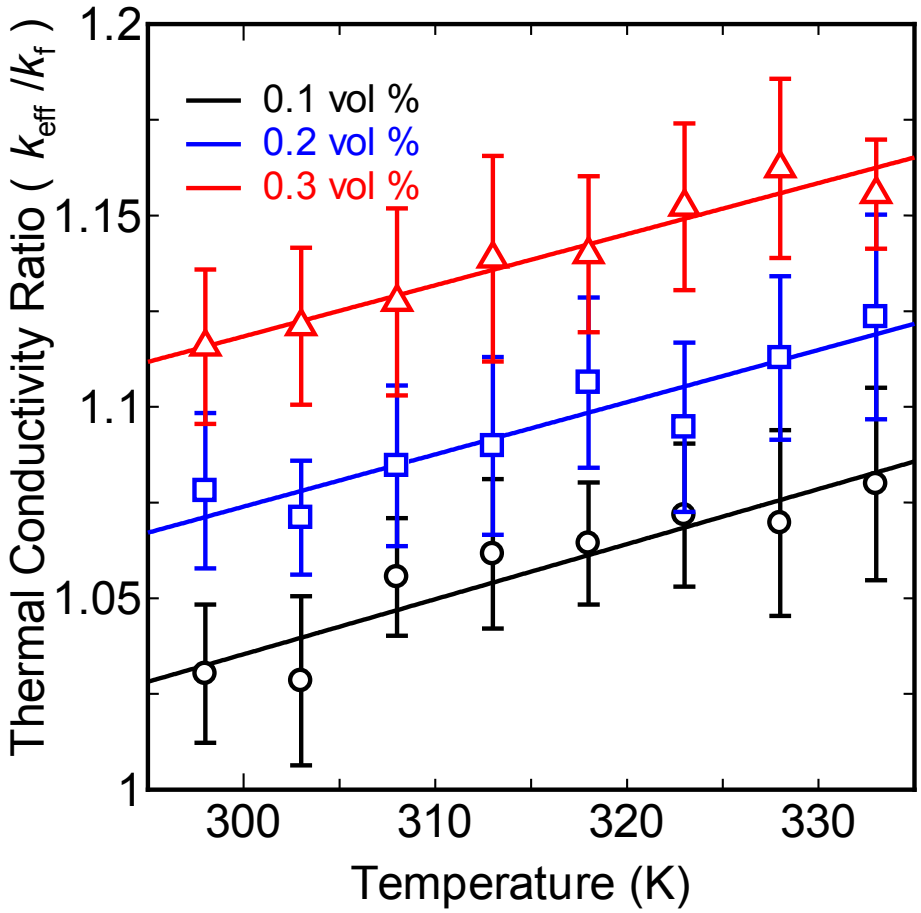

Figure 3.5: Thermal conductivity increase as a function of fluid temperature in water

From Figure 3.6, it is evident that the fluid effective thermal conductivity enhancement remains the same with respect to temperature irrespective of whether the fluid is heated or cooled (no hysteresis). This clearly rules out the possibility of **"time-dependent aggregation"** [96] as a probable mechanism for the temperature-dependent thermal conductivity increase.

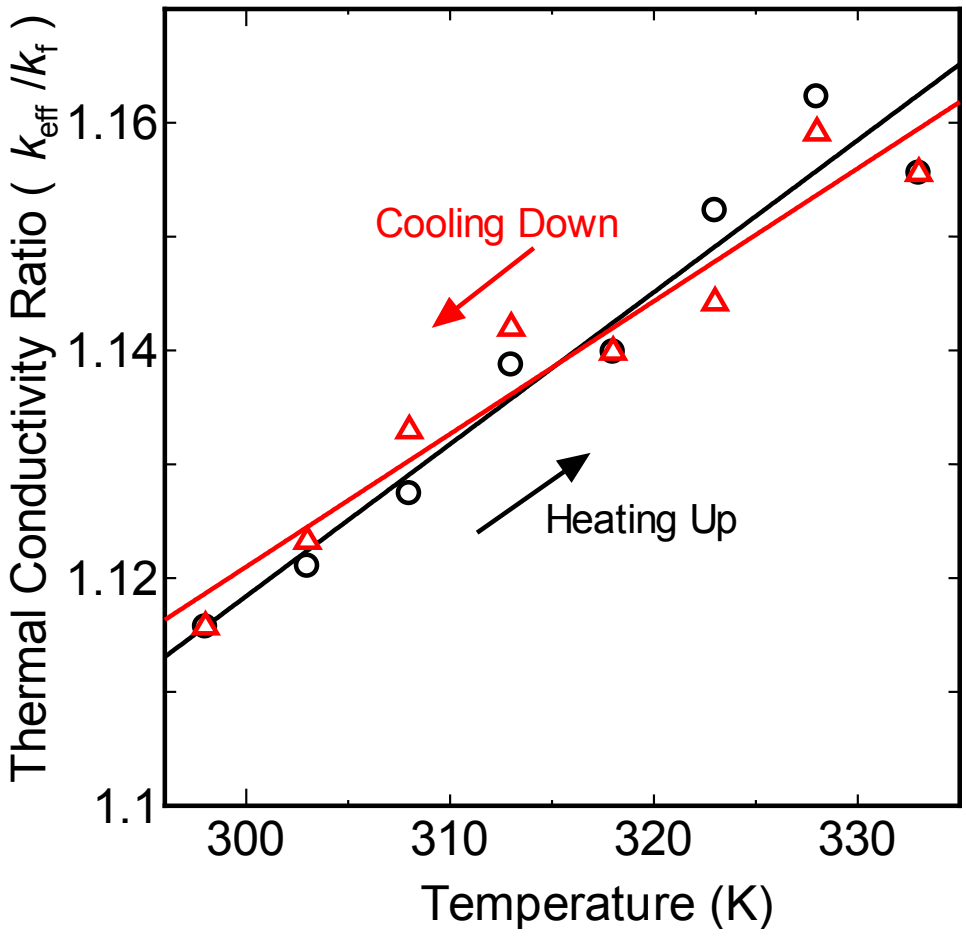

Figure 3.6: Comparison of thermal conductivity improvement during the heating and cooling process in water (SWCNT loading: 0.3 vol. %. The effective conductivity enhancement remains the same with respect to temperature irrespective of whether the fluid is heated or cooled.

Figure 3.7 shows a comparison of temperature-dependent thermal conductivity behaviour between the SWCNT/water and the SWCNT/EG based nanofluids. This Figure shows that the SWCNT/EG nanofluids did not exhibit temperature dependent enhancement, while a different trend is observed in the case of SWCNT/water nanofluid.

The difference in temperature dependent thermal conductivity variation could possibly indicate the critical role of Brownian motion in the fluid. Brownian motion depends on the fluid temperature and viscosity. Gupta and Kumar [124] suggested that the Brownian motion can enhance the thermal conductivity at higher temperatures up to 6 %. Computational modeling of SWCNTs in water using random movement of Brownian thermal walkers, Duong et al. [125] reported that temperature-based increase in thermal conductivity of water due to the enhanced diffusion of heat walkers.

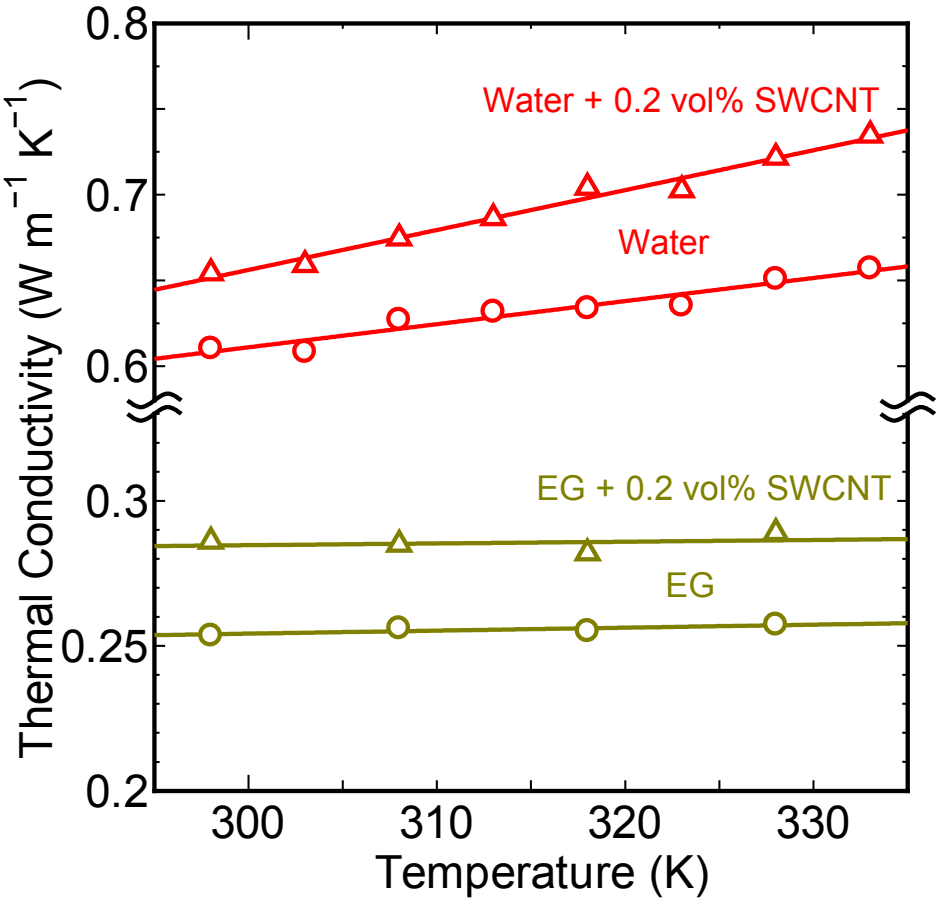

Figure 3.7: Temperature dependent thermal conductivity in SWCNT/water and SWCNT/EG nanofluids. Open circles correspond to base fluid measurements and open triangles correspond to SWCNT nanofluids.

Tsyboulski et al. [126] experimentally found the translational diffusion coefficient of SWCNTs (D_{SWCNT}) in water range from 0.3 to 6 $\mu m^2/s$, which is much lower than the diffusion coefficient of water (D_W = 0.413 mm^2/s). However, the SWCNTs also exhibit rotational diffusion (D_r) which can be estimated using Broersma theory as follows [127]:

$$D_r = \frac{3k_B T}{\pi\eta}\frac{\ln(L/d)-\gamma}{L^3} \tag{3.1}$$

In equation (3.1), L and d denote the length and diameter of the nanotube, respectively. k_B is the Boltzmann constant, T is the fluid temperature, η is the fluid viscosity and γ is the end correction coefficient (usually γ is assumed to be 0.8).

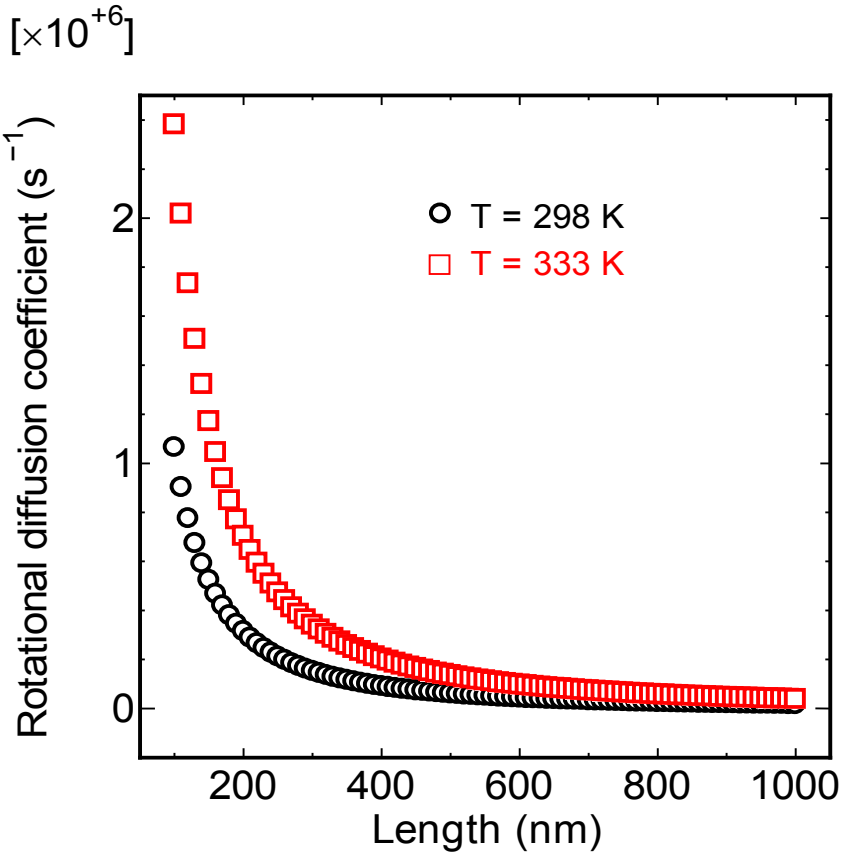

Figure 3.8: Rotational diffusion co-efficient of water based nanofluid as a function of SWCNT length.

Equation (3.1) shows the rotational diffusion is inversely proportional to the cube length of the SWCNTs which is shown in Figure 3.8. A simple calculation assuming a SWCNT length of 250 nm and diameter of 1 nm gives a rotational diffusion of approximately 1000 s^{-1}. As the temperature is increased, the viscosity of the fluid reduces which further improves the rotational diffusion of SWCNTs. Yunker et al.[128] showed that short aspect ratio ellipsoids predominantly undergo rotational diffusion while large aspect ratio particles exhibited both mixed rotational and translational diffusion.

As previously discussed, the length distribution of SWCNTs in the present study is from 100 to 600 nm. It is thus possible to conclude that the high rotational diffusion induced by the presence of shorter SWCNTs lead to the temperature dependent increase in thermal conductivity. Since viscosity of EG is much higher (~ 35 times) than that of water, the influence of rotational diffusion is less pronounced in the SWCNT/EG nanofluid, thus does not cause any improvement in conductivity at higher temperature.

Xie et al. [60] reported a thermal conductivity increase of only 7 % with 1 vol % MWCNT suspensions. Assael et al. [61] reported an increase between 20 % and 40 % at 0.6 vol % of MWCNT loading at room temperature. Ding et al. [69, 70] reported a strong temperature dependent increase for aqueous suspensions consisting of MWCNTs. An increase of up to 80 % was reported at a MWCNT loading of 1 wt % and at a temperature of 303 K. Nasiri et al. [71] recently reported the temperature dependent thermal conductivity increase of aqueous suspensions consisting of SWCNTs dispersed using SDS as the surfactant. An increase of up to 35 % at a temperature of 323 K and a nanotube loading of 0.25 wt % was reported in their

work. Similar temperature-dependent enhancement has also been reported by Glory et al. [129] for a water-based nanofluid. The present experimental thermal conductivity increase is marginally lower than the previous reports. Proper characterization and systematic experiments, like the present case, need to be performed to minimize the discrepancy among experimental results from different research groups.

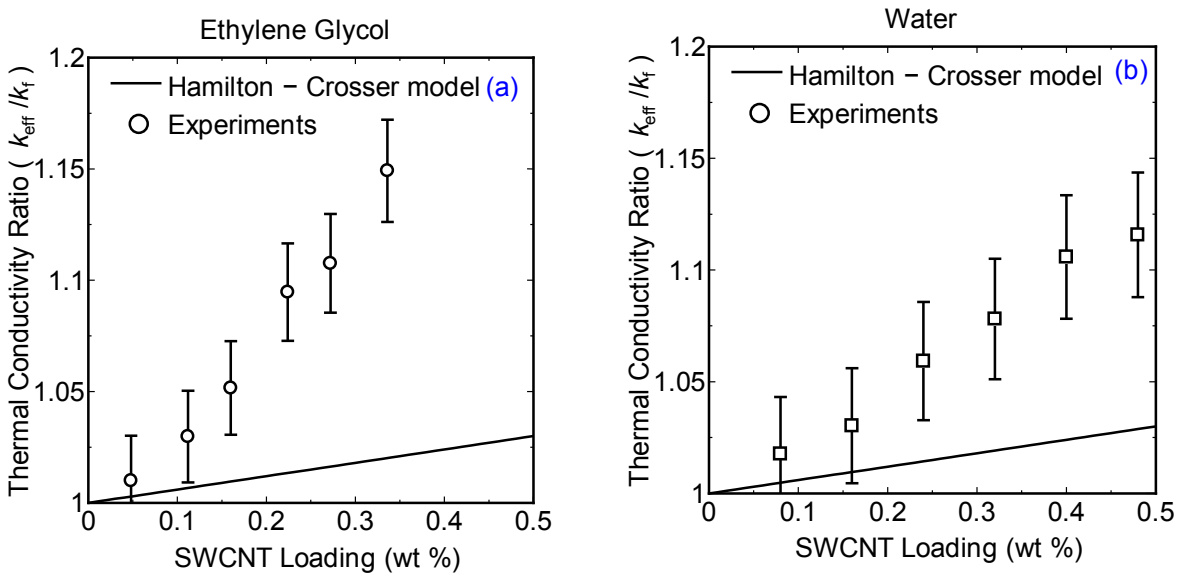

Figure 3.9: (a) Thermal conductivity enhancement of ethylene glycol compared with H-C model. (b) Thermal conductivity enhancement of water compared with H-C model.

Figure 3.9 (a & b) shows the comparison of experimental results against the predictions of Hamilton-Crosser model. In both the cases, H-C model predicts constant thermal conductivity improvement irrespective of the base fluid thermal conductivity. Experimental results of EG show a six fold improvement in thermal conductivity when compared to the H-C predictions while water showed a fourfold enhancement.

Experimental results were compared further compared with the effective medium theory (EMT) [103] and the Yamada–Ota model [111,112]. For the present model calculations, a fluid thermal conductivity of 0.252 W m^{-1} K^{-1} for EG and 0.598 W m^{-1} K^{-1} for water SWCNT thermal conductivity of 1750 $Wm^{-1}K^{-1}$, aspect ratio of 350, and thermal boundary resistance (TBR) of 10^{-8} m^2 K W^{-1} [105,106] were used.

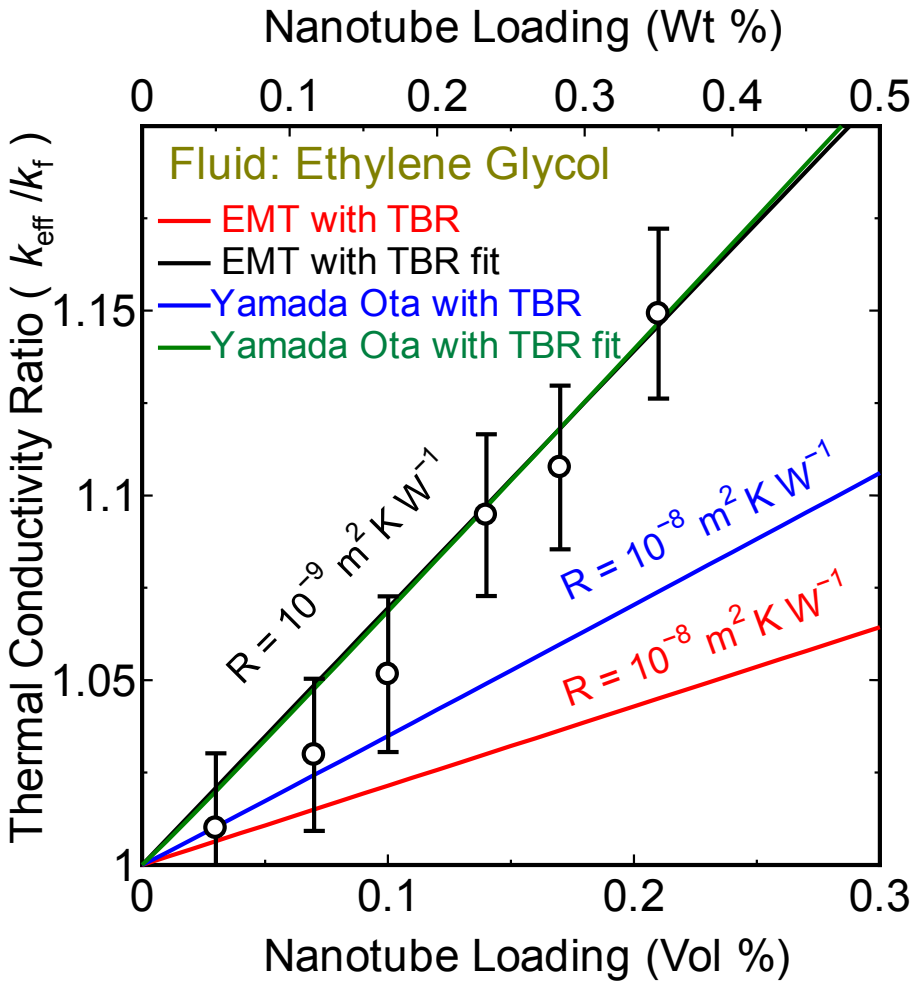

Figure 3.10: Comparison of experimental results of EG/SWCNT nanofluid with EMT model and Yamada-Ota model.

Figure 3.10 and 3.11 shows the comparison of the model calculations with the present experimental results at room temperature for ethylene glycol and water respectively. EMT theory predicts lesser enhancement, while the modified Yamada–Ota model predicts an enhancement that is marginally less than the experimental results for both the cases. Nevertheless, it can be understood from both models that the TBR plays a detrimental role in reducing the effective conductivity of the nanofluid, despite the high thermal conductivity of SWCNTs.

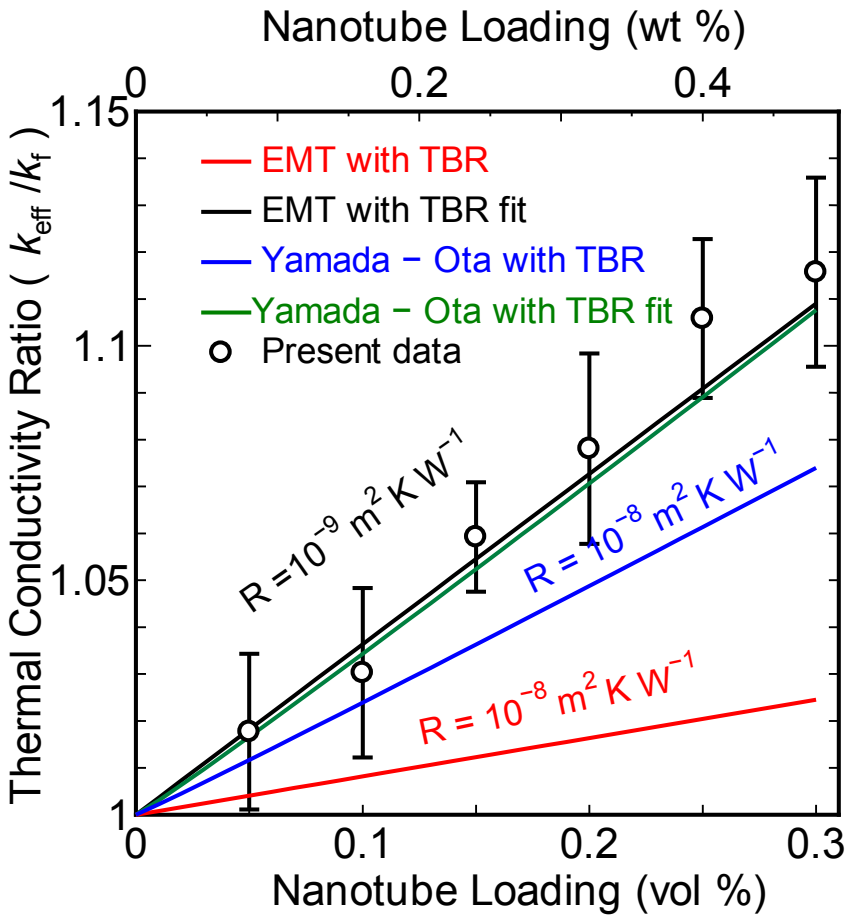

Figure 3.11: Comparison of experimental results of water with EMT model and Yamada-Ota model.

By considering TBR as an unknown parameter in the EMT model and using the measured thermal conductivity increase, the interfacial resistance was estimated to be 4.2 $\times 10^{-9}$ m^2 K W^{-1} for ethylene glycol and 2.8 $\times 10^{-9}$ m^2 K W^{-1} for water. Similar calculation for Yamada-Ota model yields a TBR of 8.9 $\times 10^{-9}$ m^2 K W^{-1} for ethylene glycol and 6.8 $\times 10^{-9}$ m^2 K W^{-1} for water respectively. This corresponds to a thermal boundary conductance (inverse of TBR) in the range of 250-350 MWm^{-2} K^{-1} (EMT fit) and 100 - 145 MW m^{-2} K^{-1} (Yamada–Ota fit) respectively. It is important to note that the estimated TBR value is one order of magnitude lower than the previous experimental report by Huxtable et al. [105] for SDS-encapsulated SWCNTs. Cherkasova and Shan [68] reported TBR of similar order of magnitude for SDBS-encapsulated MWCNTs in water. It need to be noted that such a low TBR obtained from the EMT fit is clearly striking and contradicts the existing experimental and simulation results. The principal reason for this low TBR was that the EMT model does not take into account the effective length (percolated networks) and aggregation effects in the model.

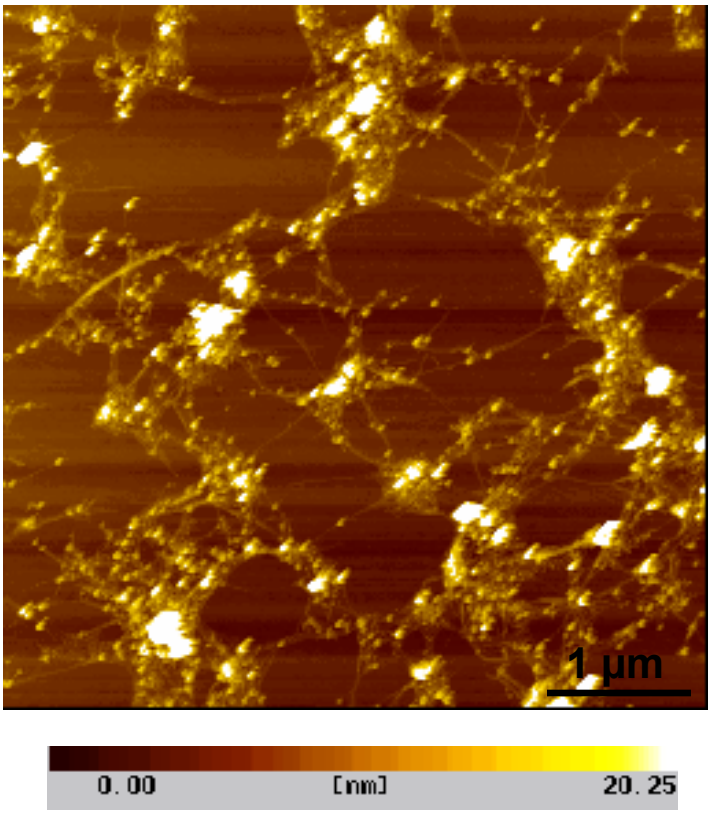

Figure 3.12: AFM visualization of 0.05 vol % SWCNTs. The presence of smaller aggregates and percolated networks to form a long heat transport path is clearly seen.

To clarify the effective length distribution, AFM measurements at a higher concentration of 0.05 vol % SWCNT nanofluid to visualize the percolation behaviour and to calculate the effective length of SWCNTs in the actual suspension which is shown in Figure 3.12. Figure 3.12 clearly shows the presence of small aggregates and connected networks having a percolation path of few micrometers. In Figure 2.9, AFM image taken at very low concentration of 0.005 vol %, the SWCNTs seem to be highly isolated while in Figure 3.12 such a feature is difficult to notice. Since Figure 3.12 corresponds to a concentration much higher than the percolation threshold of 0.0152 vol % (based on electrical conductivity measurements), it is possible to conclude the SWCNTs are in connected networks, although

the exact heat transport length is difficult to measure with our current experimental tools. When the thermal boundary resistance (TBR) is evaluated from models by using the mean aspect ratio as 350 (length 350 nm, diameter 1 nm) obtained from the measured thermal conductivity enhancement, results in an extremely low value of TBR. The low TBR resulting from this fitting is physically unreasonable and contradictory to the experimental results reported in reference [105, 106]. To obtain a TBR which is consistent with the existing literature evidence, by assuming an effective percolation length as of 1.5 - 2.5 μm (aspect ratio 1500 - 2500) and by fitting the experimental data again gives a realistic TBR of (2.1 – 2.8) $\times 10^{-8}$ m^2 K W^{-1} and (4.9 – 8.6) $\times 10^{-8}$ m^2 K W^{-1} for EMT and Yamada–Ota models, respectively. The present values are in good agreement with the existing experimental results.

It is evident from the present experimental results that the large TBR remains a hindrance in increasing the thermal conductivity of the fluid despite the high conductivity of SWCNTs. Based on MD simulations, Xu and Buehler [130] reported that the thermal boundary conductance for bare SWCNT-SWCNT junctions varies from 0.1 to 1 GWm^{-2} K^{-1}, and infiltration of a polymer matrix will further improve the conductance by a maximum of 40 %. Their simulations give an indication that by proper manipulation of TBR much higher thermal conductivity increase can be obtained in nanofluids as well as in nano composites. Besides, the authors also report that coating the CNT surface with metal layers like Au, Ni or Cu can further minimize TBR. This way of metal coating also has additional benefit that the metal layers also contribute to thermal conduction via electron transport. Both the methods are experimentally feasible techniques. However we believe functionalization with materials like polyethylene glycol (PEG) will be the right direction to minimize TBR as metal coating

will further increase the viscosity of the fluid. Such a way of PEG functionalized SWCNTs also have many medical applications [131].

3.4 Viscosity of Nanofluids and Nanofluids Favourability

Figure 3.13 shows the comparison of viscosities of SWCNT/water nanofluids measured using a Cannon Fenske viscometer measured at a constant shear rate. Figure 3.13 shows that the viscosity of the nanofluids increased with increasing SWCNT concentration. The viscosity of the nanofluid decreased as the temperature increased, thus exhibiting similar behaviour of the base fluid.

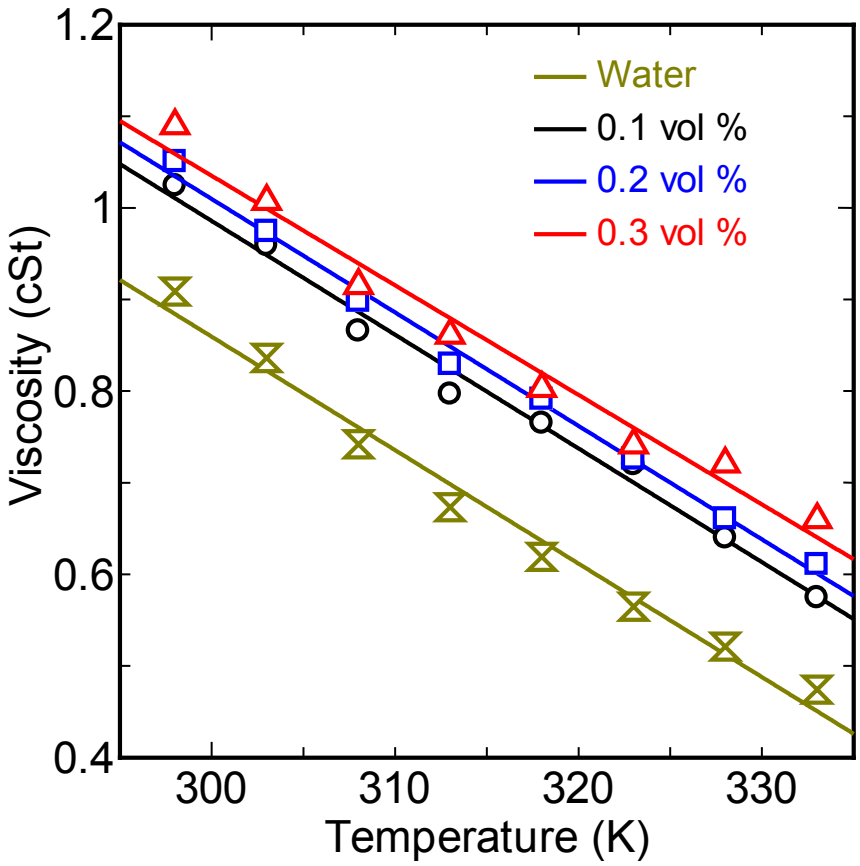

Figure 3.13: Viscosity of SWCNT/water nanofluids

Functional dependence of the viscosity on the temperature of fluid is given by Arrhenius equation as follows [132]

$$\eta = \eta_{\infty} e^{E_a/RT} \tag{3.2}$$

In equation 3.2, η_{∞} is the fluid viscosity at infinite temperature, E_a is the activation energy to the fluid flow, R is the Universal gas constant and T is the temperature in Kelvin. The activation energy and infinite-temperature viscosity are parameters that reflect the fluid behavior. These parameters can be extracted from experimental measurements through the logarithmic form of the Arrhenius equation. Figure 3.14 shows the logarithmic plot of viscosity as a function of inverse of the temperature for SWCNT/water nanofluids. Table 3.1 shows the activation energy of water and water/SWCNT based nanofluids obtained from the Arrhenius plot shown in figure 3.14.

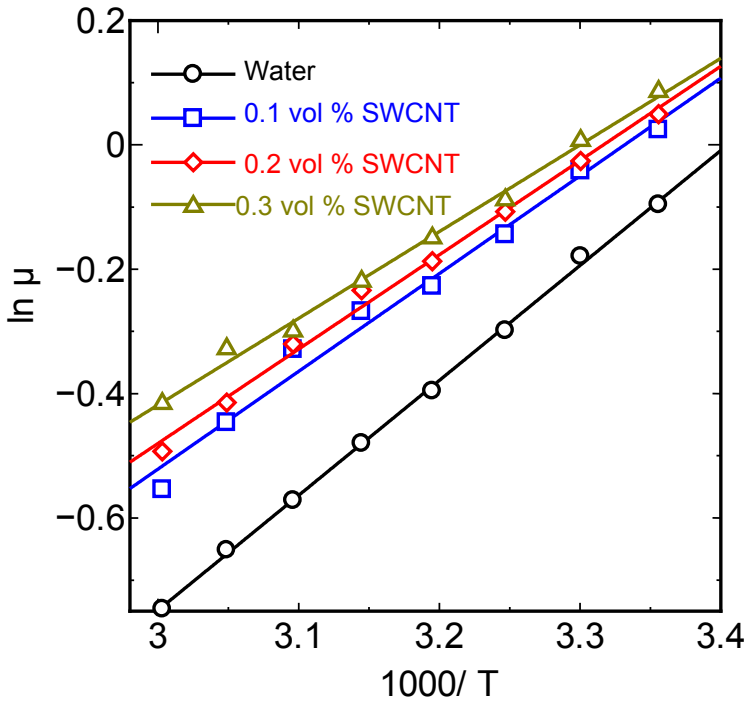

Figure 3.14: Arrhenius Plot of viscosity of SWCNT/water nanofluids.

Table 3.1: Activation Energy of SWCNT/water nanofluids from viscosity measurements

Fluid	Activation Energy (KJ/mol)
Water	15.37
0.1 vol %	13.1
0.2 vol %	12.61
0.3 vol %	11.59

It appears that the addition of SWCNTs to the water tend to decrease the activation energy of the fluid. For nanofluids suspensions, physical interpretation of the activation energy (E_a) has not been developed yet. In general, the activation energy is the energy barrier, which must be overcome, in order for the fluid layers to move past each other. A large E_a indicates that it is more difficult for the fluid layers to move past each other. In fluids the activation energy reflects attraction forces between molecules of the fluid [31]. By analogy in nanofluids E_a values may still reflect attraction forces between molecules of base fluid but their interactions are modified due to the presence of nanoparticles. It need to be noted that similar decrease in the activation energy of water and EG based nanofluids has been reported in the literature with different shapes of aluminum oxide nanoparticles [31].

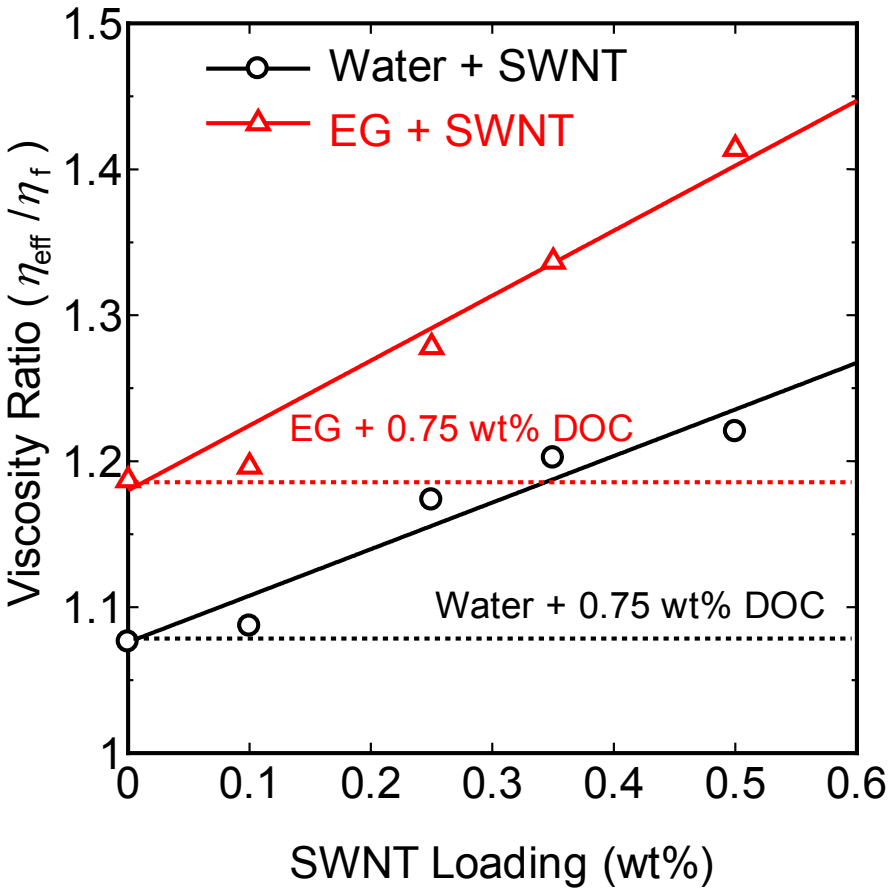

Figure 3.15: Effective viscosity of water and EG based nanofluids with SWCNT inclusions.

Figure 3.15 shows the effective improvement in the viscosity of water and EG based nanofluids. It can be seen from figure 3.15 that the introduction of surfactant gradually increases the viscosity of the base fluid. Moreover, the enhancement in viscosity is much more pronounced than the thermal conductivity improvement for both the fluids.

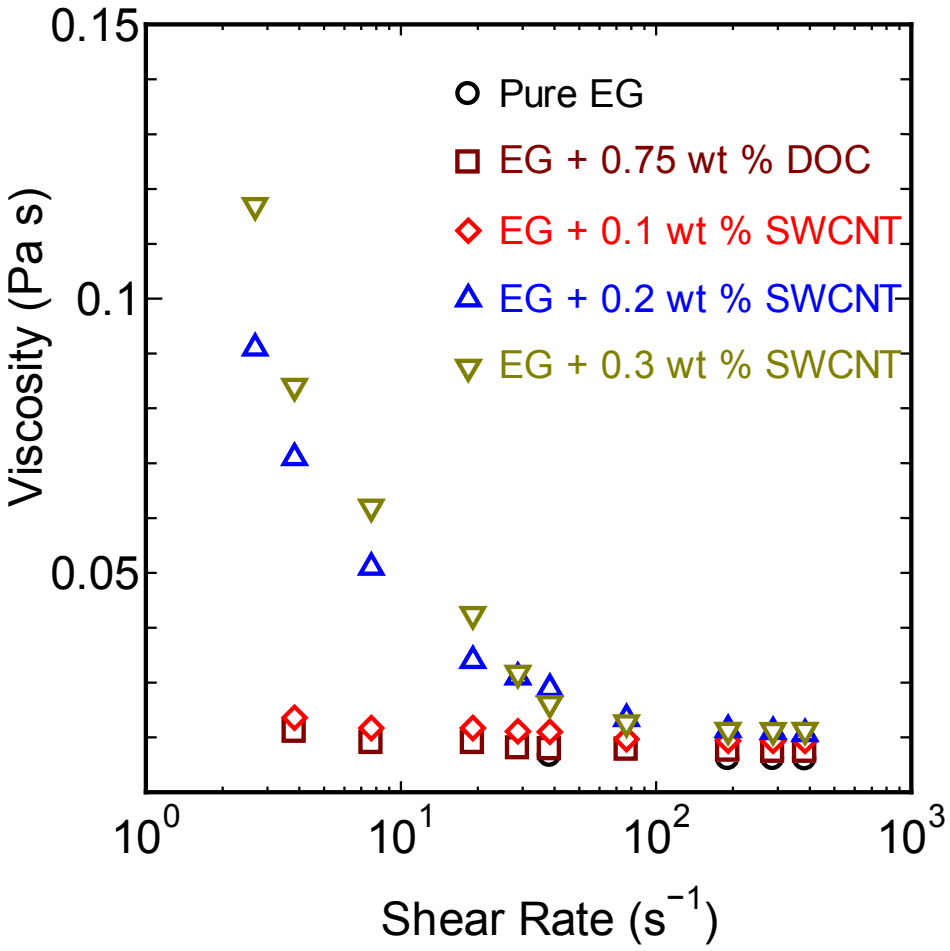

Figure 3.16: Shear Rate dependent viscosity of EG/SWCNT based nanofluids.

Figure 3.16 shows the variation of viscosity with shear rate for EG based nanofluids at room temperature. The viscosity did appreciably vary for shear rates below 100 s^{-1} indicating a clear non -newtonian behavior. However, for shear rates above 100 s^{-1} no appreciable change is noticed. This gives an impression that at low shear rates the fluid behaves non-Newtonian, however at appreciable higher shear rates a Newtonian behaviour is noticed. Current experimental results are in consistent with the previously reported non-Newtonian shear thinning behaviour at appreciably lower shear rates [70, 116-118]. The lower viscosity values

obtained from the glass capillary viscometer is due to its normal operating shear rate of higher than 100 s^{-1} [102].

The effectiveness of such nanofluids depends on the nature of fluid flow in a flow circulating system. Lower viscosity implies lower pumping power that is advantageous for the industrial application. A quantitative expression derived by Prasher et al. [133] for fully developed laminar flow suggests that the use of nanofluid will be beneficial if the increase in the viscosity is less than four times of the increase in in the thermal conductivity. In the present case, the increase in viscosity was approximately three times higher than the thermal conductivity enhancement measured at room temperature. This strong increase in viscosity will have adverse effects in practical applications of such nanofluids. This clearly shows that despite the higher thermal conductivity enhancement efficiencies of such nanofluids will be low due to the higher pumping power required. Hence, to obtain efficient coolant the viscosity need to be reduced by developing better preparation techniques. Reducing the thermal interface resistance of the SWCNTs with proper functionalization and utilization of higher aspect ratio materials will help to improve the thermal conductivity of such fluids.

3.5 Conclusions

In this chapter, the effective thermal conductivity of ethylene glycol and water is presented. Electrical conductivity measurements revealed a sharp increase in electrical conductivity near the percolating threshold, while no such behaviour was noticed for thermal conductivity. Effective thermal conductivity of the nanofluids increases with increasing nanotube loading.

Effective thermal conductivity of the water based nanofluids showed an additional 3–5% increase in conductivity with increasing temperature. Temperature based thermal conductivity enhancement observed in water is attributed to the role of rotational diffusion effects due to the shorter length of nanotubes rather than time dependent aggregation. EG based nanofluids showed a marginal non-linear tendency which is possibly due to the higher degree of agglomeration in such fluids. The difference in degree of agglomeration is clearly evidenced based on the optical absorption, dynamic light scattering and photoluminescence measurements. The experimental results were compared with some existing literature results for MWCNT suspensions. Viscosity of the SWCNT nanofluids increased with increasing SWCNT concentration and showed a threefold increase compared to the thermal conductivity enhancement. Especially EG based nanofluids show a non-Newtonian behaviour at lower shear rates. The experimental results were compared with Nan's effective medium theory and the Yamada–Ota model, the latter of which performed better than effective medium theory and was in good agreement with the experimental data. The critical role of thermal boundary resistance which limits the effective thermal conductivity improvement was discussed, and possible ways to minimize the thermal boundary resistance was recommended as a scope for future research.

Chapter 4

Effect of Carbon Nano Additive Dimensionality in the Thermal Conductivity Enhancement of Nanofluids

4.1 Introduction

In the present chapter systematic investigation of the thermal conductivity enhancement of water, and ethylene glycol in the presence of spherical and two-dimensional carbon nano inclusions is presented. Single-walled carbon nanohorns and exfoliated graphite nanoplatelets were used as the nano inclusions. Thermal conductivity measurements were carried out using a transient hot-wire technique for different temperature and loadings of nano inclusions. It was found that two-dimensional inclusions lead to higher thermal conductivity improvement followed by one-dimensional and spherical inclusions. The potential mechanism behind the thermal conductivity enhancement and the critical yet detrimental role of thermal boundary resistance in limiting the heat conduction is discussed, and the experimental results are compared with classical heat conduction models and other results in the literature.

4.2. Materials and Methods

Single walled carbon nanohorns (SWCNH) and exfoliated graphite nanoplatelets (GnP) were used as the nano inclusions in this work. Figure 4.1 shows the SEM visualization of SWCNH and GnP. SWCNH used in this study typically have diameter in the range 1-3 nm and length of 20-50 nm. Due to the less dense nature of SWCNHs, the material is dispersed in the base

fluids without using any additional surfactant. GnP used in this study typically have a length of upto 25 μm and diameter of 4-10 nm. Figure 4.2 shows the TEM visualization of SWCNH and GnP.

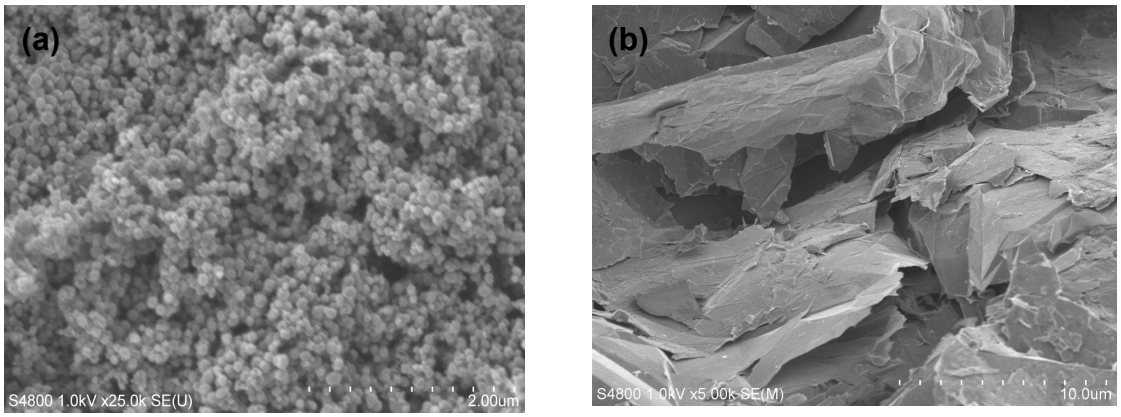

Figure 4.1: Scanning electron microscopy visualization of (a) Single Walled Carbon Nanohorns (SWCNH) (b) Exfoliated Graphite Nanoplatelets (GnP)

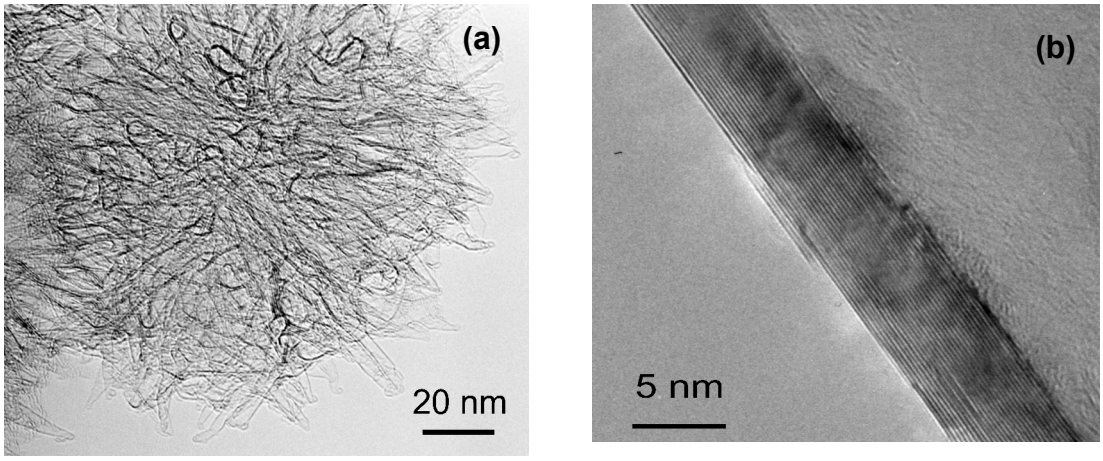

Figure 4.2: Transmission electron microscopy visualization of (a) Single Walled Carbon Nanohorns (SWCNH) (b) Exfoliated Graphite Nanoplatelets (xGnP)

To disperse the GnP in water and EG, sodium deoxycholate (DOC) is used as the surfactant. The nanofluids were subjected to bath sonication for 90 minutes followed by a tip sonication for a period of 30 minutes with a power level of 200 W. AFM visualization of the exfoliated platelets post sonication is shown in Figure 4.3. From Figure 4.3 it can be noticed that the length of the flakes is in the range of few µm long and the thickness distribution lies in the range 4-10 nm.

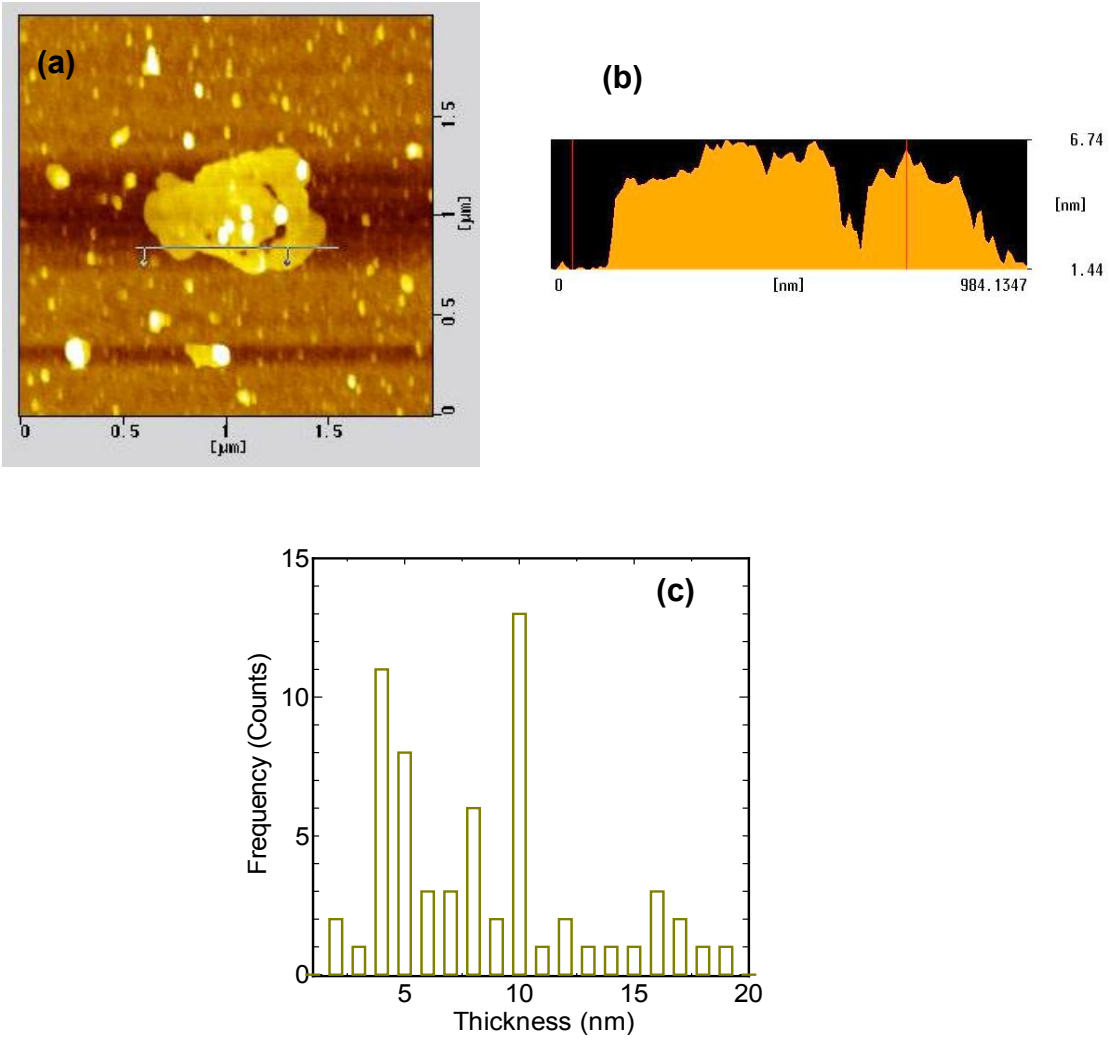

Figure 4.3: AFM visualization of xGnP. The graphite flake thickness distribution lies in the range of 4-10 nm predominantly.

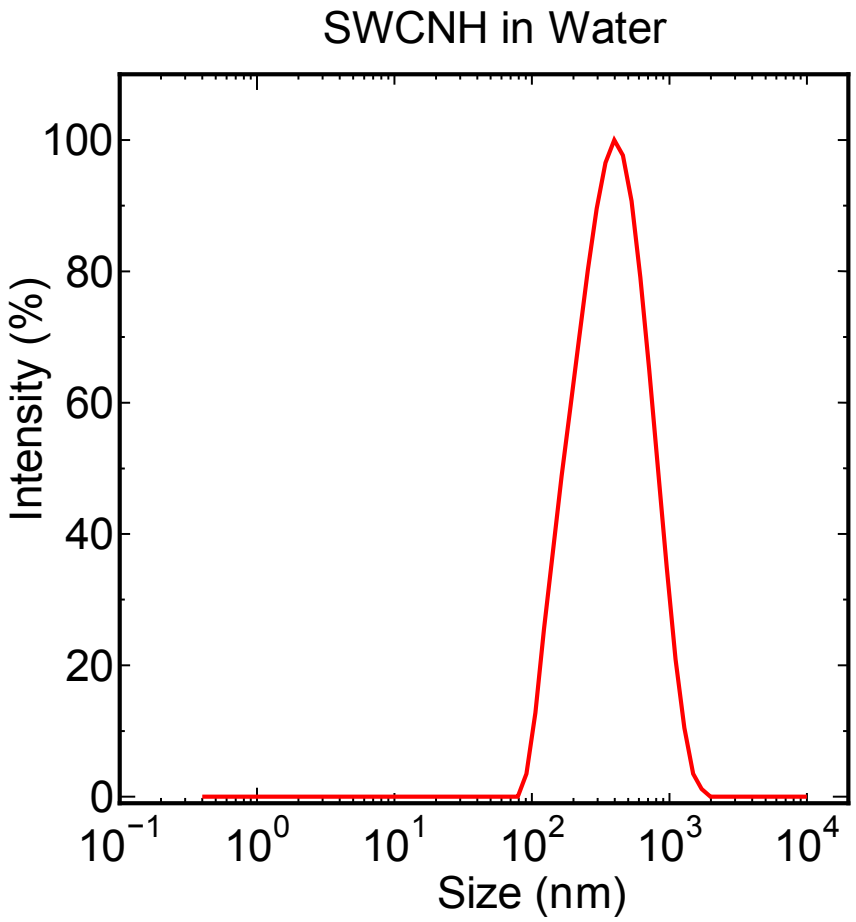

Figure 4.4: Size distribution of SWCNH in water

Figure 4.4 and 4.5 shows the size distribution of SWCNH in water and ethylene glycol respectively. It can be seenfrom figure 4.4 that the in the case of water the size distribution is rather broad and 100 nm - 1 μm with a maximum peak around 400 nm. This shows that the SWCNH is dispersed in water better compared to the case of ethylene glycol. Figure 4.5 shows the size distribution in ethylene glycol is rather compact with a narrow size distribution with a maximum peak around 800 nm. This observation is in consistent with the

size distribution of SWCNTs in different base fluids where ethyleen glycol always demosntrated a tencdency to exist in the form of aggregates compared to the case of water.

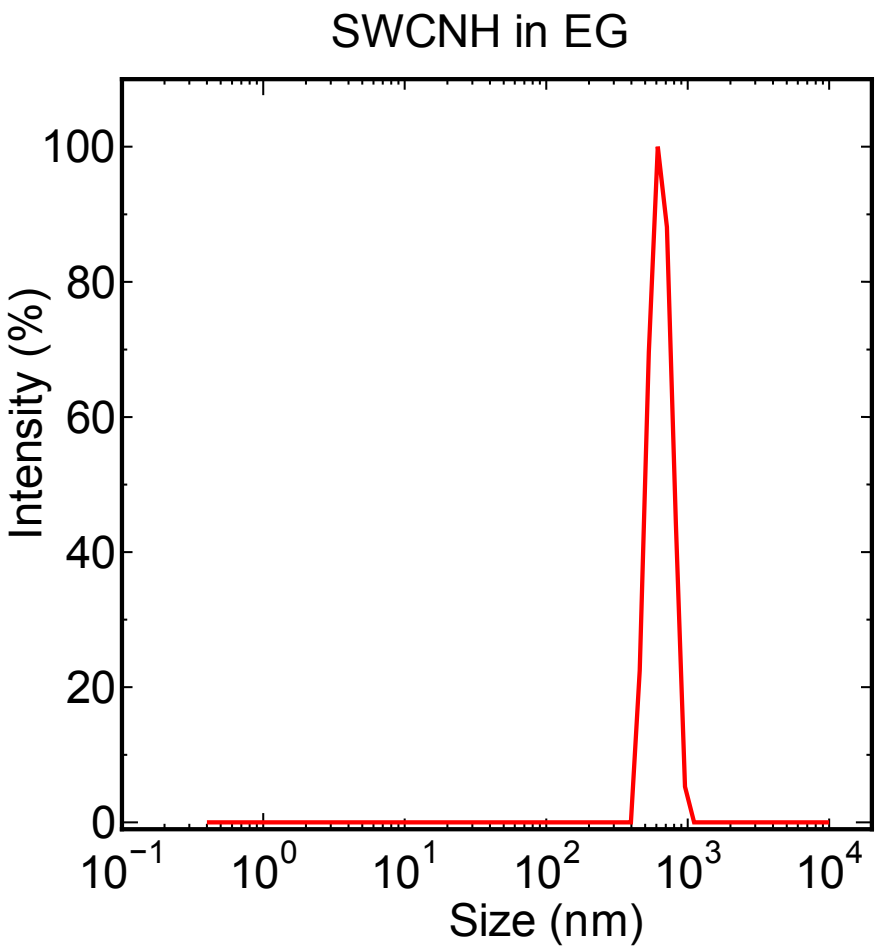

Figure 4.5: Size distribution of SWCNH in EG

4.3 Enhanced Thermal Conductivity with SWCNH and GnP

Thermal conductivity measurements were carried out using the transient hot wire technique for different loadings of nano inclusions in water and ethylene glycol. Figure 4.6 shows the thermal conductivity enhancement of water with SWCNH inclusions along with the

predictions of Maxwell's model. The thermal conductivity increases linearly with increasing SWCNH loading for the weight fraction ranging from 0.5 wt % - 2 wt %. Figure 4.6 shows that the experimental results are in consistent with the predictions of Maxwell's model. It is possible to conclude that for well dispersed nano inclusions the predictions of classical models is still valid.

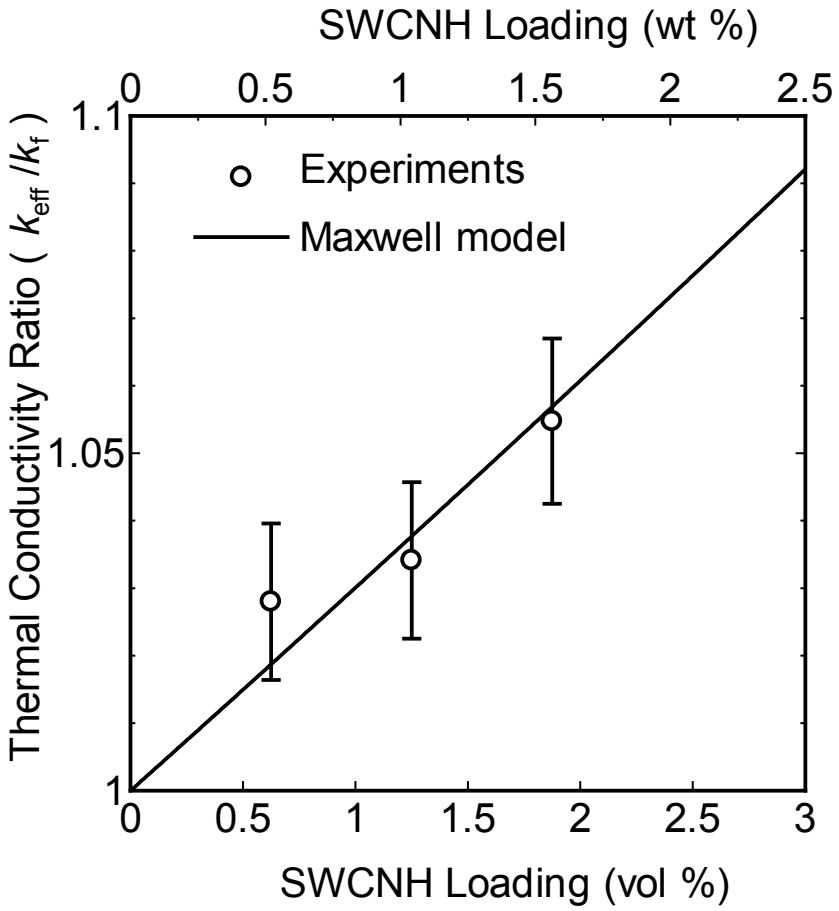

Figure 4.6: Enhanced thermal conductivity of Water as a function of SWCNH Loading and comparison with theoretical models. Predictions of Maxwell's model are in good agreement with the experimental results.

Figure 4.7 shows the thermal conductivity enhancement of SWCNH based nanofluids in ethylene glycol along with the predictions of theoretical models. A larger improvement is

seen in the case of ethylene glycol compared to the case of water. This observation is in contradiction to the Maxwell's theory [12] where the theory predicts a constant enhancement irrespective of the base fluid conductivity when the additive materials' conductivity is much higher than the base fluid conductivity. Interestingly, the enhancement noticed is twice the predictions of Maxwell's model which is consistent with previous report of CuO suspensions in Ethylene glycol [134] and nano-diamond suspensions in mineral oil [28].

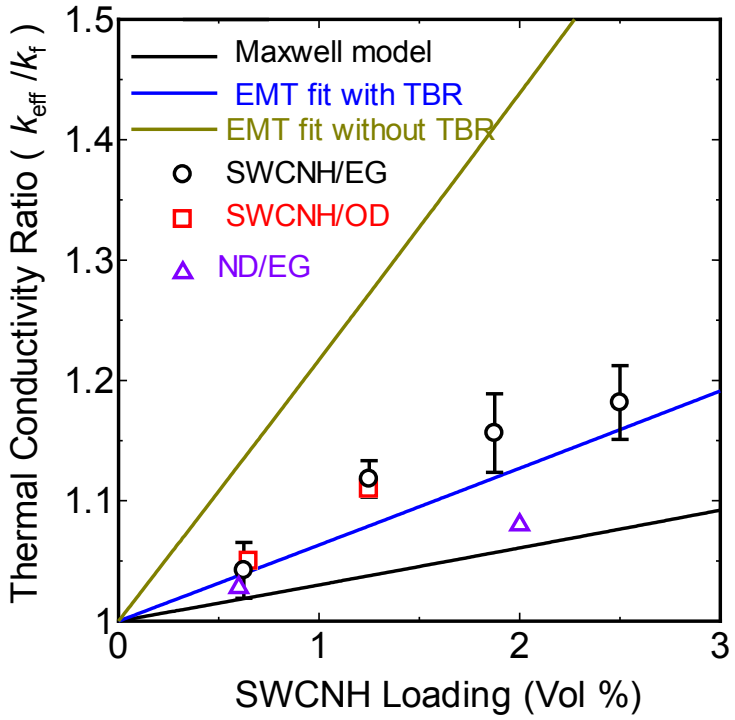

Figure 4.7: Enhanced thermal conductivity of EG as a function of SWCNH Loading and comparison with theoretical models. The experimental results are approximately a factor 2 higher than the predictions of Maxwell's model. Similar results are obtained for SWCNH/Octadecane (OD) suspensions. For Nano-diamond/Ethylene Glycol suspensions the enhancement is marginally higher than Maxwell model's prediction. The experimental results are fitted using EMT model assuming the aggregates to acts as rods of aspect ratio 10. EMT model predictions with and without the presence of TBR is also shown.

The deviation from the predictions of Maxwell model is possibly due to the level of aggregation noticed in ethylene glycol as noticed from the DLS results. The experimental results are fitted using EMT model [103] assuming the aggregates to form rods of aspect ratio 10 and taking the interfacial resistance into account. The interfacial resistance used in the calculations is of the order 10^{-8} $m^2K\ W^{-1}$. From figure 4.6 and 4.7 and based on the DLS results it is possible to conclude that for sufficiently well dispersed samples, thermal conductivity enhancement is rather limited and is in consistent with the predictions of classical models. When the suspensions tend to form aggregates a deviation from the classical models predictions may be more pronounced. The contradictory thermal conductivity enhancements reported in the literature for different nanofluid suspensions may possibly due to the different level of aggregation and the lack of proper characterization methods to evaluate the size distribution of the nanomaterials in different fluids. The present experimental results show a marginal deviation from the Maxwell model's predictions. However, the percentage of enhancement is still less enough than the case of SWCNT based nanofluids.

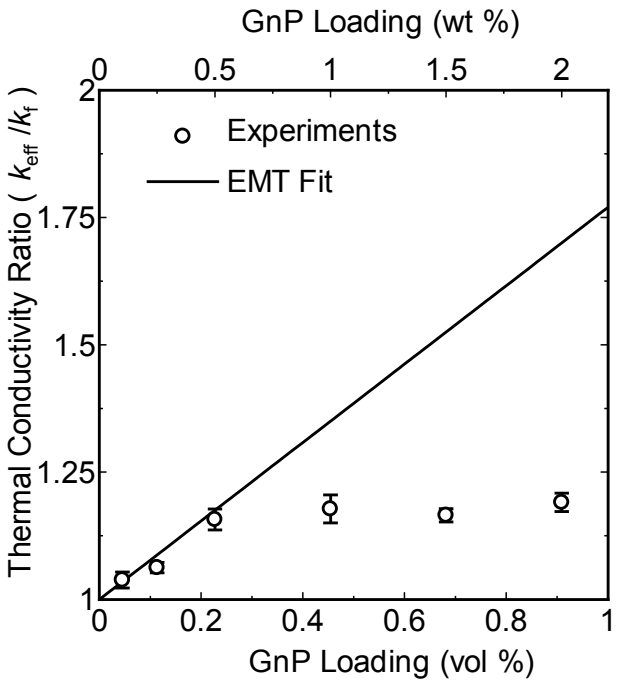

Figure 4.8: Enhanced thermal conductivity of water/GnP nanofluids and comparison with EMT prediction.

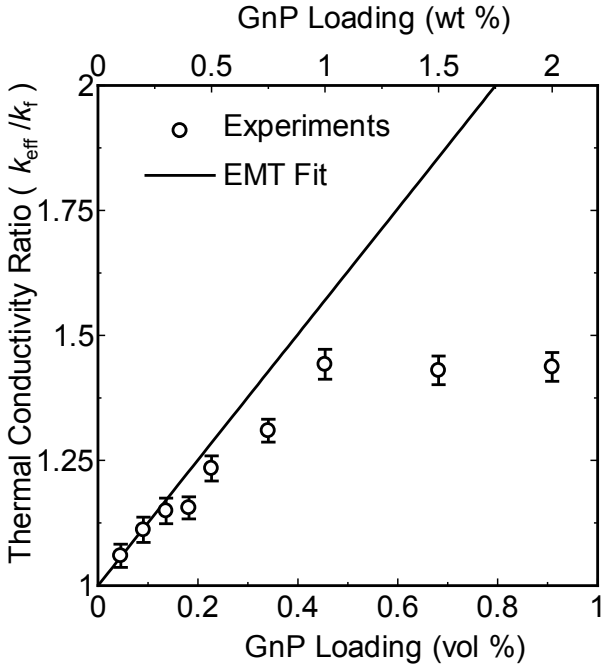

Figure 4.9: Enhanced thermal conductivity of EG/GnP nanofluids and comparison with EMT prediction.

Figure 4.8 and figure 4.9 shows the thermal conductivity enhancement of water and ethylene glycol with GnP inclusions along with the predictions of EMT model [103] assuming the GnP fakes as oblate spheroids and taking the interface resistance into account. Unlike the case of SWCNH, the thermal conductivity enhancement increases linearly upto a certain loading and remains saturated beyond a certain loading. A maximum enhancement of 17 % is noticed for water at 0.2 vol % and 43 % for EG at 0.5 vol %. Beyond the respective loadings increasing the loading of GnP does not increase the thermal conductivity of the base fluid.

The present experimental results are contradictory to the predictions of EMT model where the thermal conductivity increases with increasing nanomaterials loading. EMT model fail to explain the saturation behaviour observed in GnP based nanofluids. The present results are also contradictory to the recent results of Baby et al. [135] where the authors show 'anomalous' enhancement at very low concentration of graphene loading and also that of Zheng et al. [136] where the authors show a non-linear enhancement upto 1 vol % (2.2 wt %) in ethylene glycol and PAO based nanofluids. Besides, they also reported that the thermal conductivity increases linearly till the electrical percolation threshold beyond that it takes a "kink" but continue to increase with a different slope [136]. The electrical percolation threshold for graphite suspensions lie in the range of 0.1 vol % - 0.3 vol %. The present experimental results are partially consistent with the previous observation. However, instead of a change in the slope as reported in the previous case, the present experiments show level-off behaviour. Such level-off behaviour was previously reported for MWCNT suspensions in water by Ding et al. [70] at room temperature. Level-off behaviour may be attributed to the

mutual interaction between the graphite platelets leading to a large interfacial thermal resistance thereby limiting the heat flow path with increasing loading of the nanoplatelets**.** Besides, amorphous carbon impurities and defects in the graphite suspensions may also contribute to the increase in thermal resistance. This scenario is not noticed in the case of spherical inclusions because of its inability to form stronger percolated networks at the material loadings considered in this present study.

In previous experiments with SWCNT suspensions in water and ethylene glycol, a small temperature dependent enhancement is noticed in the case of water but not in ethylene glycol. Here, the thermal conductivity enhancement is also evaluated as a function of temperature for fixed nanomaterial loading. Figure 4.10 shows the thermal conductivity enhancement as a function of temperature in water based nanofluids for different nano inclusions. For the case of SWCNH and GnP nano-inclusion no temperature dependent thermal conductivity enhancement is noticed. This rule out the possibility of Brownian motion and micro-convection as the possible mechanisms for heat transfer enhancement in nanofluids. As previously discussed, the small temperature based enhancement noticed in the case of SWCNT inclusions may possibility attributed to the rotational motion of shorter nanotubes and also the reduction in thermal boundary resistance at increasing temperature.

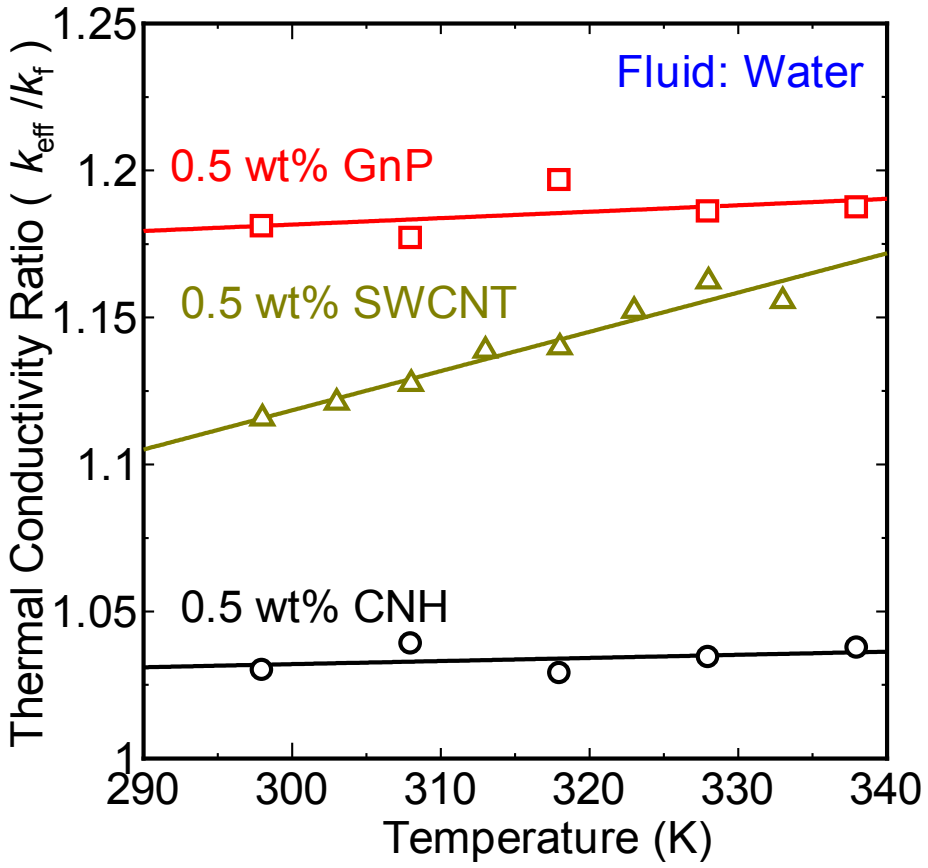

Figure 4.10: Effect of fluid temperature on the thermal conductivity enhancement in carbon based nanofluids.

4.4 Conclusions

In this chapter, the role of dimensionality of carbon allotrope in the thermal conductivity enhancement is discussed. Single walled carbon nanohorns and exfoliated graphite flakes were used as nano inclusions. SWCNH inclusions lead to modest thermal conductivity enhancement in a linear fashion while the inclusion of GnP shows a level-off behaviour. For the case of SWCNH based nanofluids in water, the experimental results are in good agreement with the predictions of Maxwell's model. However, in the case of SWCNH

inclusions in ethylene glycol, the effective enhancement is twice the predictions of Maxwell's model due to the formation of aggregates. Exfoliated graphite based nanofluids show a level-off behaviour which is contradictory to the predictions of effective medium model where the model predicts a linear enhancement with the material loading while the experimental results tend to saturate beyond a threshold loading. Further both the nano inclusions do not show any temperature dependent enhancement as previously noticed in the case of SWCNT suspensions. The experimental results also rule out the possibility of Brownian motion and Brownian assisted micro-convection as the possible heat conduction mechanisms in nanofluids and support the mechanism of particle aggregation. Based on the systematic comparisons it can be concluded that the spherical particles have low impact in thermal conductivity enhancement while SWCNTs and GnP can contribute significantly. Inability to disperse large amount of SWCNTs remains a concern while higher loading of GnP does not contribute due to large thermal resistance at higher loading.

Chapter 5

Enhanced Thermal Conduction Characteristics of Phase Change Composites with Single Walled Carbon Nanotube Inclusions

5.1 Introduction

In this chapter strikingly large contrasts in the thermal conductivity enhancement of phase change alkane in liquid and solid state with single walled carbon nanotube (SWCNT) inclusions. With a small SWCNT loading of 0.25 wt% a strikingly high 250% enhancement is achieved in the solid state and a nominal enhancement of 10% is achieved in the liquid state. The thermal conductivity contrast between solid and liquid state was found to increase with increasing SWCNT loading. The thermal conductivity contrast was more pronounced in the presence of SWCNTs compared to the presence of exfoliated graphite nanoplatelets reported in the literature.

5.2 Thermal Conductivity in Phase Change Materials

There has been considerable interest to increase the thermal conductivity of organic phase change materials using different nano inclusions. Recently, Zheng et al. [137] reported a contrasting thermal conductivity enhancement between solid and liquid states by a factor of 3.2 in *n*-hexadecane with 1 vol% loading of graphite inclusion during the first-order phase transition process. Such a contrasting enhancement for the same loading of nano inclusion is clearly surprising, and this observation was similar to previous 'anomalous' thermal

conductivity enhancements that were reported in the literature for nanofluid suspensions [10, 11, 135]. A recent review on thermal conductivity enhancement in carbon nanotube (CNT) based polymer composites shows that the significant thermal conductivity enhancement can be achieved with single walled carbon nanotubes despite the high thermal interface resistance between the nanotubes and the polymer matrix [138]. The magnitude of enhancement varies on many factors such as the type of CNT used, functionalization, purity, degree of alignment etc [138]. Especially single walled carbon nanotubes based phase change nanocomposites with its unique optical absorption properties along with improved thermal conductivity and light harvesting effects makes it a suitable candidate for novel solar thermal energy storage materials as demonstrated recently using artificially synthesized polymer/SWCNT phase change composite [139].

In this work using an organic phase change material that a contrasting thermal conductivity enhancement occurs in the solid and liquid phase when single-walled carbon nanotube dispersed using sodium deoxycholate is used as nano inclusions. A strikingly high contrast ratio of nearly 3 is achieved at an ultra-low loading of 0.25 wt%. The present experimental results show an anomalous enhancement beyond the predictions of effective medium theory in the solid state. The present work introduce an efficient way to manipulate the thermal conductivity of nano composites using one-dimensional nanomaterial inclusion by effectively controlling the heat transport path simply via temperature regulation. Such a phase change material with enhanced thermal conductivity makes it a promising candidate for thermal energy storage applications.

5.3 Materials and Methods

The exfoliated graphite nanoplatelets (GnP) used in this study was purchased from XG Sciences, USA [Grade-M, 6-10 nm thickness]. The SWCNTs used in this study were synthesized by the alcohol catalytic chemical vapour deposition (ACCVD) technique using cobalt and iron bi-metallic catalysts supported on zeolite particles (HSZ-390HUA). From AFM measurements for DOC dispersed SWCNTs we found that the length distribution lies in the range of 100 nm – 700 nm after sonication.

The synthesized SWCNTs and GnP were dispersed in *n*-Octadecane (*n*-$C_{18}H_{38}$) [99.5% purity purchased from Sigma Aldrich] whose freezing point is close to 300K, using 0.75 wt% of the surfactant sodium deoxycholate (DOC), to create stable dispersions based on our previous studies. The dispersions were subjected to sonication using an ultrasonic processor (Hielscher GmbH, UP-400S with H3/Micro Tip 3) for two hours at a power flux level of 320 W/cm^2 (80% amplification). Based on the Atomic Force Microscopy visualization (AFM) of the SWCNTs after sonication, we found that for DOC dispersed SWCNTs, the length distribution lies in the range of 100 nm – 700 nm after sonication.

Thermal conductivity measurements were carried out using the transient hot wire technique which is described elsewhere. The suitability of transient hot wire technique for liquids with nano suspensions has been questioned significantly because of the 'Brownian motion' of the nanoparticles. However, a recent benchmark study on nanofluids performed using different measurement methods clearly demonstrated the suitability of this technique for nanofluids

[32]. Additionally, the transient hot wire method has the benefit of being applicable to both fluids and solids, and is quite frequently utilized for the phase change thermal conductivity measurements of nano suspensions [140]. Hence, in this work we have used the transient hot wire method owing to its versatility in the thermal conductivity measurements of wide temperature range.

5.4 Results and Discussion

The thermal conductivity measurement results of the *n*-Octadecane (*n*-$C_{18}H_{38}$) with different loadings of GnP inclusions showed that the thermal conductivity contrast increased with higher GnP loading as shown in figure 5.1. A contrast ratio of approximately 2.1 was achieved at a GnP loading of 0.45 wt%. The present experimental enhancement with GnP were consistent than the results with graphite suspensions reported by Zheng et al.[137]

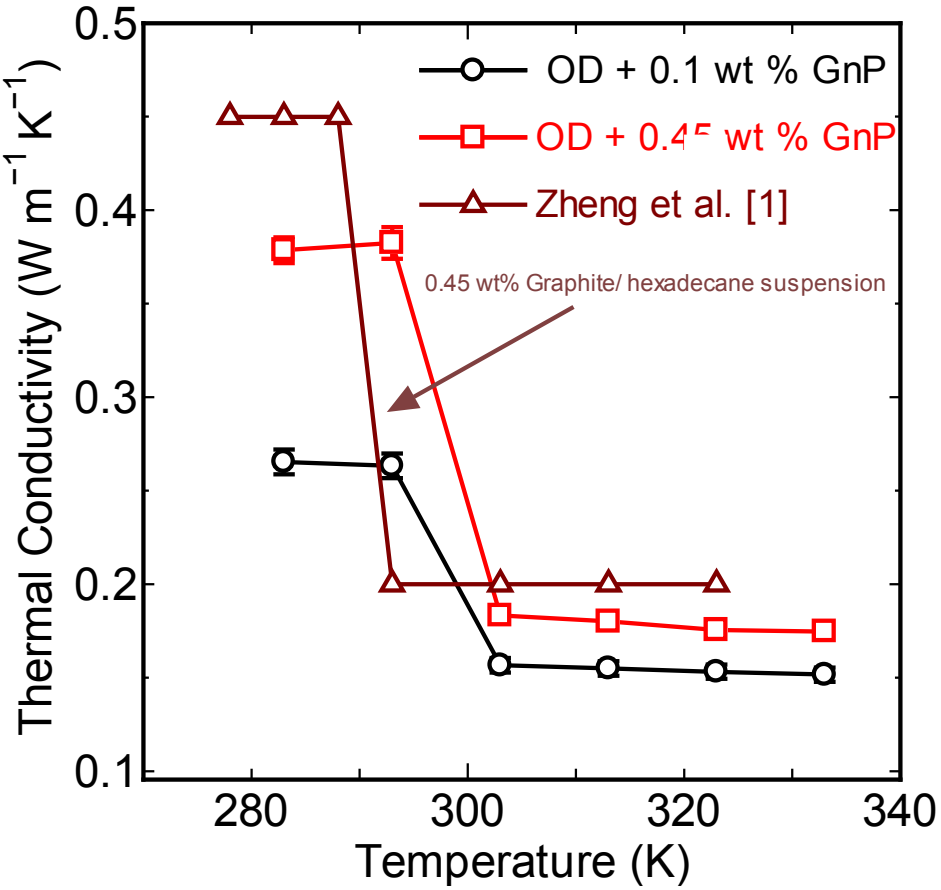

Figure 5.1: Comparison of the GnP (graphene nanoplatelets) dissolved into OD (*n*-octadecane) with different loadings and the graphite dispersed into *n*-hexadecane reported by Zheng et al. [137] Sharp increase in thermal conductivity is noticed during freezing with two dimensional graphite nanoplatelets as inclusions.

The thermal conductivity measurement results of the *n*-Octadecane (*n*-$C_{18}H_{38}$) with loadings of SWCNT inclusions and temperature as parameters showed that the thermal conductivity contrast increased with higher SWCNT loading, as shown in figure 5.2(a) and 5.2(b). The present experimental values of the pristine *n*-Octadecane (*n*-$C_{18}H_{38}$) thermal conductivity were consistent with the literature values [141]. With the inclusion of SWCNTs, a limited

improvement in thermal conductivity of 10% was noticed in liquid state while a larger improvement of 250% in the solid state was noticed with increasing SWCNT loading. The present thermal conductivity enhancement obtained in the solid state with very low loading of SWCNT is markedly superior to the results of titanium dioxide nanoparticles [142], graphene additives [143] and exfoliated graphite platelets [144]. This clearly indicates the suitability of SWCNTs as the appropriate nano filler material to enhance the thermal conductivity of organic phase change materials. Besides in this study maximum thermal conductivity contrast ratio of 2.92 was reached at much lower SWCNT loading of 0.25 wt% (~ 0.15 vol%). The present results are also superior compared with the graphite inclusion in *n*-hexadecane in which a contrast ratio of 3.2 is achieved at a much higher loading of 1 vol% [137].

In the present study, measurements are limited to low SWCNT loadings because of the difficulty in achieving good stability at higher loading of SWCNT with the current surfactant assisted dispersion method. Dispersing SWCNTs of large aspect ratio without the aid of sonication techniques or chemical functionalization methods is difficult. The former method reduces the length of the SWCNTs while the latter introduces structural defects in the SWCNTs thereby reducing the inherent thermal conductivity and also acts as defect sites to scatter phonons. However, with improved dispersion techniques and/or synthesizing SWCNTs of high purity and long aspect ratio there is a potential for achieving higher thermal conductivity contrast and higher thermal conductivity enhancement in phase change materials with nano inclusions of SWCNTs.

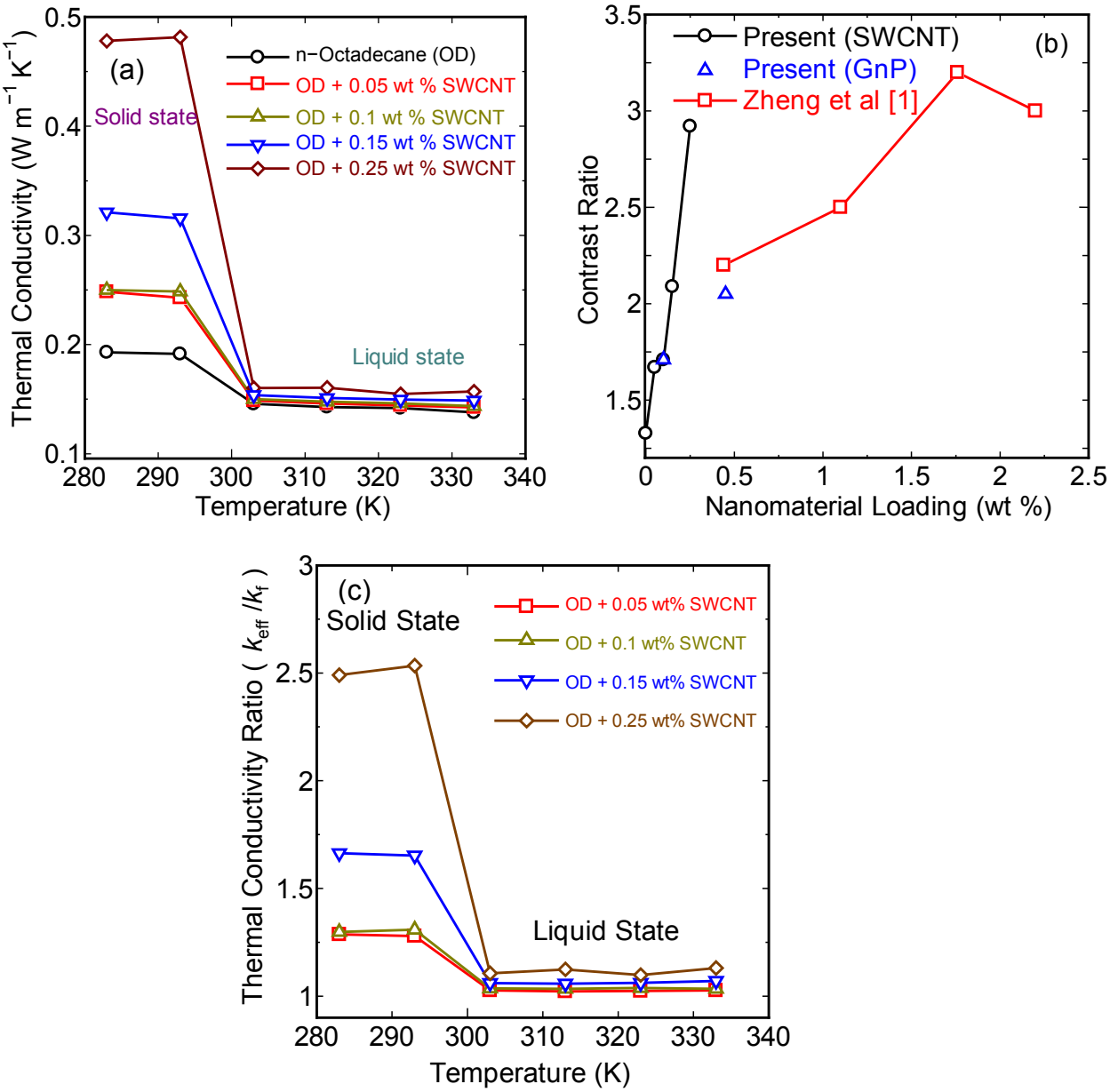

Figure 5. 2: (a) Thermal conductivity of *n*-Octadecane as a function of temperature for varying SWCNT loadings. A sharp increase in thermal conductivity in the solid state is seen. (b) Contrast ratio (solid state thermal conductivity to liquid state thermal conductivity) as a function of SWCNT loading. Maximum contrast ratio of 2.92 is achieved at a SWCNT loading of 0.25 wt%. (c) Thermal conductivity enhancement as a function of temperature for different SWCNT loading.

Higher thermal conductivity enhancement observed in the solid state possibly indicates the formation of continuous networking structure during the phase transition process. We hypothesize during freezing, when the crystals begin to nucleate forming needle like structures the SWCNTs are gradually pushed to the grain boundaries thereby leading to form a continuous quasi-2D network of bundles which in turn recovers its original form when melted back. No significant thermal conductivity improvement was noticed in the liquid state due to the absence of such continuous structures as the heat conduction is heavily limited by high interface resistance between the SWCNT and the surrounding fluid and contact resistance between SWCNTs. A recent simulation study shows that the heat transport in SWCNT materials strongly depends on the length of the nanotubes and their structural arrangement in the material [145]. Mesoscopic simulation studies of thermal conductivity of 3D SWCNT networks, quasi-2D films and self-organized networks of CNTs show strong quadratic length dependence and an order of magnitude increase in thermal conductivity due to efficient heat transport pathways caused by the CNT bundles [145]. The present thermal conductivity enhancement observed in this work can be comparable to the existing simulation results where the formation of strong network structures in the solid phase when the SWCNTs are pushed to the grain boundaries might have lead to this higher thermal conductivity enhancement.

Another possible mechanism is that alkane molecule surrounding the nanotubes when frozen to solid state exhibit a tendency to form lamellar layers along nanotube axis and exhibit two-dimensional structural ordering in planes perpendicular to the nanotube axis which is similar to the crystalline polymers [146]. Hence it may be possible that the two dimensional

structural ordering of SWCNTs and SWCNT induced molecular alignment during phase transition can lead to the high thermal conductivity enhancement of the nano composite in frozen state [146, 147].

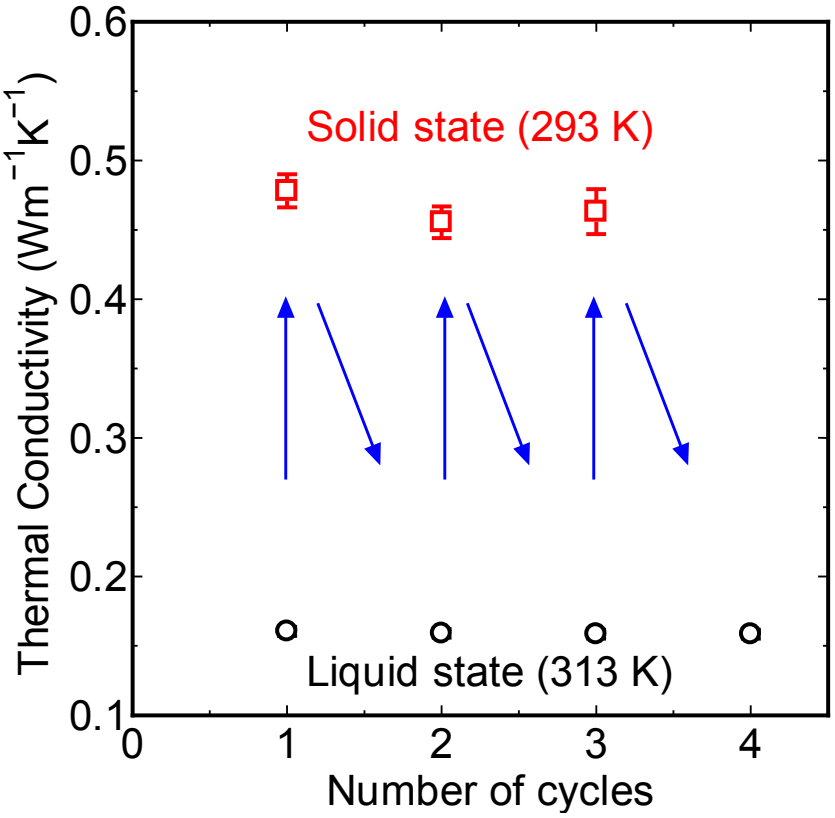

Figure 5.3: Recycling behaviour of thermal conductivity during successive phase transition cycles at SWCNT loading of 0.25 wt%. Arrows indicate the sequence of cycles.

The process remained reversible for the subsequent cycles as shown in figure 5.3. When the nano composite was reheated back to the same liquid state, the original 3D networks of the dispersions might recover or molecular disordering occurs which disrupts the crystalline structure of the alkane. Hence, the liquid state thermal conductivity enhancement remains lower than the solid state thermal conductivity.

Such reversibility and high thermal conductivity contrast is noticed irrespective of whether the inclusion is SWCNTs, or GnPs. The present experimental results show that much higher thermal conductivity contrast and high conductivity enhancement was achieved with lower loading of SWCNTs as compared to the GnP. This may possibly due to the ability of the SWCNTs to induce the formation of stronger crystalline networks than GnPs [146, 148]. Besides, the superior performance of SWCNTs over GnPs may possibly due to the tendency of alkane chain to get adsorbed on to the CNT surface and align themselves parallel to the axis of the CNT, while the alkane chains show multiple orientations on the GnP surface [149].

The effective thermal conductivity of the composites is also estimated using classical theoretical models. Assuming the SWCNTs as randomly oriented rigid ellipsoidal structures and taking into account the effect of thermal boundary resistance (TBR), the effective thermal conductivity enhancement is calculated using Maxwell-Garnett type effective medium theory (EMT) as reported by Nan et al. [103] and a modified Yamada – Ota empirical model as reported in Zheng and Hong [111,112]. For the present model calculations, we made use of the fluid state thermal conductivity of 0.143 W m^{-1} K^{-1},[11] solid state thermal conductivity of 0.193 W m^{-1} K^{-1} [141], SWCNT thermal conductivity of 1000 $Wm^{-1}K^{-1}$, and SWCNT aspect ratio (L/d) of 500 based on our atomic force microscopy (AFM) measurements. The thermal boundary resistance (TBR) was taken of the order of 10^{-8} m^2 K W^{-1} and assumed to be constant over the range of temperature tested. In these models the SWCNTs were assumed as rigid rods and the influence of the waviness of the SWCNTs was neglected.

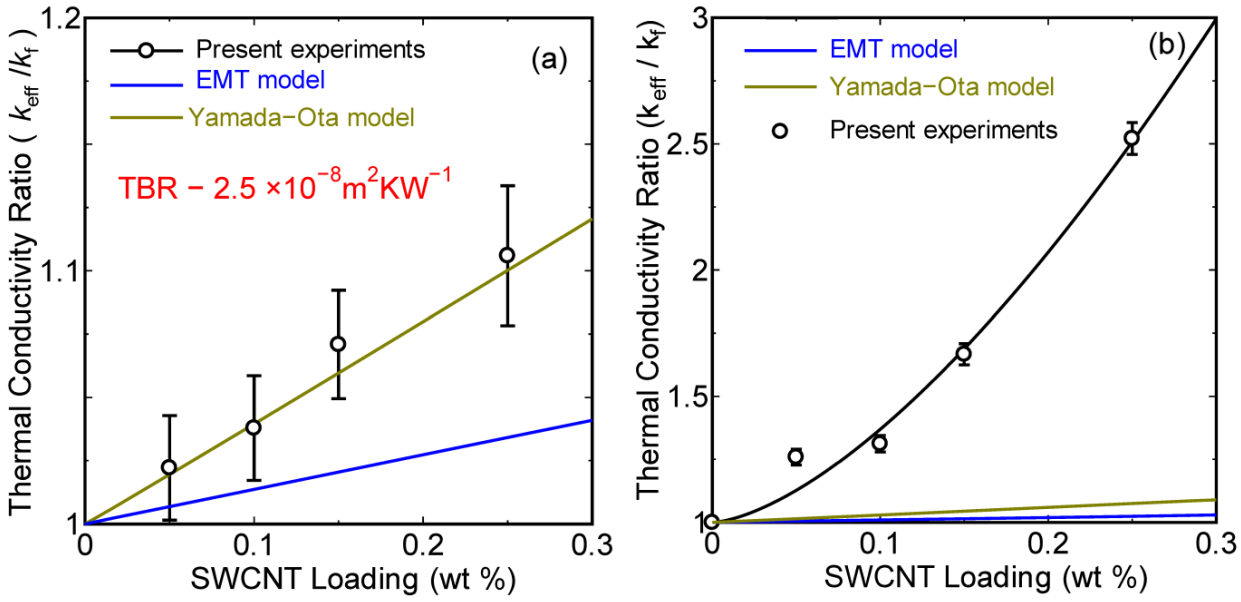

Figure 5.4: (a) Thermal conductivity enhancement in liquid state as a function of SWCNT loading. Modified Yamada-Ota model predict the present experimental results with a TBR of 2.5 x 10^{-8} m^2 K W^{-1}. EMT model prediction for the same TBR in the liquid state is marginally lesser compared to modified Yamada-Ota model. (b) Thermal conductivity enhancement in solid state as a function of SWCNT loading. The theoretical models fail to predict the enhancement in solid state as the influence of aggregation during first order phase transition is not included in the models. The experimental results were fitted with a power law equation of form $A\phi_w^b$ where A and b were fitting constants and ϕ_w is the SWCNT weight fraction. The fit parameters were 12.6 and 1.53 for A and b respectively.

Figure 5.4(a) and 4(b) show the effective thermal conductivity enhancement in liquid state and solid state along with the predictions of theoretical models. In the liquid state, the

thermal conductivity enhancement was in a linear fashion with respect to the SWCNT loading as shown in figure 3(a). The modified Yamada-Ota model can predict the experimental results with a TBR of 2.5×10^{-8} m^2 K W^{-1} (Thermal boundary conductance of 40 MW/m^2K) while the EMT model predicted a marginally lower enhancement with the same TBR. Limited experimental and numerical results exist for the boundary resistance between SWCNT and the surrounding interface. The extracted thermal boundary resistance based on our model calculations (2.5×10^{-8} m^2 K W^{-1}) is comparable with the existing experimental results for surfactant encapsulated SWCNT interfaces in water (8×10^{-8} m^2KW^{-1})[105, 106] and simulation results of SWCNTs surrounded by octane medium (3.4×10^{-8} m^2 K W^{-1}) [107].

However, both theoretical models fail to explain the high thermal conductivity enhancement noticed in the solid state. Besides, the enhancement in the solid state remains non-linear with respect to SWCNT loading while in the liquid state a linear enhancement is noticed. Failure of the classical models to explain the enhancement in solid state may due to the assumption that the thermal boundary resistance is assumed to be constant and the role of aggregation is not taken into account in the calculations. It may be possible that the thermal boundary resistance in the liquid phase and crystalline phase is different as noticed in the recent simulations [148]. Further experiments to probe the thermal boundary resistance using time domain thermoreflectance measurements will facilitate better understanding of the interface effects and help in improving theoretical models.

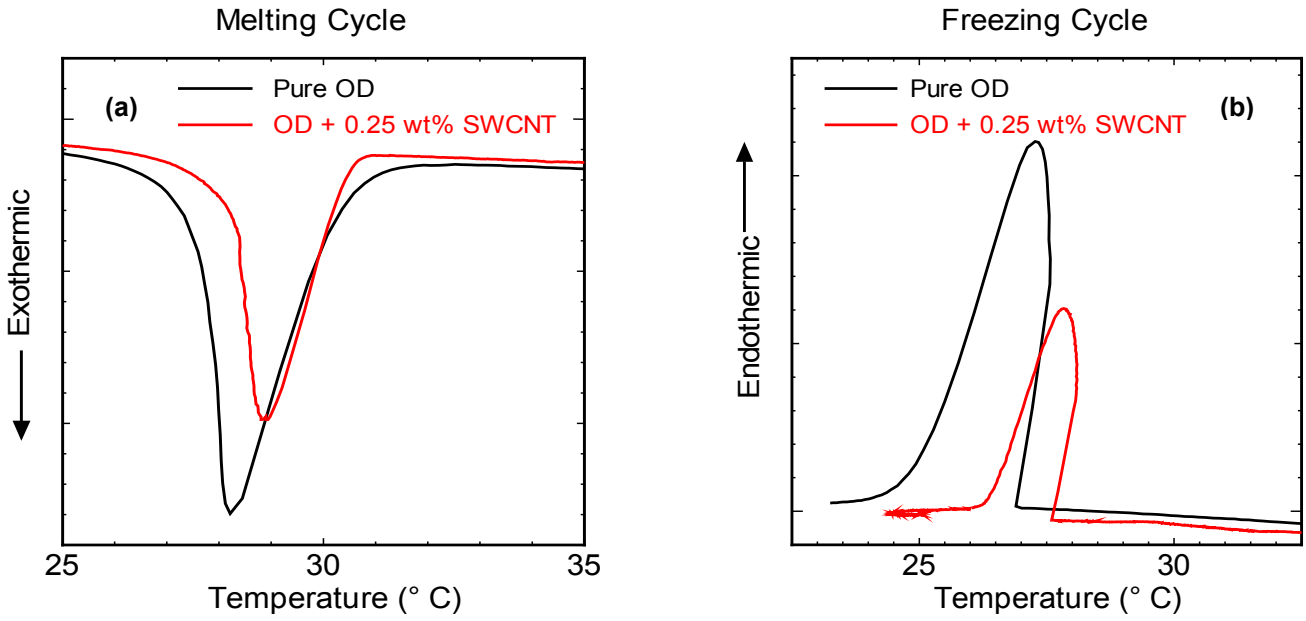

Figure 5.5: (a) Differential Scanning Calorimetry plot of melting cycle in *n*-octadecane and *n*-octadecane/SWCNT nano composite. (b) Differential Scanning Calorimetry plot of freezing cycle in *n*-octadecane and *n*-octadecane/SWCNT nano composite. Note that the peaks are shifted by 3.5 ºC for calibration correction of the DSC.

The phase change enthalpy is a critical factor which determines the thermal energy storage capacity of the PCMs. Figure 5.5 (a) and (b) shows that with the addition of 0.25 wt % SWCNT, the melting and freezing enthalpy of *n*-octadecane decreases. It is generally anticipated that the addition of nanoparticles will decrease the freezing and melting temperature of the materials. However, in this case a minor increase in the melting and freezing point is noticed. Since, the calorimetry technique used in the present experiments is not sufficiently accurate at low temperatures this future is difficult to explain. However, the decrease is approximately 30% in the case of 0.25 wt % SWCNT loading. Since some of the PCM volume is replaced by the presence of SWCNT which does not undergo phase transition a reduction in phase change enthalpy is anticipated. However, this reduction in

enthalpy limits the energy storage capability of the PCMs. Hence, further loading of SWCNT need to limited. The present results show a much higher reduction in phase change enthalpy compared to the case of 4 wt% graphene inclusions in 1-octadecanol where a 14 % decrease is reported [143].

5.5 Conclusions

In summary, contrasting thermal conductivity enhancement in phase change alkane with one-dimensional SWCNT nano inclusions and two-dimensional exfoliated GnP nano inclusions is reported. SWCNTs were far more effective at enhancing the solid/liquid thermal conductivity contrast than any other material reported to date. The potential mechanism behind the 'anomalous' thermal conduction enhancement is discussed based on the existing numerical and simulation results. The experimental results are also analyzed in the light of effective medium and Yamada-Ota models. Classical theoretical models fail to explain the contrasting thermal conductivity improvements. Recent molecular dynamics simulations show that the thermal boundary resistance in the liquid phase and crystalline phase is different which may cause this anomaly. However, experimental data of thermal interface resistance in different phases is still lacking. Further experiments to probe the thermal boundary resistance using time domain thermoreflectance measurements in the solid and liquid phase will facilitate better understanding of the interface effects and help in improving theoretical models. Further research need to focus on the development of theoretical models to explain such contrasting behaviour.

Chapter 6

Conclusions and Scope for Future Research

There are much anticipation on 'anomalous' enhancement in nanofluids thermal conductivity in the recent decade. However, the potential of nanofluids and the magnitude of thermal conductivity enhancements remains unclear due to lack of sufficient knowledge in dispersion methods and characterization techniques. To understand the real potential of nanofluids, systematic investigation of the thermal conductivity enhancement is carried out with well characterized single walled nanohorns, single walled carbon nanotubes and exfoliated graphite based nanofluids.

SWCNH based aqueous nanofluids shows enhancement in good agreement with the predictions of Maxwell's model while in the case of non-aqueous nanofluids a deviation from the Maxwell's model occurs possibly due to the aggregate formation. The thermal conductivity enhancement in non-aqueous nanofluids was found to be twice the predictions of Maxwell's model.

SWCNT based nanofluids shows higher enhancement than the case of spherical inclusions owing to its high aspect ratio. Experimental results are in reasonable agreement with the predictions of effective medium theory providing a low but still reasonable magnitude of the interfacial resistance is used in calculations. The present experiments reveal that thermal conductivity enhancement in well dispersed nanofluids are modest and can be reasonably predicted with classical theoretical models.

Contrasting thermal conductivity enhancement in phase change alkane is found with nano inclusions. SWCNT inclusions show an 'anomalous' improvement in the solid state at a very

low loading while the enhancement in liquid state is minimal. Mechanism behind this phase dependent enhancement is still unclear and the classical models cannot explain this behaviour. Such a phase change material with enhanced thermal conductivity makes it a promising candidate for thermal energy storage applications.

Perspectives for Future Research

The present results clearly demonstrate the inefficiency of spherical inclusions as the potential material for nanofluid applications. Despite, SWCNT suspensions show a higher viscosity enhancement compared to the thermal conductivity enhancement, there does still exist a possibility to utilize this material by carefully manipulating the interface resistance. Further research should focus on manipulating the thermal boundary resistance by functionalizing nano-materials with appropriate covalent bonding or decorating with a metal nanoparticle to minimize the resistance between the nano inclusion and the surrounding medium. Experiments need to be performed to probe the thermal boundary resistance in the solid crystalline phase and liquid phase of alkanes to understand the unusual thermal conduction noticed in phase change materials. This will facilitate better understanding of the interface effects and help in improving theoretical models. Effective medium theory needs to be improved to take into account by considering the interaction between CNTs in different fluids, defect level, and poly-dispersive nature of material aspect ratio, the role of percolation and contact resistances between the nano inclusions.

Bibliography

[1] International Technology Roadmap for Semiconductors: Assembly and Packaging. www.itrs.net.

[2] Prasher R., Thermal interface materials: historical perspective, status, and future directions, Proceedings of the IEEE, 2006; 94(8): 1571- 1586.

[3] Garimella S, Singhal V, Dong L, On-chip thermal management with microchannel heat sinks and integrated micropumps, Proceedings of the IEEE,2006; 94(8): 1534- 1548.

[4] Ahuja AS. Augmentation of Heat Transport in Laminar-Flow of Polystyrene Suspensions .1. Experiments and Results. Journal of Applied Physics. 1975;46(8):3408-16.

[5] Choi SUS, Siginer DA, Wang HP. Enhancing thermal conductivity of fluids with nanoparticles, developments and applications of non-newtonian flows, FED- vol 231/MD; 1995.

[6] Daungthongsuk W, Wongwises S. A critical review of convective heat transfer of nanofluids. Renewable & Sustainable Energy Reviews. 2007;11(5):797-817.

[7] Fan J, Wang LQ. Review of Heat Conduction in Nanofluids. Journal of Heat Transfer-Transactions of the ASME. 2011;133(4).

[8] Kleinstreuer C, Feng Y. Experimental and theoretical studies of nanofluid thermal conductivity enhancement: a review. Nanoscale Research Letters. 2011;6.

[9] Masuda H, Ebata A, Teramae K, Hishinuma N. Netsu Bussei. 1993;4:227.

[10] Eastman JA, Choi SUS, Li S, Yu W, Thompson LJ. Anomalously increased effective thermal conductivities of ethylene glycol-based nanofluids containing copper nanoparticles. Applied Physics Letters. 2001;78(6):718-20.

[11] Patel HE, Das SK, Sundararajan T, Sreekumaran Nair A, George B, Pradeep T. Thermal conductivities of naked and monolayer protected metal nanoparticle based nanofluids: Manifestation of anomalous enhancement and chemical effects. Applied Physics Letters. 2003;83(14):2931-3.

[12] Maxwell JC. A Treatise on Electricity and Magnetism; 1891.

[13] Moghadassi AR, Hosseini SM, Henneke DE. Effect of CuO Nanoparticles in Enhancing the Thermal Conductivities of Monoethylene Glycol and Paraffin Fluids. Industrial and Engineering Chemistry Research. 2010; 49:1900.

[14] Patel HE, Sundararajan T, Das SK. An experimental investigation into the thermal conductivity enhancement in oxide and metallic nanofluids. Journal of Nanoparticle Research. 2010;12: 1015-31.

[15] Tijerina JT, Narayanan TN, Gao G, Rohde M, Tsentalovich DA, Pasquali M, Ajayan PM, Electrically Insulating Thermal Nano-Oils Using 2D Fillers, ACS Nano, 2012; 6(2):1214-1220.

[16] Yu W, Xie H, Chen L, Li Y. Enhancement of thermal conductivity of kerosene-based Fe3O4 nanofluids prepared via phase-transfer method. Colloids and Surfaces A 2010;355:109-13.

[17] Parekh K, Lee HS. Magnetic field induced enhancement in thermal conductivity of magnetite nanofluid. Journal of Applied Physics, 2010;107:09A310.

[18] Gallego MJP, Lugo L, Legido JL, Pineiro MM. Enhancement of thermal conductivity and volumetric behavior of FexOy nanofluids. Journal of Applied Physics 2011;110:014309.

[19] Guo SZ, Li Y, Jiang JS, Xie HQ. Nanofluids Containing -Fe_2O_3 Nanoparticles and Their Heat Transfer Enhancements. Nanoscale Research Letters 2010;5:1222-7.

[20] Shima PD, Philip J, Raj B. Synthesis of Aqueous and Nonaqueous Iron Oxide Nanofluids and Study of Temperature Dependence on Thermal Conductivity and Viscosity. The Journal Physical Chemistry C 2010;114:18825-33.

[21] Das SK, Putra N, Thiesen P, Roetzel W. Temperature dependence of thermal conductivity enhancement for nanofluids. Journal of Heat Transfer-Transactions of the ASME. 2003;125(4):567-74.

[22] Sundar LS, Sharma KV. Thermal conductivity enhancement of nanoparticles in distilled water. International Journal of Nanoparticles. 2008;1:66-77.

[23] Teng TP, Hung YH, Teng TC, Moa HE, Hsu HG. The effect of alumina/water nanofluid particle size on thermal conductivity. Applied Thermal Engineering. 2010;30:2213-8.

[24] Jha N, Ramaprabhua S. Thermal conductivity studies of metal dispersed multiwalled carbon nanotubes in water and ethylene glycol based nanofluid. Journal of Applied Physics. 2009;106:084317.

[25] Paul G, Philip J, Raj B, Das PK, Manna I. Synthesis, characterization, and thermal property measurement of nano-Al95Zn05 dispersed nanofluid prepared by a two-step process. International Journal of Heat and Mass Transfer. 2011;54:3783-8.

[26] Kole M, Dey TK. Thermal conductivity and viscosity of Al2O3 nanofluid based on car engine coolant. Journal of Physics D: Applied Physics 2010;43 (31):315501.

[27] Shalkevich N, Escher W, Burgi T, Michel B, Ahmed LS, Poulikakos D. On the Thermal Conductivity of Gold Nanoparticle Colloids. Langmuir 2010;26: 663-70.

[28] Branson BT, Beauchamp PS, Beam JC, Lukeheart CM, Davidson JL, Nanodiamond nanofluids for enhanced thermal conductivity. ACS Nano 2013; 7(4): 3183-3189.

[29] Yang B, Han ZH. Temperature-dependent thermal conductivity of nanorod-based nanofluids. Applied Physics Letters, 2006;89: 083111.

[30] Duangthongsuk W, Wongwises S. Measurement of Temperature-Dependent Thermal Conductivity and Viscosity of TiO2-Water Nanofluids. Experimental and Thermal Fluid Science. 2009; 33: 706-14.

[31] Timofeeva EV, Routbort JL, Singh D. Particle shape effects on thermophysical properties of alumina nanofluids. Journal of Applied Physics 2009;106:014304.

[32] Buongiorno J, Venerus DC, Prabhat N, McKrell T, Townsend J, Christianson R, et al. A benchmark study on the thermal conductivity of nanofluids. Journal of Applied Physics. 2009;106(9).

[33] Godson L, Raja B, Lal DM, Wongwises S. Enhancement of heat transfer using nanofluids-An overview. Renewable & Sustainable Energy Reviews. 2010;14(2):629-41.

[34] Ozerinc S, Kakac S, Yazicioglu AG. Enhanced thermal conductivity of nanofluids: a state-of-the-art review. Microfluidics and Nanofluidics. 2010;8(2):145-70.

[35] Philip J, Shima PD, Thermal properties of nanofluids, Advances in Colloid and Interface Science.2012; 183-184: 30-45.

[36] Iijima S. Nature. 1991;354:56.

[37] Dresselhaus MS, Dresselhaus G, Jorio A, Unusual properties and structure of carbon nanotubes, Annual Review of Materials Research. 2004; 34 (34): 247-278.

[38] Balandin A. Thermal properties of graphene and nanostructured carbon materials, Nature Materials.2011, 10, 569-581.

[39] Hone J, Whitney M, Piskoti C, Zettl A. Thermal conductivity of single-walled carbon nanotubes. Physical Review B. 1999;59(4):R2514-R6.

[40] Kim P, Shi L, Majumdar A, McEuen PL. Thermal transport measurements of individual multiwalled nanotubes. Physical Review Letters. 2001;87(21).

[41] Yu CH, Shi L, Yao Z, Li DY, Majumdar A. Thermal conductance and thermopower of an individual single-wall carbon nanotube. Nano Letters. 2005;5(9):1842-6.

[42] Pettes MT, Shi L. Thermal and Structural Characterizations of Individual Single-, Double-, and Multi-Walled Carbon Nanotubes. Advanced Functional Materials. 2009;19(24):3918-25.

[43] Fujii M, Zhang X, Xie HQ, Ago H, Takahashi K, Ikuta T, et al. Measuring the thermal conductivity of a single carbon nanotube. Physical Review Letters. 2005;95(6).

[44] Choi TY, Poulikakos D, Tharian J, Sennhauser U. Measurement of the thermal conductivity of individual carbon nanotubes by the four-point three-omega method. Nano Letters. 2006;6(8):1589-93.

[45] Choi TY, Poulikakos D, Tharian J, Sennhauser U. Measurement of thermal conductivity of individual multiwalled carbon nanotubes by the 3-omega method. Applied Physics Letters. 2005;87(1).

[46] Wang ZL, Tang DW, Li XB, Zheng XH, Zhang WG, Zheng LX, et al. Length-dependent thermal conductivity of an individual single-wall carbon nanotube. Applied Physics Letters. 2007;91(12).

[47] Wang ZL, Tang DW, Zheng XH, Zhang WG, Zhu YT. Length-dependent thermal conductivity of single-wall carbon nanotubes: prediction and measurements. Nanotechnology. 2007;18(47).

[48] Pop E, Mann D, Wang Q, Goodson K, Dai HJ. Thermal conductance of an individual single-wall carbon nanotube above room temperature. Nano Letters. 2006;6(1):96-100.

[49] Li Q, Liu C, Wang X, Fan S, Measuring the thermal conductivity of individual carbon nanotubes by the Raman shift method. Nanotechnology, 2009; 20(14): 145702.

[50] Hansen JP, McDonald IR, Theory of Simple Liquids, 2nd ed.,Academic, London:1986.

[51] Lukes JR, Zhong HL. Thermal conductivity of individual single-wall carbon nanotubes. Journal of Heat Transfer-Transactions of the ASME. 2007;129(6):705-16.

[52] Berber S, Kwon YK, Tomanek D. Unusually high thermal conductivity of carbon nanotubes. Physical Review Letters. 2000;84(20):4613-6.

[53] Osman MA, Srivastava D. Nanotechnology. 2001;12:21.

[54] Padgett CW, Brenner DW. Influence of chemisorption on the thermal conductivity of single-wall carbon nanotubes. Nano Letters. 2004;4(6):1051-3.

[55] Moreland JF, Freund JB, Chen G. The disparate thermal conductivity of carbon nanotubes and diamond nanowires studied by atomistic simulation. Microscale Thermophysical Engineering 2004;8(1):61-9.

[56] Maruyama S. A molecular dynamics simulation of heat conduction of a finite length single-walled carbon nanotube. Microscale Thermophysical Engineering 2003;7(1):41-50.

[57] Che JW, Cagin T, Goddard WA. Thermal conductivity of carbon nanotubes. Nanotechnology. 2000;11(2):65-9.

[58] Mingo N, Broido DA. Carbon nanotube ballistic thermal conductance and its limits. Physical Review Letters. 2005;95(9).

[59] Choi SUS, Zhang ZG, Yu W, Lockwood FE, Grulke EA. Anomalous thermal conductivity enhancement in nanotube suspensions. Applied Physics Letters. 2001;79(14):2252-4.

[60] Xie H, Hohyun L, Wonjin Y, Mansoo C. Nanofluids containing multiwalled carbon nanotubes and their enhanced thermal conductivities. Journal of Applied Physics. 2003;94(8).

[61] Assael MJ, Chen CF, Metaxa I, Wakeham WA. Thermal conductivity of suspensions of carbon nanotubes in water. International Journal of Thermophysics. 2004;25(4):971-85.

[62] Assael MJ, Metaxa IN, Arvanitidis J, Christofilos D, Lioutas C. Thermal conductivity enhancement in aqueous suspensions of carbon multi-walled and double-walled nanotubes in the presence of two different dispersants. International Journal of Thermophysics. 2005;26(3):647-64.

[63] Hwang Y, Lee JK, Lee CH, Jung YM, Cheong SI, Lee CG, et al. Stability and thermal conductivity characteristics of nanofluids. Thermochimica Acta. 2007;455(1-2):70-4.

[64] Choi TY, Maneshian MH, Kang B, Chang WS, Han CS, Poulikakos D. Measurement of the thermal conductivity of a water-based single-wall carbon nanotube colloidal suspension with a modified 3-omega method. Nanotechnology. 2009;20(31).

[65] Liu MS, Lin MCC, Huang IT, Wang CC. Enhancement of thermal conductivity with carbon nanotube for nanofluids. International Communications in Heat and Mass Transfer. 2005;32(9):1202-10.

[66] Yang Y, Grulke EA, Zhang ZG, Wu GF. Thermal and rheological properties of carbon nanotube-in-oil dispersions. Journal of Applied Physics. 2006;99(11).

[67] Nanda J, Maranville C, Bollin SC, Sawall D, Ohtani H, Remillard JT, et al. Thermal conductivity of single-wall carbon nanotube dispersions: Role of interfacial effects. Journal of Physical Chemistry C. 2008;112(3):654-8.

[68] Cherkasova AS, Shan JW. Particle Aspect-Ratio and Agglomeration-State Effects on the Effective Thermal Conductivity of Aqueous Suspensions of Multiwalled Carbon Nanotubes. Journal of Heat Transfer-Transactions of the ASME. 2010;132(8).

[69] Wen DS, Ding YL. Effective thermal conductivity of aqueous suspensions of carbon nanotubes (carbon nanotubes nanofluids). Journal of Thermophysics and Heat Transfer. 2004;18(4):481-5.

[70] Ding YL, Alias H, Wen DS, Williams RA. Heat transfer of aqueous suspensions of carbon nanotubes (CNT nanofluids). International Journal of Heat and Mass Transfer. 2006;49(1-2):240-50.

[71] Nasiri A, Shariaty-Niasar M, Rashidi A, Amrollahi A, Khodafarin R. Effect of dispersion method on thermal conductivity and stability of nanofluid. Experimental Thermal and Fluid Science. 2011;35(4):717-23.

[72] Keblinski P, Phillpot SR, Choi SUS, Eastman JA. Mechanisms of heat flow in suspensions of nano-sized particles (nanofluids). International Journal of Heat and Mass Transfer. 2002;45(4):855-63.

[73] Eastman JA, Phillpot SR, Choi SUS, Keblinski P. Annual Review of Materials Research. 2004;34:6.

[74] Keblinski P. , Cahill D.G. Comment on “Model for HeatConduction in Nanofluids”, Physical Review Letters. 2005; 95, 209401.

[75] Tsai TH, Kuo LS, Chen PH, Yang CT. Effect of viscosity of base fluid on thermal conductivity of nanofluids. Applied Physics Letters. 2008;93(23).

[76] Lee D, Kim JW, Kim BG. A new parameter to control heat transport in nanofluids: Surface charge state of the particle in suspension. Journal of Physical Chemistry B. 2006;110(9):4323-8.

[77] Gao JW, Zheng RT, Ohtani H, Zhu DS, Chen G. Experimental Investigation of Heat Conduction Mechanisms in Nanofluids. Clue on Clustering. Nano Letters. 2009;9(12):4128-32.

[78] Biercuk MJ, Llaguno MC, Radosavljevic M, Hyun JK, Johnson AT, Fischer JE. Carbon nanotube composites for thermal management. Applied Physics Letters. 2002;80(15):2767-9.

[79] Hamilton R, Crosser O. Industrial and Engineering Chemistry Fundamentals. 1962;1(3):187.

[80] Hashin Z, Shtrikman S. Journal of Applied Physics. 1962;33:3125.

[81] Maruyama S, Kojima R, Miyauchi Y, Chiashi S, Kohno M. Low-temperature synthesis of high-purity single-walled carbon nanotubes from alcohol. Chemical Physics Letters. 2002;360(3-4):229-34.

[82] Saito R, Dresselhaus G, Dresselhaus MS. Trigonal warping effect of carbon nanotubes. Physical Review B. 2000;61(4):2981-90.

[83] Araujo PT, Doorn SK, Kilina S, Tretiak S, Einarsson E, Maruyama S, et al. Third and fourth optical transitions in semiconducting carbon nanotubes. Physical Review Letters. 2007;98(6).

[84] Chen LF, Xie HQ. Surfactant-free nanofluids containing double- and single-walled carbon nanotubes functionalized by a wet-mechanochemical reaction. Thermochimica Acta. 2010;497(1-2):67-71.

[85] Xie H, Chen L. Review on the Preparation and Thermal Performances of Carbon Nanotube Contained Nanofluids. Journal of Chemical and Engineering Data. 2011;56(4):1030-41.

[86] Jiang LQ, Gao L, Sun J. Journal of Colloid and Interface Science. 2003;260:89.

[87] Zhang X, Gu H, Fujii M. Effective thermal conductivity and thermal diffusivity of nanofluids containing spherical and cylindrical nanoparticles. Journal of Applied Physics. 2006;100(4).

[88] Garg P, Alvarado JL, Marsh C, Carlson TA, Kessler DA, Annamalai K. An experimental study on the effect of ultrasonication on viscosity and heat transfer performance of multi-wall carbon nanotube-based aqueous nanofluids. International Journal of Heat and Mass Transfer. 2009;52(21-22):5090-101.

[89] Bonaccorso F, Hasan T, Tan PH, Sciascia C, Privitera G, Di Marco G, et al. Density Gradient Ultracentrifugation of Nanotubes: Interplay of Bundling and Surfactants Encapsulation. Journal of Physical Chemistry C. 2010;114(41):17267-85.

[90] Zhao P, Einarsson E, Xiang R, Murakami Y, Maruyama S. Controllable Expansion of Single-Walled Carbon Nanotube Dispersions Using Density Gradient Ultracentrifugation. The Journal of Physical Chemistry C. 2010;114(11):4831-4.

[91] Zhao P, Einarsson E, Lagoudas G, Shiomi J, Chiashi S, Maruyama S. Tunable separation of single-walled carbon nanotubes by dual-surfactant density gradient ultracentrifugation. Nano Research. 2011;4(7):623-34.

[92] Mazer NA, Carey MC, Kwasnick RF, Benedek GB. Quasielastic light scattering studies of aqueous biliary lipid systems. Size, shape, and thermodynamics of bile salt micelles. Biochemistry. 1979;18(14):3064-75.

[93] Hagen A, Hertel T. Quantitative analysis of optical spectra from individual single-wall carbon nanotubes. Nano Letters. 2003;3(3):383-8.

[94] Bachilo SM, Strano MS, Kittrell C, Hauge RH, Smalley RE, Weisman RB. Structure-assigned optical spectra of single-walled carbon nanotubes. Science. 2002;298(5602):2361-6.

[95] Venerus DC, Kabadi MS, Lee S, Perez-Luna V. Study of thermal transport in nanoparticle suspensions using forced Rayleigh scattering. Journal of Applied Physics. 2006;100(9).

[96] Gharagozloo PE, Eaton JK, Goodson KE. Diffusion, aggregation, and the thermal conductivity of nanofluids. Applied Physics Letters. 2008;93(10).

[97] Carslaw HS, Jaeger JC. Conduction of Heat in Solids; 1959.

[98] Nagasaka Y, Nagashima A. Absolute Measurement of the Thermal-Conductivity of Electrically Conducting Liquids by the Transient Hot-Wire Method. Journal of Physics E : Scientific Instruments. 1981;14(12):1435-40.

[99] Healy JJ, de Groot JJ, Kestin J. The theory of the transient hot-wire method for measuring thermal conductivity. Physica B. 1976;82(2):392-408.

[100] American Society of Testing and Materials, Standard test method for thermal conductivity of liquids, ASTM D-2717; 2009: 95-98.

[101] Diguilio R, Teja AS. Thermal-Conductivity of Poly(Ethylene Glycols) and Their Binary-Mixtures. Journal of Chemical and Engineering Data. 1990;35(2):117-21.

[102] http://www.cannoninstrument.com/cfr.htm

[103] Nan C-W, Birringer R, Clarke DR, Gleiter H. Effective thermal conductivity of particulate composites with interfacial thermal resistance. Journal of Applied Physics. 1997;81(10):6692-9.

[104] Kapitza PL, Heat transfer and superfluidity of helium II. Physical Review.1941; 60, 354-355.

[105] Huxtable ST, Cahill DG, Shenogin S, Xue LP, Ozisik R, Barone P, Usrey M, Strano MS, Siddons G, Shim M, Keblinski P. Interfacial Heat Flow in Carbon Nanotube Suspensions. Nature Materials. 2003; 2, 731-734.

[106] Kang SD, Li SC, Lee ES, Cho YW, Kim YH, Lyeo H, Lee. YH. Interfacial Thermal Conductance Observed to be Higher in Semiconducting than Metallic Carbon Nanotubes. ACS Nano. 2012; 6, 3853-3860.

[107] Shenogin S, Xue LP, Ozisik R, Keblinski P, Cahill DG. Role of Thermal Boundary Resistance on the Heat Flow in Carbon-Nanotube Composites. Journal of Appied Physics. 2004; *95,* 8136-8144.

[108] Carlborg CF, Shiomi J, Maruyama S. Thermal boundary resistance between single walled carbon nanotubes and surrounding matrices. Physical Review B. 2008; 78, 205406-1-8.

[109] Schmidt AJ, Alper JD, Chiesa M, Chen G, Das SK, Schifferli KH, Probing the Gold Nanorod-Ligand-Solvent Interface by Plasmonic Absorption and Thermal Decay. The Journal of Physical Chemistry C.2008; 112: 13320-13323.

[110] Park J, Huang J, Wang W, Murphy CJ, Cahill DG. Heat transport between Au nanorods, surrounding liquids and solid supports. The Journal of Physical Chemistry C.2012; 116: 26335-26341.

[111] Yamada E, Ota T. Effective Thermal-Conductivity of Dispersed Materials. Heat and Mass Transfer. 1980;13(1-2):27-37.

[112] Zheng YZ, Hong HP. Modified model for effective thermal conductivity of nanofluids containing carbon nanotubes. Journal of Thermophysics and Heat Transfer. 2007;21(3):658-60.

[113] A. Einstein. Eine neue bestimmung der molek¨uldimensionen. Ann. Physik., 1096,19:289–306.

[114] Mooney M. The viscosity of concentrated suspensions of spherical particles. Journal of Colloidal Science. 1951; 6,162-170.

[115] Krieger IM, Dougherty. A mechanism for non-newtonian flow in suspensions of rigid spheres. Transactions of the Society of Rheology. 1959; 3,137-152.

[116] Phuoc TX, Massoudi M, Chen RH. Viscosity and thermal conductivity of nanofluids containing multi-walled carbon nanotubes stabilized by chitosan, International Journal of Thermal Sciences. 2011;50:12-18.

[117] Lee J, Gharagozloo P, Kolade B, Eaton J, Goodson K. Nanofluid convection in microtubes. Journal of Heat Transfer. 2010; 132: 092401-1-5.

[118] Halelfadl S, Estellé P, Aladag B, Doner N, Maré T. Viscosity of carbon nanotubes water-based nanofluids: Influence of concentration and temperature. International Journal of Thermal Sciences. 2013;71:111-117.

[119] Ruan BL, Jacobi AM. Heat transfer characteristics of multiwall carbon nanotube suspensions (MWCNT nanofluids) in intertube falling-film flow. International Journal of Heat and Mass Transfer. 2012;55(11-12):3186-95.

[120] Stauffer D, Aharnoy A. Introduction to The Percolation Theory; 1991.

[121] Hernandez JJ, Garcia-Gutierrez MC, Nogales A, Rueda DR, Kwiatkowska M, Szymczyk A, et al. Influence of preparation procedure on the conductivity and transparency

of SWCNT-polymer nanocomposites. Composites Science and Technology. 2009;69(11-12):1867-72.

[122] Chatterjee T, Yurekli K, Hadjiev VG, Krishnamoorti R. Single-walled carbon nanotube dispersions in poly(ethylene oxide). Advanced Functional Materials. 2005;15(11):1832-8.

[123] Shenogina N, Shenogin S, Xue L, Keblinski P. On the lack of thermal percolation in carbon nanotube composites. Applied Physics Letters. 2005;87(13).

[124] Gupta A, Kumar R. Role of Brownian motion on the thermal conductivity enhancement of nanofluids. Applied Physics Letters. 2007;91(22).

[125] Duong HM, Papavassiliou DV, Mullen KJ, Wardle BL, Maruyama S. Calculated Thermal Properties of Single-Walled Carbon Nanotube Suspensions. Journal of Physical Chemistry C. 2008;112(50):19860-5.

[126] Tsyboulski DA, Bachilo SM, Kolomeisky AB, Weisman RB. Translational and rotational dynamics of individual single-walled carbon nanotubes in aqueous suspension. ACS Nano. 2008;2(9):1770-6.

[127] Broersma S. Rotational Diffusion Constant of a Cylindrical Particle. Journal of Chemical Physics. 1960;32(6):1626-31.

[128] Yunker PJ, Chen K, Zhang ZX, Ellenbroek WG, Liu AJ, Yodh AG. Rotational and translational phonon modes in glasses composed of ellipsoidal particles. Physical Review E. 2011;83(1).

[129] Glory J, Bonetti M, Helezen M, Mayne-L'Hermite M, Reynaud C. Thermal and electrical conductivities of water-based nanofluids prepared with long multiwalled carbon nanotubes. Journal of Applied Physics. 2008;103(9).

[130] Xu ZP, Buehler MJ. Nanoengineering Heat Transfer Performance at Carbon Nanotube Interfaces. ACS Nano. 2009;3(9):2767-75.

[131] Shim M, Kam NWS, Chen RJ, Li YM, Dai HJ. Functionalization of carbon nanotubes for biocompatibility and biomolecular recognition. Nano Letters. 2002;2(4):285-8.

[132] Larson RG. The Structure and Rheology of Complex Fluids, 1999, Oxford University Press, New York.

[133] Prasher R, Song D, Wang J, Phelan P. Measurements of nanofluids viscosity and its implications for thermal applications. Applied Physics Letters; 2006; 89**:** 133108.

[134] Garg J, Poudel B, Chiesa M, Gordon JB, Ma JJ, Wang JB, Ren ZF, Kang YT, Ohtani H, Nanda J, Mckinley GH, Chen G, Enhanced thermal conductivity and viscosity of copper nanoparticles in ethylene glycol nanofluid. Journal of Applied Physics. 2008; 103: 074301.

[135] Baby TT, Ramaprabhu S, Investigation of thermal and electrical conductivity of graphene based nanofluids. Journal of Applied Physics. 2010; 108:124308-1-6.

[136] Zheng R, Gao J, Wang J, Feng S-P, Ohtani H, Wang J, et al. Thermal Percolation in Stable Graphite Suspensions. Nano Letters. 2011;12(1):188-92.

[137] Zheng R, Gao J, Wang J, Chen G. Reversible temperature regulation of electrical and thermal conductivity using liquid–solid phase transitions. Nature Communications. 2011;2:289.

[138]. Han Z, Fina A, Thermal Conductivity of Carbon Nanotubes and Their Polymer Nanocomposites: A Review. Progress in Polymer Science. 2011; 36: 914-944.

[139]. Wang Y, Tang B, Zhang S, Single-Walled Carbon Nanotube/ Phase Change Material Composites: Sunlight-Driven, Reversible, Form-Stable Phase Transitions for Solar Thermal Energy Storage. Advanced Functional Materials. 2013**:** DOI: 10.1002/adfm.201203728.

[140]. Khodadadi JM, Fan L, Babaei H, Thermal Conductivity Enhancement of Nanostructured-Based Colloidal Suspensions Utilized as Phase Change Materials for Thermal Energy Storage: A Review. Renewable and sustainable Energy Reviews. 2013**;** 24: 418-444.

[141] Powell RW, Challoner AR, Seyer WF. Correspondence. Measurement of Thermal Conductivity of n-Octadecane. Industrial & Engineering Chemistry. 1961;53(7):581-2.

[142] Liu YD, Zhou YG, Tong MW, Zhou XS. Experimental study of thermal conductivity and phase change performance of nanofluids PCMs. Microfluidics and Nanofluidics. 2009;7(4):579-84.

[143] Yavari F, Fard HR, Pashayi K, Rafiee MA, Zamiri A, Yu Z, et al. Enhanced Thermal Conductivity in a Nanostructured Phase Change Composite due to Low Concentration Graphene Additives. The Journal of Physical Chemistry C. 2011;115(17):8753-8.

[144] Sari A, Karaipekli A. Thermal conductivity and latent heat thermal energy storage characteristics of paraffin/expanded graphite composite as phase change material. Applied Thermal Engineering. 2007;27(8-9):1271-7.

[145] Volkov AN, Zhigilei LV. Scaling Laws and Mesoscopic Modeling of Thermal Conductivity in Carbon Nanotube Materials. Physical Review Letters. 2010;104(21).

[146] Wei CY. Structural phase transition of alkane molecules in nanotube composites. Physical Review B. 2007;76(13).

[147] Yang JS, Yang CL, Wang MS, Chen BD, Ma XG. Crystallization of alkane melts induced by carbon nanotubes and graphene nanosheets: a molecular dynamics simulation study. Physical Chemistry Chemical Physics. 2011;13(34):15476-82.

[148] Babaei H, Keblinski P, Khodadadi JM. Thermal conductivity enhancement of paraffins by increasing the alignment of molecules through adding CNT/graphene. International Journal of Heat and Mass Transfer. 2013;58(1-2):209-16.

[149] Xu JZ, Chen T, Yang CL, Li ZM, Mao YM, Zeng BQ, et al. Isothermal Crystallization of Poly(L-lactide) Induced by Graphene Nanosheets and Carbon Nanotubes: A Comparative Study. Macromolecules. 2010;43(11):5000-8.

Appendix

A. Signal Analysis of the Transient Hot Wire Setup

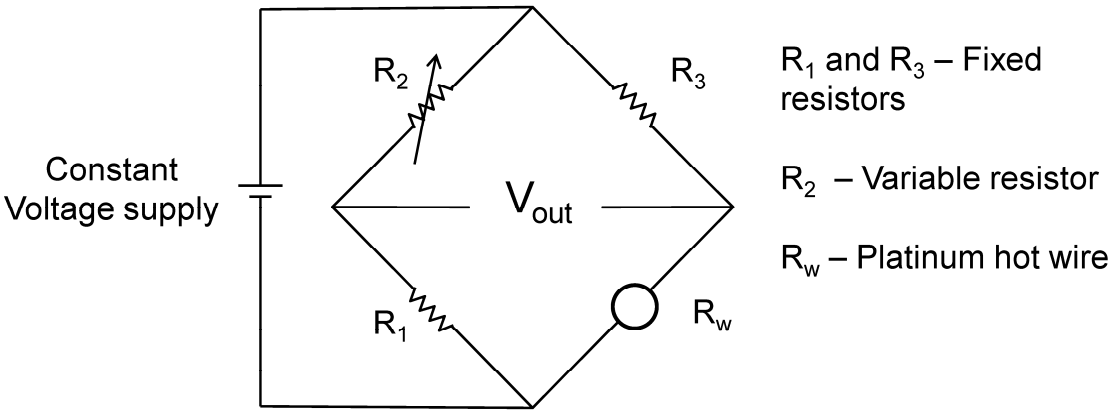

Figure A.1 : Scheamtic of the THW setup

The condition for the balance of Wheatstone bridge is

$$\frac{R_1}{R_2} = \frac{R_w}{R_3} \tag{A.1}$$

In equation A.1, R_1 and R_3 are fixed resistors and R_2 is the adjustable resistor and R_w is the resistance of the hot wire. When the bridge balance is disturbed bya supplying a constant voltage (V_{in}), the output voltage V_{out} can be calculated using the Kirchoff's law which is as follows.

$$\frac{V_{out}}{V_{in}} = \left[\frac{R_{wt}}{R_{wt} + R_3} - \frac{R_1}{R_1 + R_2} \right] \tag{A.2}$$

Here R_{wt} is the resistance of the hot wire at every time step. Simplifying equation A.2, R_{wt} can be calculated s follows:

$$R_{wt} = \frac{AR_3}{1-A} \tag{A.3}$$

Where

$$A = \left[\frac{V_{out}}{V_{in}} + \frac{1}{1+\frac{R_3}{R_w}} \right] \tag{A.4}$$

Voltage drop across the hot wire (V_{Rw}) is given by the eqation (A.5) as follows:

$$V_{Rw} = \frac{V_{in} R_{wt}}{R_{wt} + R_3} \tag{A.5}$$

Heat flux per unit length (q) at any instant of time is then calculated from the R_{wt}, V_{Rw} and length of the hot wire (L_w). This is shown in equation (A.6).

$$q = \frac{(V_{Rw})^2}{R_{wt} L_w} \tag{A.6}$$

The temperature change of the hot wire is calculated from the change in resistance of the hot wire R_{wt} and the temperature coefficient of resistance of the platinum hot wire (α) which is shown in equation (A.7).

$$\Delta T = \frac{\Delta R_w}{\alpha R_w} \tag{A.7}$$

Finally, thermal conductivity of the fluid is then calculated as follows (A.8)

$$k = \frac{q}{4\pi} \left(\frac{d \ln(t)}{d\Delta T} \right) \tag{A.8}$$

B. Uncertainty Analysis of the Transient Hot Wire Setup

The thermal conductivity of the fluid from the transient hot wire setup is calculated as shown below:

$$k = \frac{q}{4\pi}\left(\frac{d\ln(t)}{d\Delta T}\right) \tag{B.1}$$

Rearranging the equation in terms of the measured resistancechange as a function of time gives

$$k = \alpha R_w \frac{q}{4\pi}\left(\frac{d\ln(t)}{d\Delta R_w}\right) = k = \alpha R_w \frac{q}{4\pi}\left(\frac{1}{B}\right)$$

Where, $B=\left(\frac{d\ln(t)}{d\Delta R_w}\right)^{-1}$ (B.2)

The uncertainties in the measured quantities can be written as follows:

$$\delta k = \sqrt{\left(\frac{\delta q}{q}\right)^2 + \left(\frac{\delta \alpha}{\alpha}\right)^2 + \left(\frac{\delta R_w}{R_w}\right)^2 + \left(\frac{\delta B}{B}\right)^2} \tag{B.3}$$

It need to be noted here that the uncertaintiy in the heat flux per unit length depends on multiple quantities such as change in voltage drop across the hot wire, change in wire resistance and inaccuracy in the hot wire length.Hence, the uncertainity due to heat flux per unit length can be further calculated as follows:

$$\delta q = \sqrt{\left(\frac{\delta V_{RW}}{V_{RW}}\right)^2 + \left(\frac{\delta L_w}{L_w}\right)^2 + \left(\frac{\delta R_{wt}}{R_{wt}}\right)^2} \tag{B.4}$$

Furthermore, the uncertainty in wire voltage is further dependent on the voltage input and the resistance of the hot wire and another resistance which is in serires with it. So, the uncertainty in voltage supply to the wire can be further written as follows:

$$\delta V_{RW} = \sqrt{\left(\frac{\delta V_{in}}{V_{in}}\right)^2 + \left(\frac{\delta R_{wt}}{R_{wt}}\right)^2 + \left(\frac{\delta R_3}{R_3}\right)^2} \tag{B.5}$$

The uncertainty in total resistance change of the hot wire for a period of time can be further written as follows:

$$\delta R_{wt} = \sqrt{\left(\frac{\delta V_{in}}{V_{in}}\right)^2 + \left(\frac{\delta V_{out}}{V_{out}}\right)^2 + \left(\frac{\delta R_1}{R_1}\right)^2 + \left(\frac{\delta R_2}{R_2}\right)^2 + \left(\frac{\delta R_3}{R_3}\right)^2} \tag{B.6}$$

The temperature co-efficient of resistance as a function of temperature is measured as 0.00384 Ω/°C which is very close to the literature value of 0.00393 Ω/°C which gives an uncertainty of 2.29 %. The uncertainty from least square fitting error is negligible and lies in the range of 0.1 %. The over-all uncertainity of the transient hot wire setup is tabulated below:

Uncertainty	(%)
$\frac{\delta V_{in}}{V_{in}}$	0.67
$\frac{\delta V_{out}}{V_{out}}$	1
$\frac{\delta R_1}{R_1}$	0.1
$\frac{\delta R_2}{R_2}$	0.2
$\frac{\delta R_3}{R_3}$	0.1
$\frac{\delta R_{wt}}{R_{wt}}$	1.22
$\frac{\delta L_w}{L_w}$	0.2
$\frac{\delta V_{Rw}}{V_{Rw}}$	1.39
$\frac{\delta q}{q}$	1.87
$\frac{\delta \alpha}{\alpha}$	2.29
$\frac{\delta B}{B}$	0.1
$\frac{\delta k}{k}$	2.8

C. Background Correction of Optical Absorbance from Ethylene Glycol Based Nanofluids

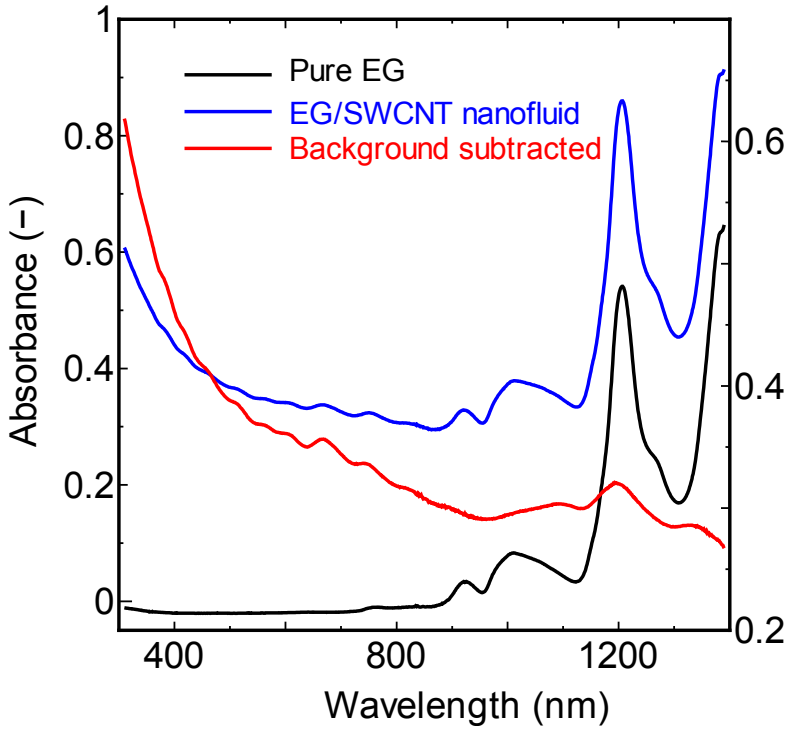

Figure C1: Optical absorbance spectra of EG/SWCNT based nanofluid.

The optical absorbance measurements was perofrmed by considering pure water as the background. However, ethylene glycol has strong absorption in the near-infra red region. Hence, to obtain the absorption spectra of EG/SWCNT nanofluid, two measurements were performed. First, the optical spectra of annofluid is measured followed by the absoprtion spectra of pure ethylene glycol. The red line in figure shows the absorption spectra of nanofluid after subtracting the effects of pure fluid. The broad peak in the infra red regin and smaller peakd in the visible region shows the presence of SWCNTs.

D.Dynamic Light Scattering, Optical Absorption and Photoluminescene Spectra of SWCNT/Water Nanofluids of Varying Concentrations

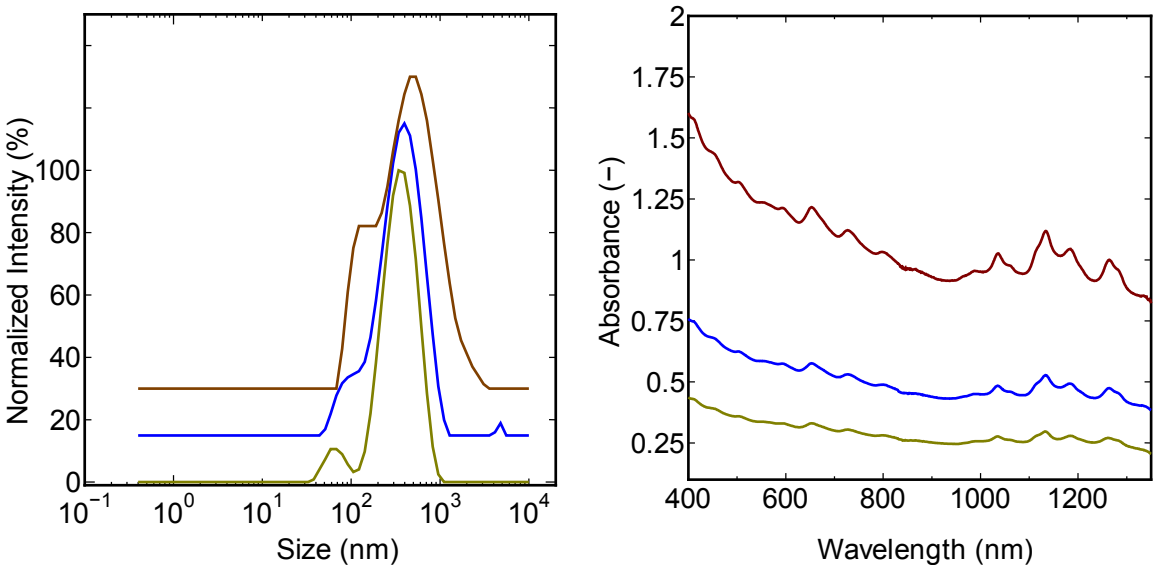

Figure D1: DLS and corresponding OAS results of 0.001 wt % , 0.0025 wt % and 0.005 wt % SWCNT/water nanofluid suspensions.

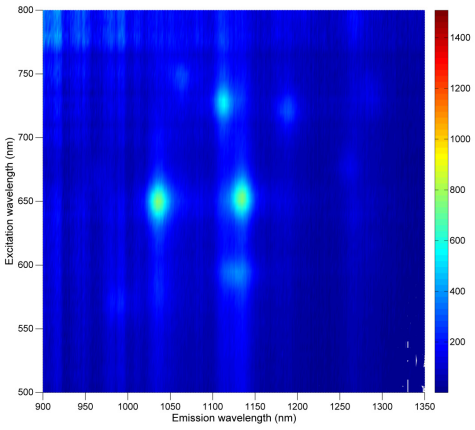

Figure D2: PL spectroscopic results of 0.001 wt % SWCNT/water nanofluid suspensions.

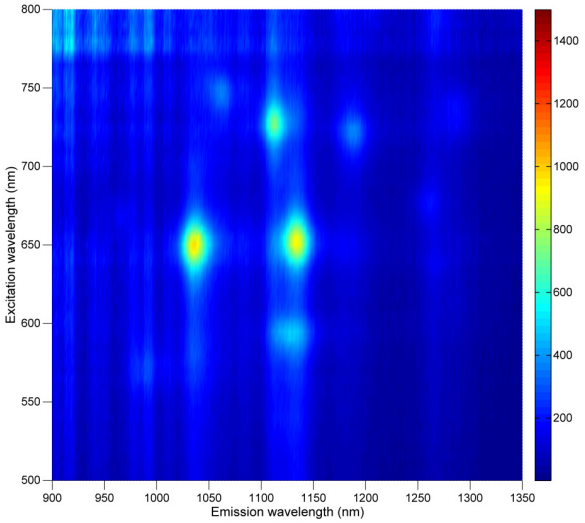

Figure D3: PL spectroscopic results of 0.0025 wt % SWCNT/water nanofluid suspensions.

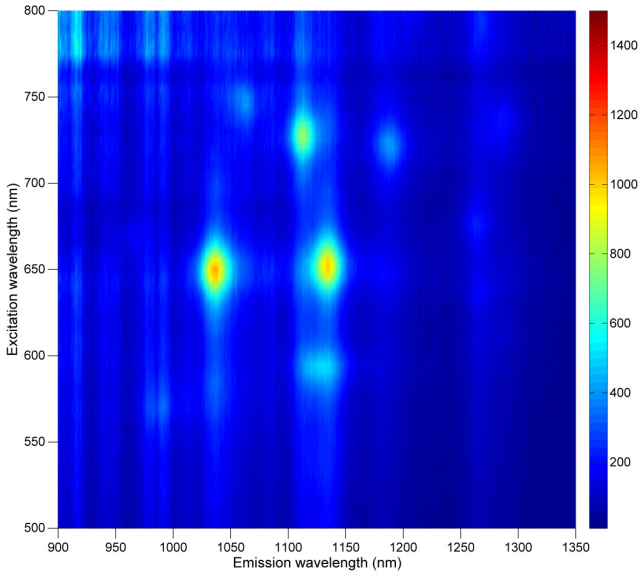

Figure D4: PL spectroscopic results of 0.005 wt % SWCNT/water nanofluid suspensions.

From figure D1 – D4, the optical absorbance and PL spectra clearly reveals efficeint isolation obtained by the DOC surfactant. However , the DLS results show two distinct features and

the smaller peak increase with increasing SWCNT concentration. Since the DLS measurements assume the rods as equivalent spheres, it is possible to assume that the smaller intensity peaks origniate from the individual SWCNTs. While the dominant peak can be attributed to the presence of smaller bundles.

E. Electrical Conductivity Measurement using Linear Sweep Voltage Supply

Electrical conductivity measurements reported in the chapter 3 was performed by connecting the sample to a digital multi-meter. The experimental results were further confirmed for pure fluid and nanofluid suspensions by performing additional measurements using a applied voltage and measuring the change in current for the samples (linear sweep method).

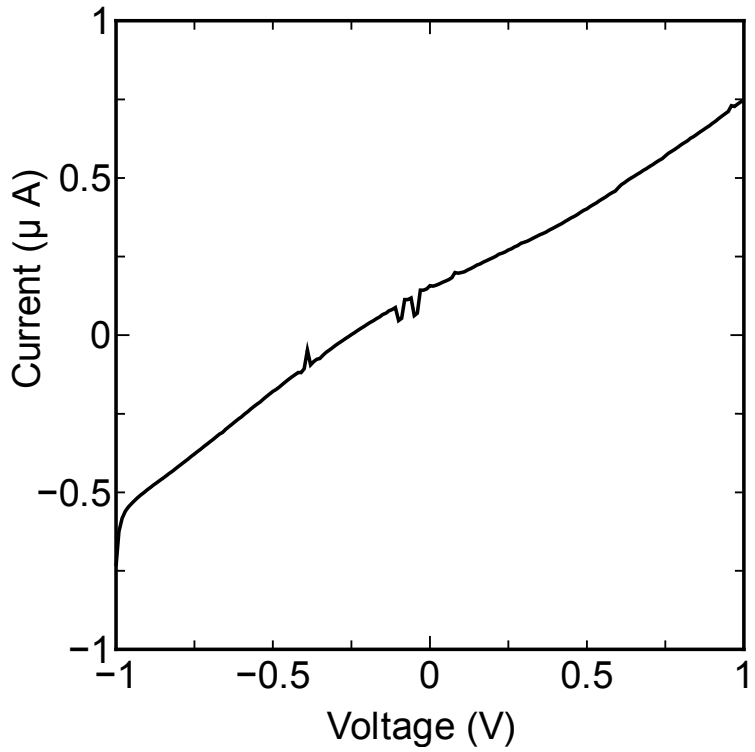

Figure E1: I-V curve of pure water

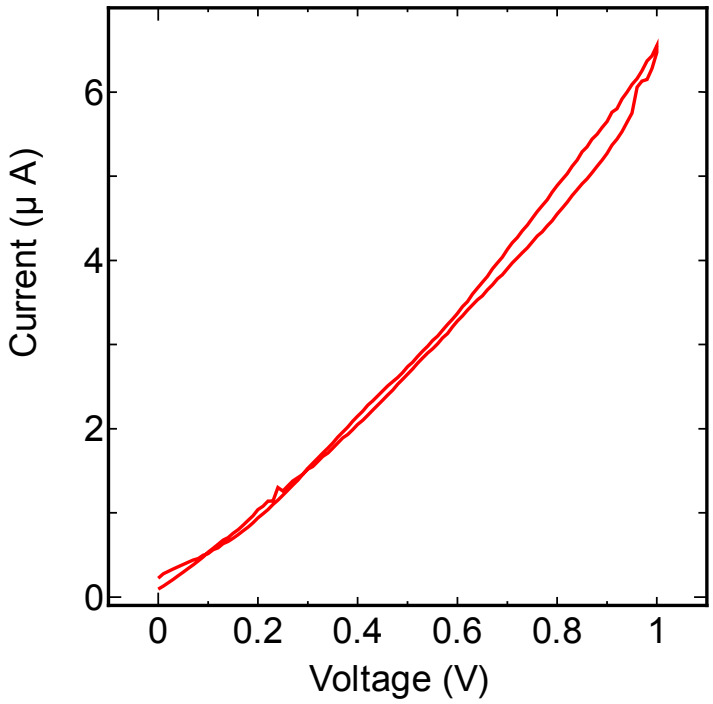

Figure E2: I-V curve of 0.25 wt % SWCNT/water nanofluid.

The experimental electrical conductivity of pure water and 0.25 wt % SWCNT obtained from this method is 5.93 μS cm^{-1} and 69 μS cm^{-1} . This meaasurement is in consistent with the previous results obtained using simple digital multimeter.

F. Shear Rate Data of Cannon Fenske Viscometer

CANNON INSTRUMENT COMPANY®
PO Box 16 • 2139 High Tech Road • State College • PA • 16804-0016 • USA
814 353 8000 • 800 676 6232 • FAX 814 353 8007

SHEAR RATE DATA

Cannon-Fenske Routine ♦ Cannon- Ubbelohde ♦ Cannon- Ubbelohde Dilution Viscometers

Equation: $\text{ShearRate} = \frac{4\,V}{\pi\, r^3 t}$

Tube Size	Efflux Volume (ml)	Capillary Radius (cm)	Viscosity (cSt)	Efflux Time (sec)	Shear Rate (Sec^{-1})
25	1.5	0.015	0.4	200	2830
			1.6	800	708
50	3.0	0.022	0.8	200	1790
			3.2	800	450
75	3.0	0.0265	1.6	200	1025
			6.4	800	256
100	3.0	0.0315	3.0	200	612
			12.0	800	153
150	3.0	0.039	7.0	200	321
			28.0	800	80.3
200	3.0	0.0505	20	200	148
			80	800	37
300	3.0	0.0625	50	200	78
			200	800	19.5
350	3.0	0.075	100	200	45.1
			400	800	11.3
400	3.0	0.094	240	200	23.3
			960	800	5.84
450	3.0	0.115	500	200	12.6
			2000	800	3.15
500	3.0	0.155	1600	200	5.15
			6400	800	1.29
600	3.0	0.200	4,000	200	2.29
			16,000	800	0.597
650	3.0	0.228	9,000	200	1.67
			36,000	800	0.46
700	3.0	0.278	20,000	200	0.89
			80,000	800	0.22

G. Influence of Sonication Time on the Thermal Conductivity Enhancement

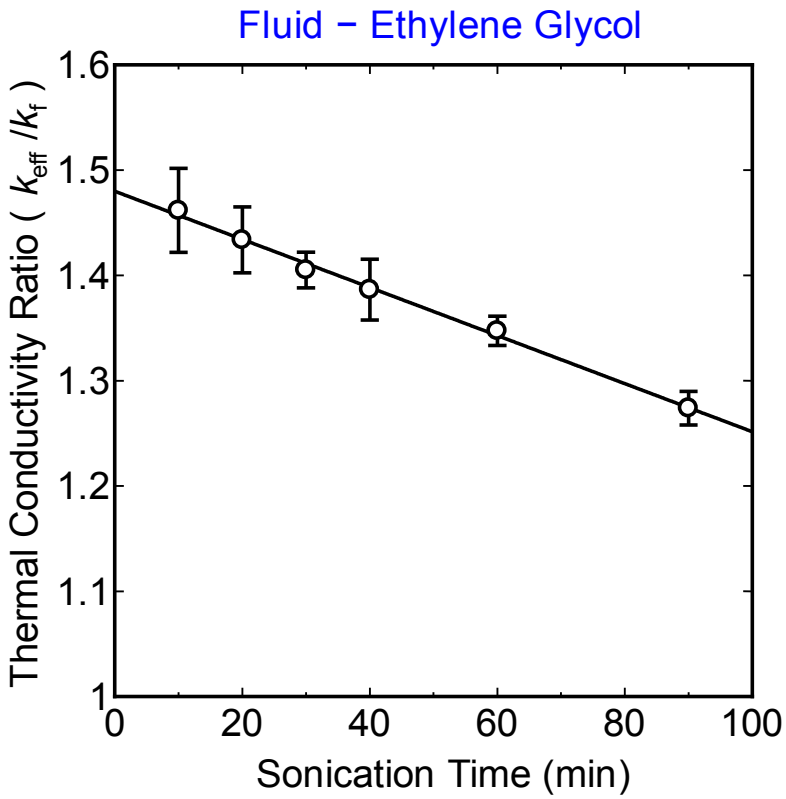

Figure G 1: Influence of sonication conditions on the thermal conductivity enhancement of EG/GnP nanofluids.

Figure G 1 shows that the effective thermal conductivity enhancement decreases with increasing sonication time. This is due to the reduction in size of the flakes as the sonication time is increased. To achieve higher enhancement larger flakes are required. However, very low sonication conditions are ineffieicent to maintain the stability of the suspensions. Hence, it is desirable to develop better dispersions methods to obtain maximm thermal conductivity enhancement.

H Viscosity Measurements of SWCNH and GnP based Nanofluids

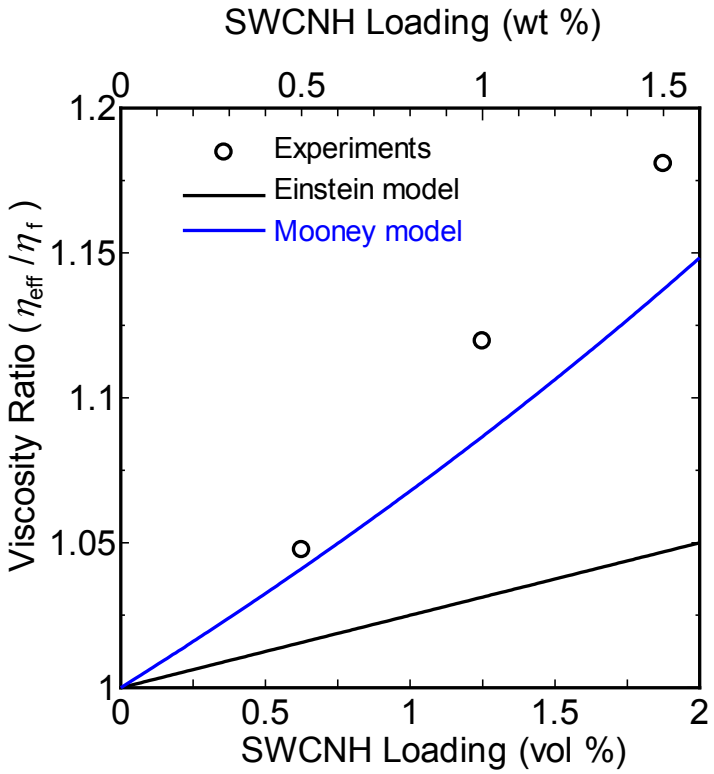

Figure H1: Viscosity enhancement of water/SWCNH based nanofluids along with theoretical predictions.

The viscosity measurements of SWCNH and GnP based nanofluids is shown in figure H1-H5. In all cases, EG based nanofluids show a non-Newtonian shear thinning behaviour. Similarly the increase in viscosity is much more pronounced compared to the enhancement of thermal conductivity as seen in chapter 4 of the thesis. Comparison of the viscosity enhancement with the Einstein model show that it under-estimates the viscosity enhancement. Mooney's model predicts reasonable enhancement for water based nanofluids while it fails for the EG suspensions.

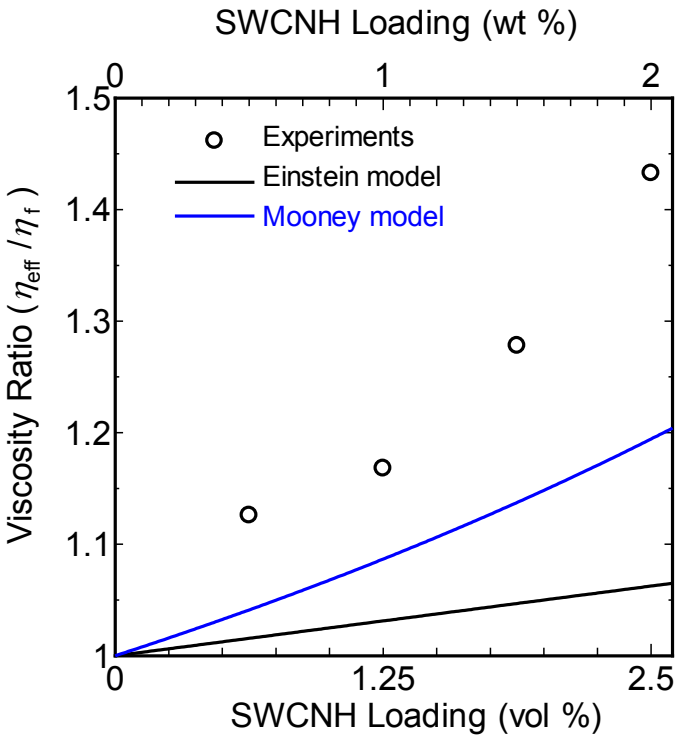

Figure H2: Viscosity enhancement of EG/SWCNH based nanofluids along with theoretical predictions.

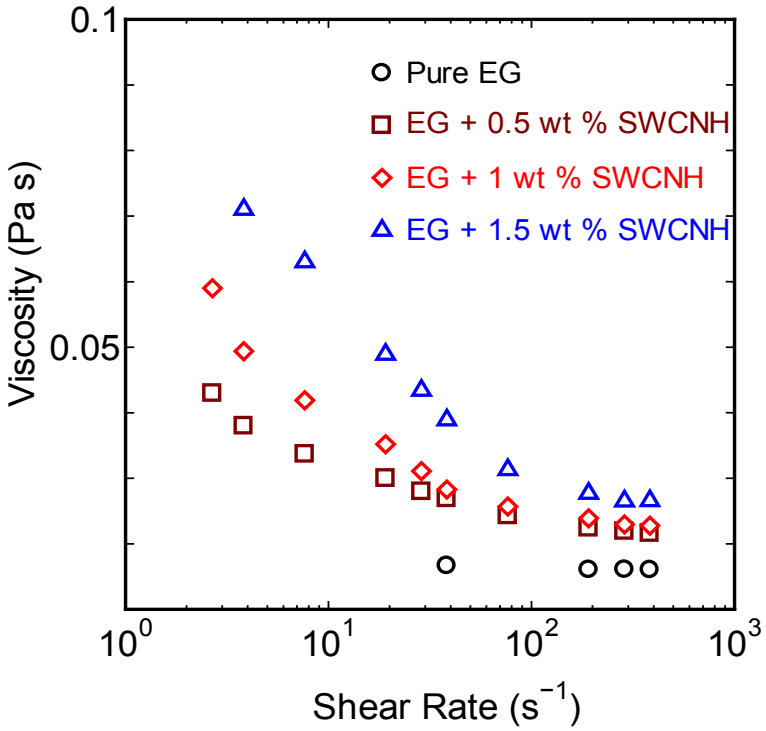

Figure H3: Shear Rate dependent viscosity of EG/SWCNH based nanofluids

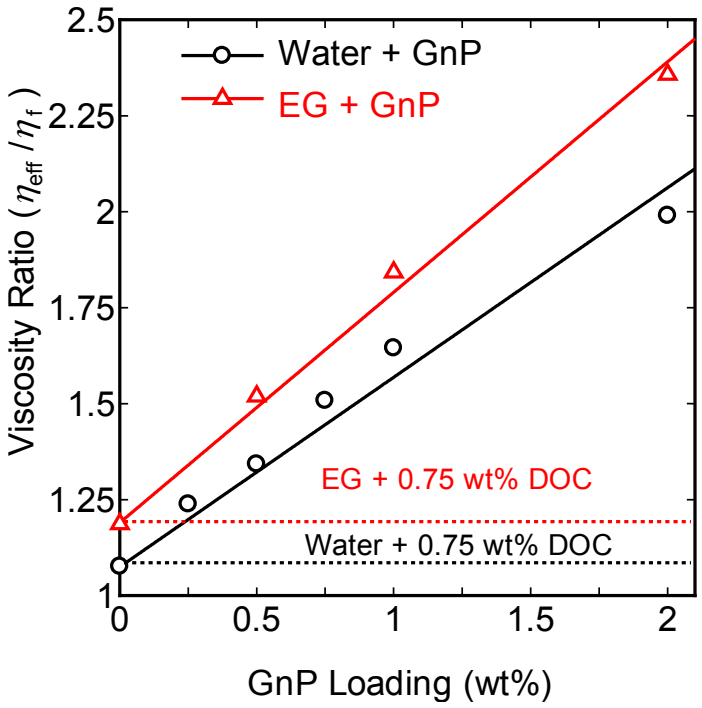

Figure H4: Viscosity enhancement of Water and EG/GnP based nanofluids along with theoretical predictions.

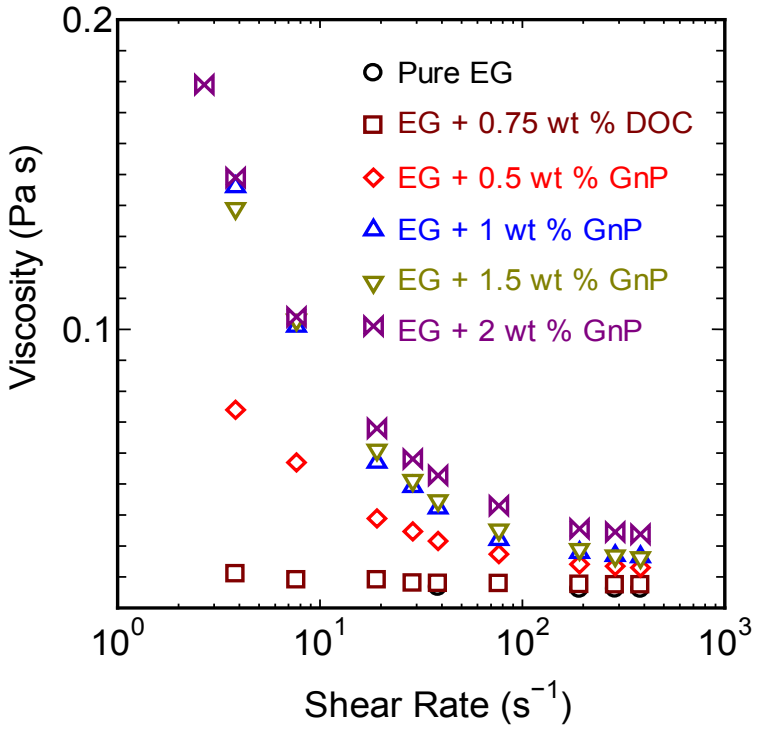

Figure H5: Shear Rate dependent viscosity of EG/SWCNH based nanofluids

I. One Dimensional Steady State Measurements of Phase Change Nanocomposites

The thermal conductivity of phase change nano composites with carbon nanotube inclusions were also measured using a one-dimensional steady state measurement method. The schematic representation of the meaasurement setup is shown in figure I 1.

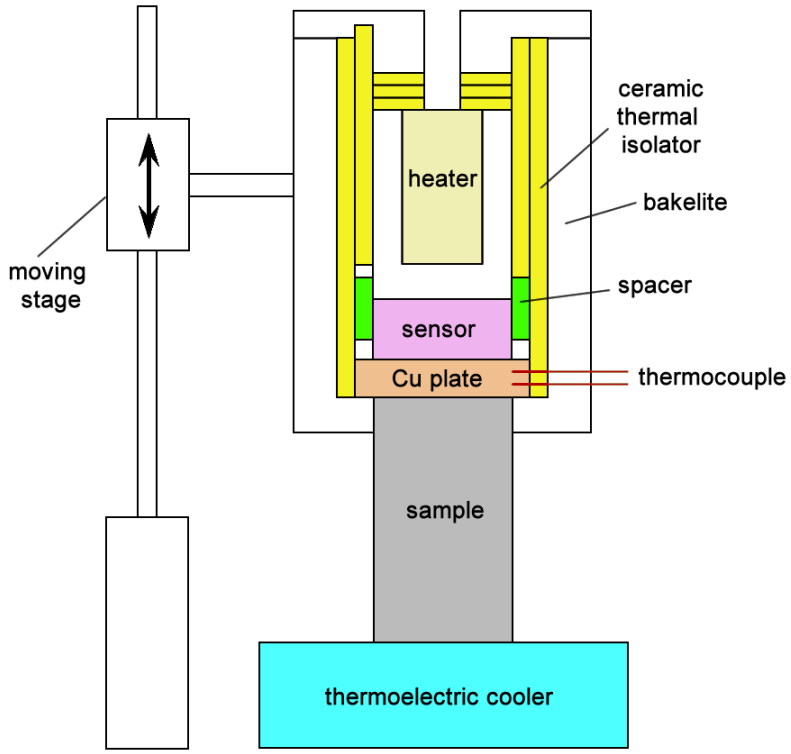

Figure I 1: Schematic Represntation of the 1D - Steady State Heat Conduction Experimental Setup.

The experimental setup consists of a heater which is surrounded by a ceramic thermal insulator. Below the heater, a heat flux sensor is placed which is connected to the data acquistion system. Below th heat flux sensor, a copper plate is placed and the temperature of

the copper plate is measured using a k-type thermcouples. The entire assembly is mounted on a bakelite mould. The bakelite mould is connected to a movable stand. The sample to be tested is placed on a thermoelectric cooler which is maintained at a tempearute of 273 K. A uniform DC power supply is given to the heater to introduce a temperature graident. The tempearaute of the copper plate and the corresponding heat flux is monitored using the data acquistion system. The experiment is allowed to run for a period of 30 minutes to ensure that the steady state condtion is reached. From the measured temperature conditions, heat flux per unit area (q) results and the length of the sample (L), the thermal conductivity of the sample is calculated using the Fourier's law as follows:

$$k = \frac{qL}{\Delta T} \qquad \text{(I. 1)}$$

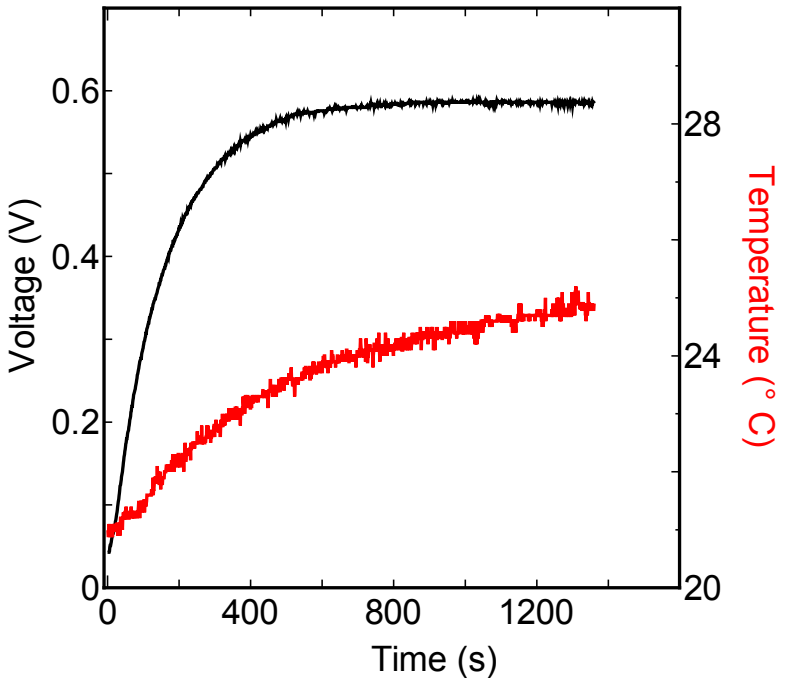

Figure I 2: Raw data of the temperature profile of the sample

A typical temperature profile and the corresponding heat flux results are shown in figure I 2. From the measurements sample of diamter 10 mm and length 15 mm, 20 mm and 25 mm is used. From the measured tempearture of the sample and the heat flux signal, the thermal conductivity of the sample is directly calculated using the expression (I 1). The **thermal conductivity of pristine n-octadecane** and **0.25 wt % n-octadecane/ SWCNT composite** is estimated as **0.172 ± 0.025 Wm^{-1} K^{-1}** and **0.351 ± 0.013 Wm^{-1} K^{-1}**.

J. Contrasting Thermal Conductivity in Phase Change Alkanes with SWCNH inclusions

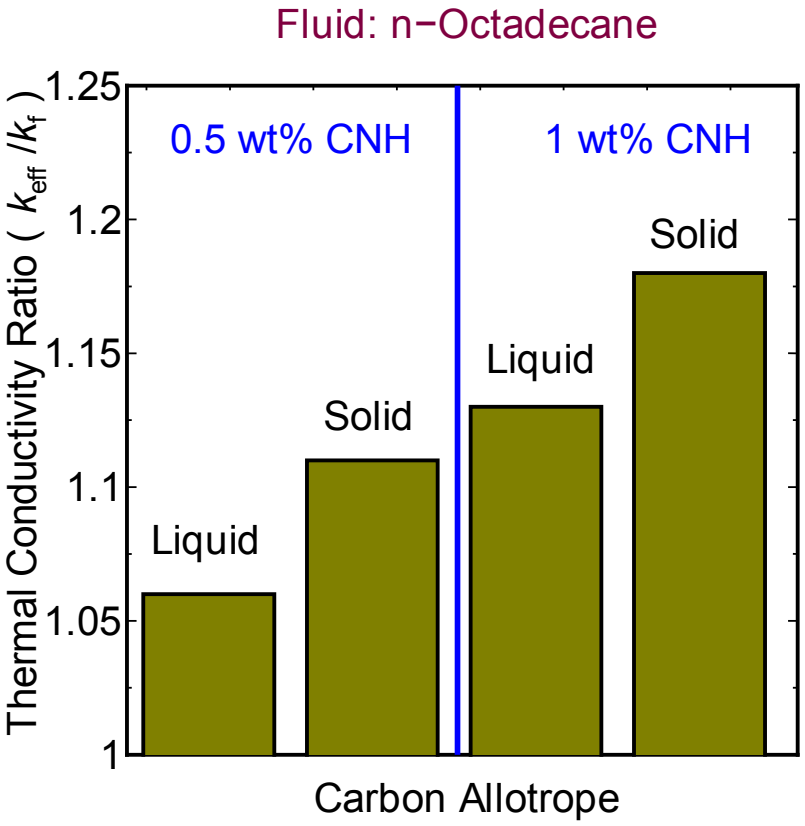

Figure J 1: Thermal Conductivity enhancement in n-octadecane for solid and liquid state.

The thermal conductivity increases with increasing SWCNH loading in both the liquid and solid state. The enahncement in solid state is quite higher the liquid state. However, the magnitue of enhancemetn in solid state is not much higher compared to the case of SWCNT and GnP inclusions.

List of Publications

1. **S. Harish**, K. Ishikawa, S. Chiashi, J. Shiomi, S. Maruyama, Anomalous Thermal Conduction Characteristics of Phase Change Composites with Single Walled Carbon Nanotube Inclusions, The Journal of Physical Chemistry C, *Volume 117, Issue 29, 2013, pp 15409-15413.*

2. **S. Harish**, K. Ishikawa, E. Einarsson, S. Aikawa, S. Chiashi, J. Shiomi, S. Maruyama, Enhanced thermal conductivity of ethylene glycol with single walled carbon nanotube inclusions, International Journal of Heat and Mass Transfer, *Volume 55, Issue 13-14, 2012, pp 3885-3890.*

3. **S. Harish**, K. Ishikawa, E. Einarsson, S. Aikawa, T. Inoue, P. Zhao, M. Watanabe, S. Chiashi, J. Shiomi, S. Maruyama, Temperature dependent thermal conductivity increase of aqueous nanofluid with single walled carbon nanotube inclusion, Materials Express, *Volume 2, Issue 3, 2012, pp 213-223.*

4. **S. Harish**, Godson Asirvatham, Jefferson Bose, A. Bensely, Experimental analysis of parallel plate and cross-cut pin fin heat sinks for electronic cooling applications, Thermal Science, *Volume 14, Issue 1, 2010, pp 147-156.*

5. **S. Harish**, A. Bensely, D. Mohan Lal, A. Rajadurai, Gyöngyvér B. Lenkey, Microstructural study of cryogenically treated En31 bearing steel, Journal of Materials Processing Technology*, Volume 209, Issue 7, 2009, pp 3351-3357*.

6. **S. Harish**, D. Peter Michael, A. Bensely, D. Mohan Lal, A. Rajadurai, Mechanical property investigation of natural fiber coir composite, Materials Characterization*, Volume 60, Issue 1, 2009, pp 44-49.*

7. P. Elayiaraja, **S. Harish**, L. Wilson, A. Bensely , D. M. Lal, Experimental investigation on heat transfer characteristics of metal foam heat sink for electronic cooling applications, Experimental Heat Transfer**,** *Volume 23, Issue 3, 2010, pp 185-195.*

8. A. Bensely, D. Senthilkumar, **S.Harish,** D. Mohan Lal, G. Nagarajan, A. Rajadurai, Pete Paulin, Cryogenic Treatment of Gear Steel, Gear solutions Magazine, October 2011.

9. A. Bensely, L. Shyamala, **S. Harish** , D. Mohan Lal, G. Nagarajan, Krzysztof Junik, A. Rajadurai, Fatigue behaviour and fracture mechanism of cryogenically treated En 353 steel, Materials & Design*, Volume 30, Issue 8, 2009, pp 2955-2962.*

10. T. Thurakitseree, C. Kramberger, P. Zhao, S. Aikawa, **S.Harish,** S. Chiashi, E. Einarsson, S. Maruyama, Diameter controlled and Nitrogen doped vertically aligned single wall carbon nanotubes, Carbon, *Volume 50, Issue 7, 2012, pp 2635-2640.*

11. R.Xiang, B.Hou, E.Einarsson, P.Zhao, **S.Harish**, K.Morimoto, Y.Miyauchi, S.Chiashi, Z.Tang, S. Maruyama, Carbon atoms in ethanol do not contribute equally to formation of single-walled carbon nanotubes, ACS Nano, *Volume 7, Issue 4, 2013, pp 3095-3103.*

12. **S.Harish**, K. Ishikawa, E. Einarsson, S.Aikawa, M.Watanabe, S. Chiashi, J. Shiomi, S. Maruyama, Thermal conductivity of single walled carbon nanotube suspensions in ethylene glycol: Experiments and Theoretical Limits, Proceedings of the 4th International Symposium on Heat Transfer and Energy conversion, January 2012, Guangzhou, China.

13. **S.Harish**, K. Ishikawa, E. Einarsson, T. Inoue, S. Chiashi, J. Shiomi, S. Maruyama, Enhanced thermal conductivity of water with surfactant encapsulated and individualized single walled carbon nanotube dispersions, Proceedings of the ASME 3rd Micro/Nanoscale Heat and Mass Transfer International conference**,** March 2012, Atlanta, USA.

14. **S.Harish**, K. Ishikawa, E. Einarsson, J. Shiomi, S. Maruyama, Temperature dependent thermal conductivity enhancement of water with surfactant encapsulated single walled carbon nanotube inclusion, Proceedings of the 3rd International Forum on Heat Transfer, November 2012, Nagasaki, Japan.

15. Herbert Raj, **S. Harish,** R. Nishanth Chandran, G. Chandrasekhar, D.Mohan Lal, Numerical Simulation of R407C/R290/R600a refrigerant mixture in a HCFC22 hermetic reciprocating compressor, Proceedings of International Conference on Modeling and Simulation, 2007, India.